5-16-2024

# A Comprehensive Study on Electrospun Fibres: Application in High-Efficiency Face Masks and Coaxial Fibre Morphology Exploration

Grzegorz Gajewski
*University of Windsor*

# "A Comprehensive Study on Electrospun Fibres: Application in High-Efficiency Face Masks and Coaxial Fibre Morphology Exploration"

By

**Grzegorz Gajewski**

A Thesis

Submitted to the Faculty of Graduate Studies

through the Department of Mechanical, Automotive & Materials Engineering

in Partial Fulfillment of the Requirements for

the Degree of Master of Applied Science

at the University of Windsor

Windsor, Ontario, Canada

2024

**"A Comprehensive Study on Electrospun Fibres: Application in High-Efficiency Face Masks and Coaxial Fibre Morphology Exploration"**

by

**Grzegorz Gajewski**

APPROVED BY:

_____

M. Mirhasani

Department of Electrical & Computer Engineering

_____

A. Edrisy

Department of Mechanical, Automotive & Materials Engineering

_____

A.R. Riahi, Advisor

Department of Mechanical, Automotive & Materials Engineering

April 12, 2024

# DECLARATION OF ORIGINALITY

I hereby certify that I am the sole author of this thesis and that no part of this thesis has been published or submitted for publication.

I certify that, to the best of my knowledge, my thesis does not infringe upon anyone's copyright nor violate any proprietary rights and that any ideas, techniques, quotations, or any other material from the work of other people included in my thesis, published or otherwise, are fully acknowledged in accordance with the standard referencing practices. Furthermore, to the extent that I have included copyrighted material that surpasses the bounds of fair dealing within the meaning of the Canada Copyright Act, I certify that I have obtained a written permission from the copyright owner(s) to include such material(s) in my thesis and have included copies of such copyright clearances to my appendix.

I declare that this is a true copy of my thesis, including any final revisions, as approved by my thesis committee and the Graduate Studies office, and that this thesis has not been submitted for a higher degree to any other University or Institution.

# ABSTRACT

This thesis presents a detailed investigation into the fabrication of electrospun nanofibres, focusing on their application in high-efficiency face masks and the exploration of coaxial electrospinning to understand how various parameters affect the morphology of core-shell fibres. The study begins with the optimization of electrospinning parameters for producing uniform polyvinylidene fluoride-hexafluoropropylene (PVDF-HFP) fibres, identifying a 1:1 dimethylformamide (DMF): Acetone ratio as optimal for achieving consistent fibre diameters and morphologies. This foundational work informs the subsequent development of fibrous mats, with scanning electron microscopy (SEM) images revealing the impact of solvent ratios on fibre diameter and distribution. Filtration tests demonstrate that while beaded fibres are traditionally seen as less desirable, they exhibit good filtration capabilities with significantly reduced pressure drops, challenging conventional views and suggesting potential for specific applications. Further, the thesis delves into coaxial electrospinning experiments, aiming to produce fibres with core-shell structures by manipulating electrospinning parameters such as solvent ratios, polymer concentrations, and applied voltages. Firstly, by finding working polymer solutions to create uniform fibres of each core and shell solution, then combining them to observe if the interaction between the solutions affects the final fibre. SEM analysis confirms the successful creation of core-shell fibres, highlighting the nuanced effects of these parameters on fibre morphology. A wide range of core-shell ratios are fabricated as well as core-shell fibres with multiple cores.

# DEDICATION

I would like to dedicate this thesis to my loving wife, who supported me and encouraged me during my countless hours of research and writing, I could not have completed my research and thesis without her. I would like to thank her family, my In-laws, for their support through the pandemic and afterwards.

# ACKNOWLEDGEMENTS

I am grateful to my advisor, Dr. Reza Riahi, for his invaluable guidance and support throughout this journey. His wisdom and encouragement have been pivotal to my success. I would like to thank Dr. Afsaneh Edrisy for her support through my research process and as well as contacting me for the opportunity to do my research under Dr. Riahi. My thanks to the staff of the Department of Mechanical, Automotive & Materials Engineering for their assistance and to my colleagues for their camaraderie and insights. I would like to show my gratitude to Dr. Mitra Mirhassani for taking the time to be on my committee. Most importantly, I express my gratitude to my wife who has pushed me in the right direction when I was unmotivated and was there for me when my days ran long. Finally, to my family, who have provided unwavering support and encouragement from the beginning of this process.

# TABLE OF CONTENTS

# LIST OF TABLES

# LIST OF FIGURES

# LIST OF ABBREVIATIONS/SYMBOLS

PVDF-HFP… Poly(vinylidene fluoride-co-hexafluoropropylene)

PPE… Personal protective equipment

DMF… Dimethylformamide

PS…Polystyrene

THF… Tetrahydrofuran

PVDF…Polyvinylidene fluoride

PLA…Polylactic Acid

PP…Polypropylene

PE…Polyethylene

NP…Nano Particles

NT…Nanotubes

QF…Quality Factor

η…Filtration Efficiency

ΔP… Change in Pressure

DNA…Deoxyribonucleic Acid

ZnO…Zinc Oxide

TiO2…Titanium Dioxide

SARS-CoV-2… severe acute respiratory syndrome coronavirus 2

RH…Relative Humidity

VIPS…Vapour Induced Phase Separation

CS…Chitosan

PEO…Polyethylene Oxide

CA…Cellulose Acetate

CA-A… Cellulose Acetate and Acetone

CA-D… Cellulose Acetate and DMAc

CA-AD… Cellulose Acetate with different ratios of Acetome and DMAc

DMAc… Dimethylacetamide

PGLA… Poly(glycolide-co-lactide)

CA-AD21… Cellulose Acetate with a 2:1 ratio of Acetone:DMAc

Ag-NPs…Silver Nano Particles

TEM…Transmission Electron Microscopy

PVP… Polyvinylpyrrolidone

PAN…Polyacrylonitrile

wt%...Weight Percentage

PTFE… Polytetrafluoroethylene

SEM…Scanning Electron Microscopy

PLB…Low Beaded Structure

PHB…High Beaded Structure

PUB…Ultra-high Beaded Structure

N95…US standard mask that filters out 95% of most penetrating particle size

MPPS…Most penetrating particle size

# NOMENCLATURE

nm…Nanometers

kV…Kilovolts

um…Micrometers

dyn/$cm^2$…Dyne per Square Centimeter

mN/m…Millinewtons per meter

# CHAPTER 1 - Objectives and Introduction

### *1.1 Objectives*

The objectives for this study are:

- To investigate the electrospinning process for fabricating Chitosan (CS) nanofibres with the goal of creating uniform fibres.

- To combine polyvinylidene fluoride-hexafluoropropylene (PVDF-HFP) and Chitosan (CS) nanofibres with the intent to create high-efficiency face masks, optimizing fibres to have a filtration rating and fall within the max standard limit for inhalation resistance for face masks, or 343 Pa.

- To assess the filtration capabilities and breathability of the produced nanofibre filters compared to the current face mask standard, the N95 mask.

- To explore the application of coaxial electrospinning techniques for creating core-shell fibre structures.

- After forming coaxial fibres, choose specific parameters to adjust during the fibre fabrication process.

- Analyze the coaxial fibres using both optical microscopy and SEM, and report on the findings of how these parameters change the features of the coaxial fibre.

### *1.2 Introduction*

Among the various nanofabrication techniques, electrospinning stands out for its simplicity, versatility, and efficacy in producing nanofibres with high surface area-to-volume ratios, which are ideal for a wide range of applications, including filtration, tissue engineering, drug delivery, and protective clothing. Electrospinning involves using an

electric field to draw polymer solutions or melts into ultrafine fibres. This thesis focuses on the electrospinning of polyvinylidene fluoride-hexafluoropropylene (PVDF-HFP) nanofibres, with an emphasis on their application in high-efficiency face masks and the exploration of coaxial electrospinning to understand the influence of various parameters on the morphology of core-shell fibres. The global pandemic highlighted the critical role of personal protective equipment (PPE), particularly face masks, in controlling the spread of infectious diseases. The efficiency of face masks largely depends on the filtration capabilities and breathability of the material used, parameters that directly influence the fibre morphology. Hence, optimizing the electrospinning process to produce fibres that balance filtration efficiency with breathability is paramount. This thesis builds upon this premise, starting with producing uniform PVDF-HFP fibres optimized through adjustments in the solvent ratios and electrospinning parameters. A note for the terminology used in this thesis in regards to the fibres appearance, the term "uniform fibres" is used to identify fibres that have little to no variation in their diameter across the fibre. This does not reference the overall fibre diameters amongst the various fibres in sample, the difference in fibre diameters in a given sample is known as the "fibre diameter distribution".

Moreover, coaxial electrospinning is an advanced technique to fabricate fibres with core-shell structures, offering the potential for enhanced performance in many applications. The core-shell fibres can provide a combination of mechanical properties, chemical functionalities, and structural features that are difficult to achieve with single-material fibres. By varying parameters such as polymer concentrations, solvent compositions, feed rate ratios, and electrospinning voltages, this research aims to understand their impact on fibre morphology systematically and, consequently, on the filtration performance of the fabricated face masks.

# CHAPTER 2 – Literature Review

## *2.1 Introduction*

Electrospinning has emerged as a powerful technique for producing ultrafine fibres with diameters ranging from nanometers to micrometers. The technique involves the application of a high electric field to a polymer solution or melts, forming a charged jet that is elongated and solidifies to form fibres. Electrospinning has applications in various fields, including biomedicine, energy storage, environmental remediation, and filtration. In recent years, electrospun nanofibres have received increasing attention as a potential candidate for air filtration applications, particularly in the development of face masks. The COVID-19 pandemic has highlighted the need for effective face masks to protect against respiratory droplets containing the virus. Electrospun nanofibres offer several advantages over conventional filter materials, including a high surface area-to-volume ratio, small pore size, and high filtration efficiency. Coaxial electrospinning has emerged as a promising strategy for producing nanofibres with unique properties, including core-sheath and hollow fibres. Coaxial electrospinning produces nanofibres with controlled morphology and properties. This literature review aims to provide an overview of the current state of research on electrospinning, with a particular focus on the morphology of coaxial spun nanofibres and air filtration applications. The review will begin with a discussion of the fundamentals of electrospinning, including the mechanisms involved in fibre formation and the factors that affect the morphology and properties of the resulting nanofibres. It will then explore the various materials that have been electrospun for air filtration applications, such as polymers, composites, and inclusions, and the methods used to modify their properties through coaxial electrospinning.

## *2.2 Types of Electrospinning*

Electrospinning is a versatile and widely used technique for fabricating nanofibres with applications in various fields, including biomedical engineering, materials science, and environmental engineering. This section aims to comprehensively review different electrospinning methods, including but not limited to needleless, single-needle, coaxial,

triaxial, side-by-side, and multi-needle electrospinning. The review will highlight each technique's fundamental principles, advantages, limitations, and applications.

### *2.2.1 Needleless Electrospinning*

Needleless electrospinning, which can have rotating and stationary spinnerets, has garnered significant attention for its innovative approach to eliminating metal needle use. This unique feature leads to higher production rates and ease of scalability, offering a significant advantage over traditional methods. The technique typically employs a semi-submerged rotating cylinder or spiral electrode, among other configurations that leverage the needleless method [1, 2, 3]. While the voltage required between the needle and electrode can reach excess of 30 kV, the needleless setup operates within a range of 30 kV-80 kV. The absence of a needle mitigates the risk of clogging and enables continuous nanofibre production. Needleless electrospinning has proven its efficacy in filtration, energy storage, and tissue engineering, where high-throughput fabrication is crucial.

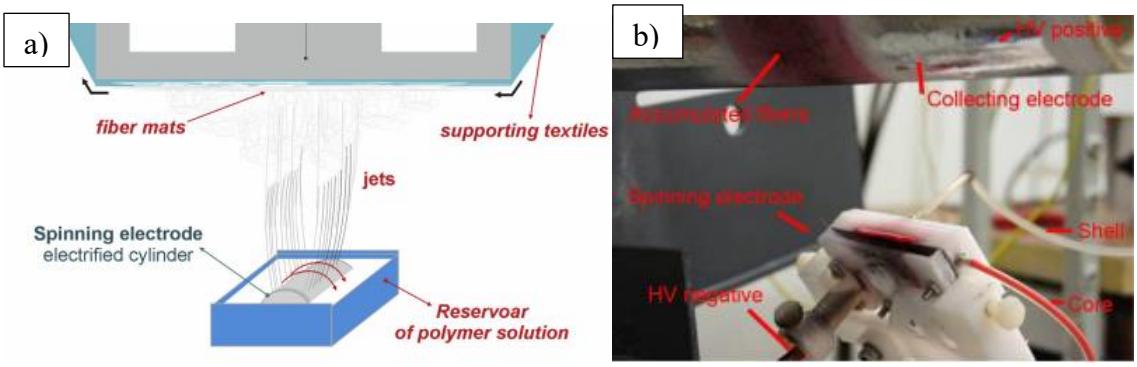


*Figure 2.1 a rotating [2] and (b) a stationary [3] needleless electrospinning set up*

### *2.2.2 Single-Needle Electrospinning*

Single-needle electrospinning is the most commonly used technique in electrospinning. It involves using a single metal needle, either round or flat, connected to a high-voltage power supply. A polymer solution or melt is dispensed through the needle, and an electric field is applied to induce the formation and elongation of nanofibres [4, 5]. Single-needle electrospinning offers excellent control over fibre morphology, diameter, and alignment. It has been extensively employed in drug delivery systems, tissue engineering scaffolds, and

filtration membranes. Single-needle electrospinning can be used to create solid fibres and a core-shell structure.

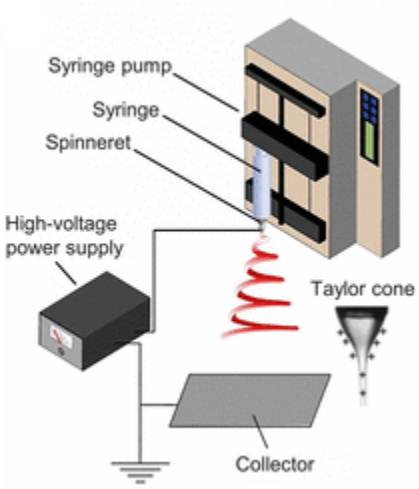


*Figure 2.2 An example of a vertical single-needle electrospinning set-up [5]*

### *2.2.3 Coaxial Electrospinning*

Coaxial Electrospinning involves the simultaneous extrusion of two or more concentrically arranged fluids through a coaxial spinneret. A polymer solution or melt is typically injected through the inner needle, while a different solution is introduced through the outer needle [6]. By adjusting the flow rates of the polymer solutions and the applied voltage, it is possible to control the morphology and properties of the resulting nanofibres. Coaxial electrospinning allows the fabrication of core-shell structured nanofibres, where the core can encapsulate active agents or functional materials. This technique has been widely utilized in controlled drug release, tissue engineering, and sensor fabrication [7].

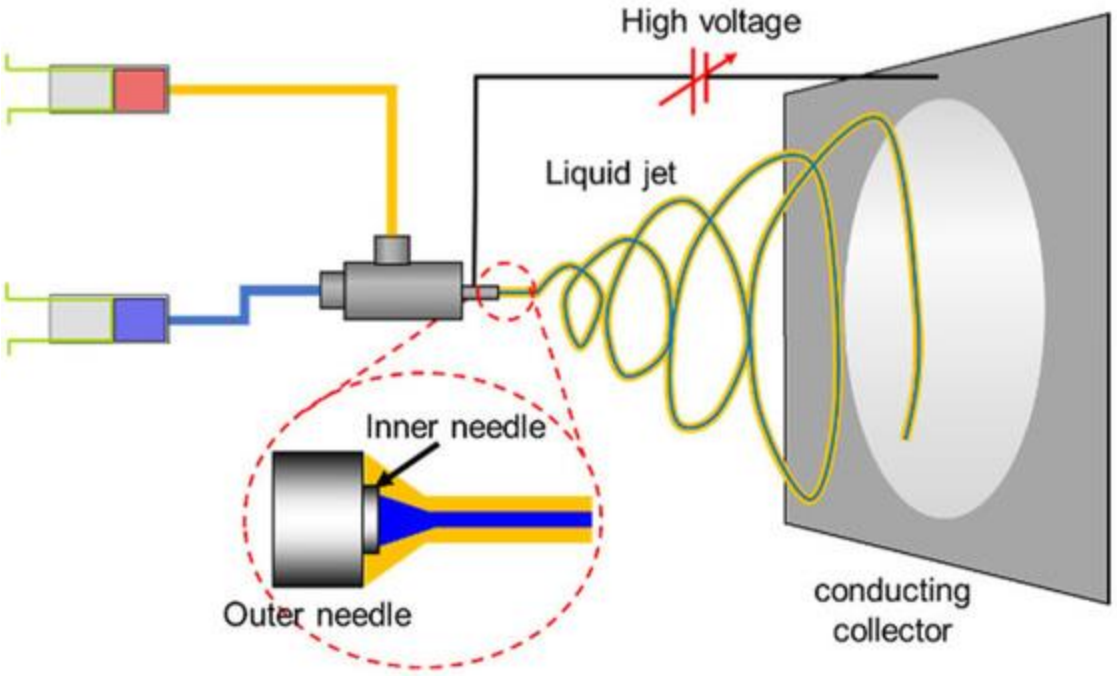


*Figure 2.3 An example of a coaxial electrospinning set up [7]*

### *2.2.4 Triaxial Electrospinning*

Triaxial electrospinning expands upon the concept of coaxial electrospinning by introducing an additional concentric layer. Triaxial electrospinning enables the simultaneous extrusion of three materials, resulting in complex hierarchical structures [8, 9]. Triaxial electrospinning provides enhanced versatility for incorporating multiple components within the nanofibre structure, such as cells, growth factors, and nanoparticles. This technique has found applications in tissue engineering, where the spatial organization of different components is crucial for mimicking native tissue structures.

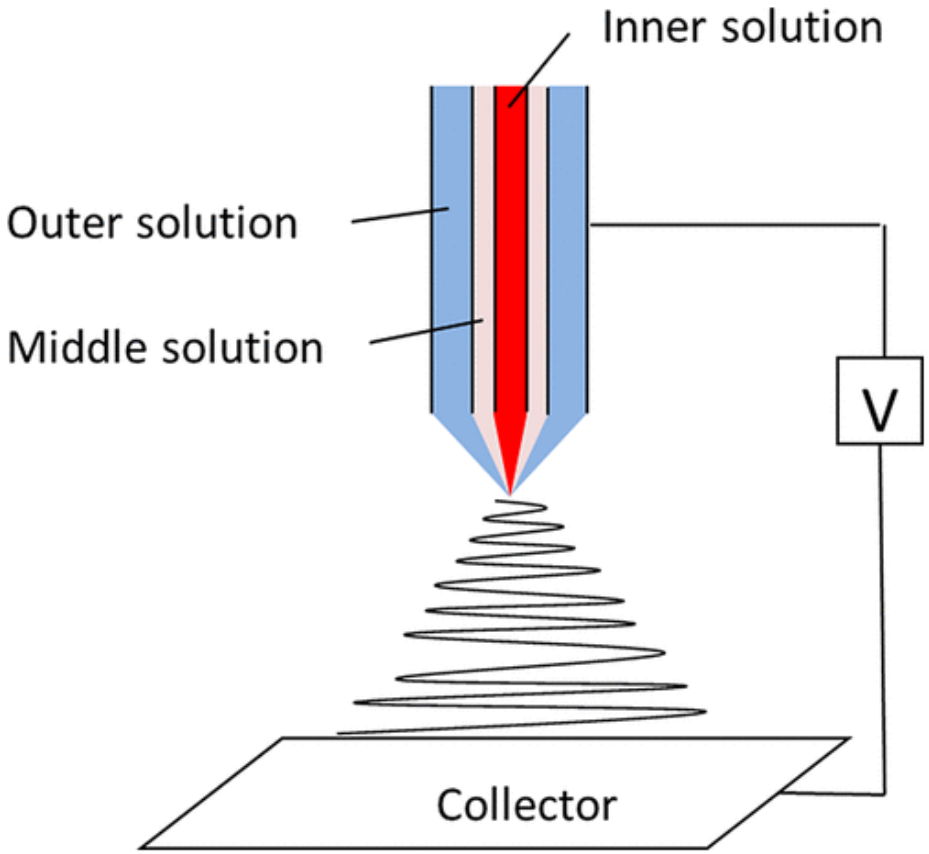


*Figure 2.4 An example of triaxial electrospinning [9]*

### *2.2.5 Side-by-Side Electrospinning*

Side-by-side electrospinning involves the simultaneous extrusion of two or more different polymers through adjacent needles [10]. The resulting nanofibres possess a side-by-side arrangement of the different polymers, allowing for functional fibres with distinct properties. Applications such as functional textiles, composite materials, and catalysts use side-by-side electrospinning.

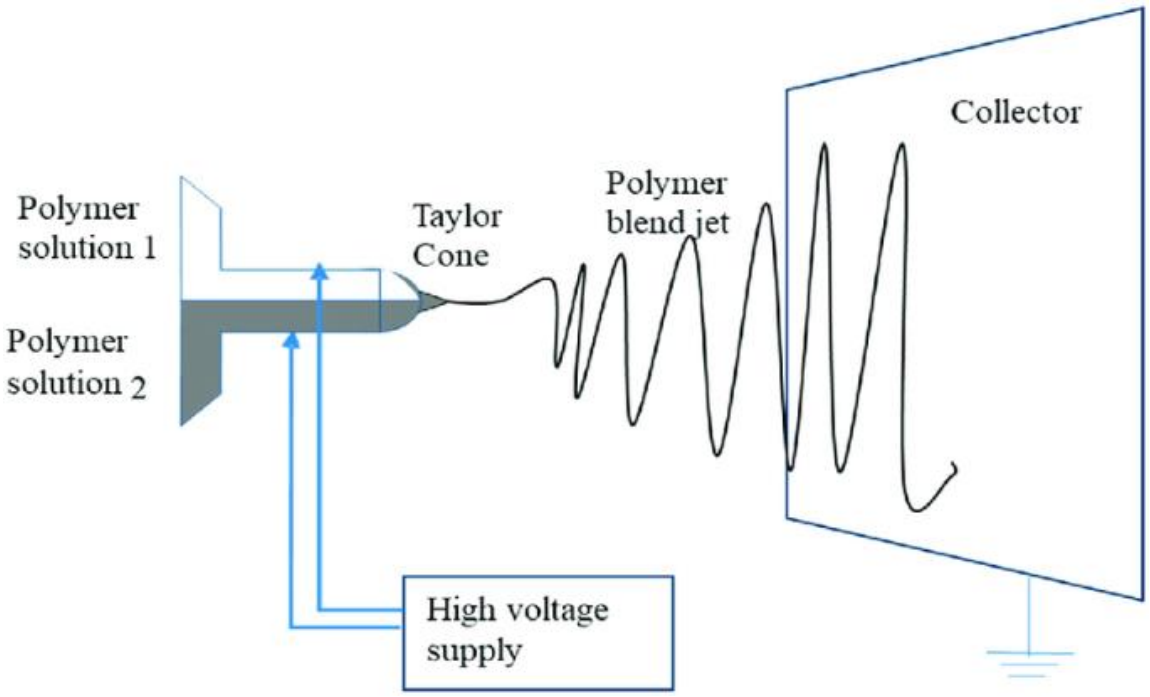


*Figure 2.5 An example of side-by-side electrospinning [10]*

### *2.2.6 Multi-needle Electrospinning*

Multi-needle electrospinning employs an array of multiple needles for simultaneous electrospinning. This technique enables the production of many nanofibres in parallel, thereby increasing the overall production rate [11]. Multi-needle electrospinning is particularly useful for large-scale nanofibre production and when high-throughput manufacturing is required. It is also used in filtration, protective clothing, and energy storage.

Grasping the distinct advantages and limitations of different electrospinning techniques is critical. It enables the fabrication of nanofibres with diverse structures and functionalities. The choice of electrospinning method hinges on the application's specific requirements, including fibre morphology, composition, scalability, and functionality. Empowering ourselves with a deep understanding of the principles and capabilities of each technique is crucial for optimizing electrospinning processes and advancing their applications in various fields. Further research and development are needed to unlock these techniques' full potential and tackle the challenges associated with electrospinning, such as scalability,

material compatibility, and process control.

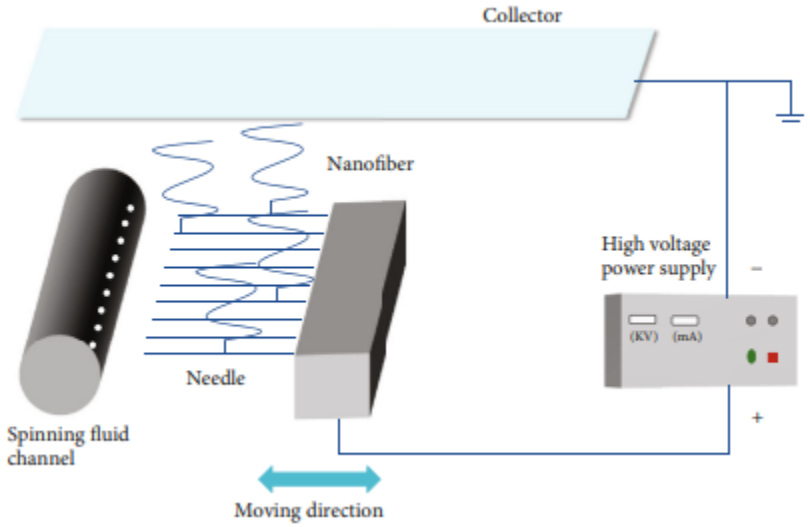


*Figure 2.6 An example of multi-needle electrospinning [11]*

### *2.3 Electrospinning Setup Parameters*

The single needle/coaxial electrospinning set-up is standard, but each parameter affects the fibres produced. In its most basic form, an electrospinning enclosure contains a solution that is fed through a spinneret; a spinneret is usually a metal needle of various, but small, diameters with a flat end, a collector a set distance from the tip of the spinneret, and a power source connected to an electrode near the spinneret and the collector [12, 13, 14] These four parts of the electrospinning set-up each have their influence on the resulting fibre. The term spinneret is used; however, it does not always mean the same type of needle. Sometimes, the solution is in a bath with a rotating cylinder, where the polymer solution coats the protruding cylinder surface, and the electric field forms Taylor cones at the portion of the solution nearest the collector.

### *2.4 Materials of Electrospinning*

The outcome of an electrospinning process is under the influence of many interrelated variables, including operating parameters (e.g., applied voltage, flow rate, collector distance, room temperature, and ambient humidity), polymer type, attributes of the solution (e.g., concentration, additives, conductivity, and surface tension) [15]. The choice of material selection, including polymers, solvents, and additives, shapes the electrospinning

process and the characteristics of the resulting nanofibres. Considerations must be involved when choosing materials to meet specific objectives, such as enhancing mechanical strength, electrical conductivity, biocompatibility, or drug encapsulation capacity.

The science of materials selection and manipulation in electrospinning is fundamental to achieving precise control over the morphology, structure, and functionality of nanofibrous materials. This knowledge is essential for developing advanced applications in fields as diverse as tissue engineering, filtration, energy storage, and drug delivery, but also demonstrates the practical relevance of this research in addressing real-world challenges.

### *2.4.1 Polymers*

More than 100 organic and synthetic polymers have been explored in solution electrospinning to produce nanofibres directly [16]. Synthetic polymers such as polystyrene and poly(vinyl chloride), poly(lactic acid), Polycaprolactone, and poly(lactic-co-glycolic acid) have been used in various applications including, but not limited to, commercial, medical, and textile fields [17, 18]. Natural biopolymers, such as chitin/chitosan, collagen, alginate, and gelatin, have been electrospun into fibres for various applications. Conductive polymers such as polyaniline and polypyrrole and other functional polymers such as poly(vinylidene fluoride) have also been used for applications in supercapacitors and piezoelectric/pyroelectric applications respectively [19, 20, 21].

### *2.4.2 Solutions*

These polymers can only be successfully electrospun if the solution meets two requirements. Firstly, the solution has to have a sufficiently high molecular weight for the polymer. The molecular weight is directly related to the amount of polymer chains in the solution. As a solution increases in molecular weight, the morphology generally changes from (1) beads only to (2) incipient fibres with beads to (3) beads-on-a-string fibres to (4) uniform fibres to (5) globular fibres or “macrobeads” [22].

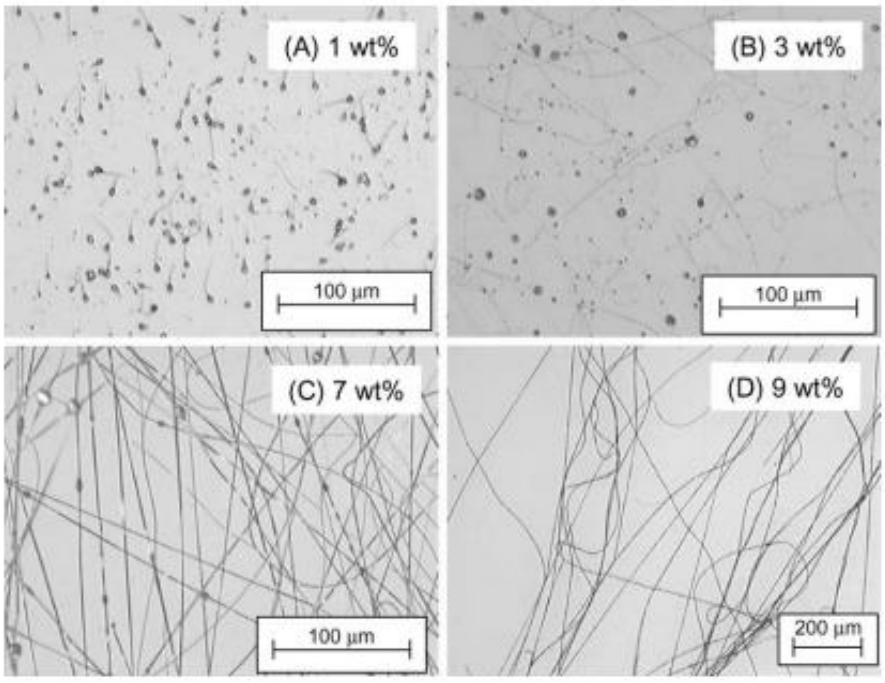


*Figure 2.7 (A) Bead only structure, (B) incipient fibres with beads, (C) beads-on-a-string fibres, (D) uniform fibres [22]*

Electrospun fibres are formed through the entanglements of polymer chains. Without enough polymer chains in the solution, the chains cannot be entangled, resulting in a solution that can only create beads; this would result in an electrospraying process. However, as the polymer solution increases, the connections between these electrospray beads start to form, and eventually, through the whipping part of the electrospinning process, these fibres stretch uniformly and can achieve nanoscale diameters.

This is the general rule for electrospinnable polymers. However, a further distinction can be made when focusing on the fibre diameters with polymers of higher and lower molecular weights. The solution requires a higher polymer chain concentration per unit for lower molecular weight polymers, resulting in lower extensibility and thicker fibres. Since each polymer chain is longer, a lower polymer chain concentration per unit is needed to create uniform fibres for a high molecular weight polymer solution. Having a lower polymer chain concentration and longer polymer chains allows for more extensibility and results in smaller-diameter fibres[22].

### *2.4.3 Solvents*

Solvents range in properties just as much as polymers in electrospinning solutions. However, not all solvents can be used with all polymers. It is apparent that not all polymers are soluble in all solvents; however, even amongst those compatible with a given polymer, its solubility is not the only factor to consider. Additionally, solubility does not directly translate to spinnability [15]. Some of the usable solvents in electrospinning are toxic. With many of the uses of electrospinning being in the medical sector or of nature to contact skin, these solvents could be better and, in some cases, restricted [23]. Solvents are an essential part of solution preparation, as any slight change in a solvent can change the morphology of the resulting fibres. Uyar et al. explored this by testing various grades of N, N-Dimethylformamide (DMF) from different suppliers (99.8%, 99%, and 98% purity). This study also found that two bottles of the same purity DMF had different conductivities. All solvents yielded fibres but they differed in fibre diameter and bead size by, at times, hundreds of nanometers, demonstrating that the purity of DMF influences when the morphology of the nanofibre changes from a bead-on-string to a uniform fibre [24].

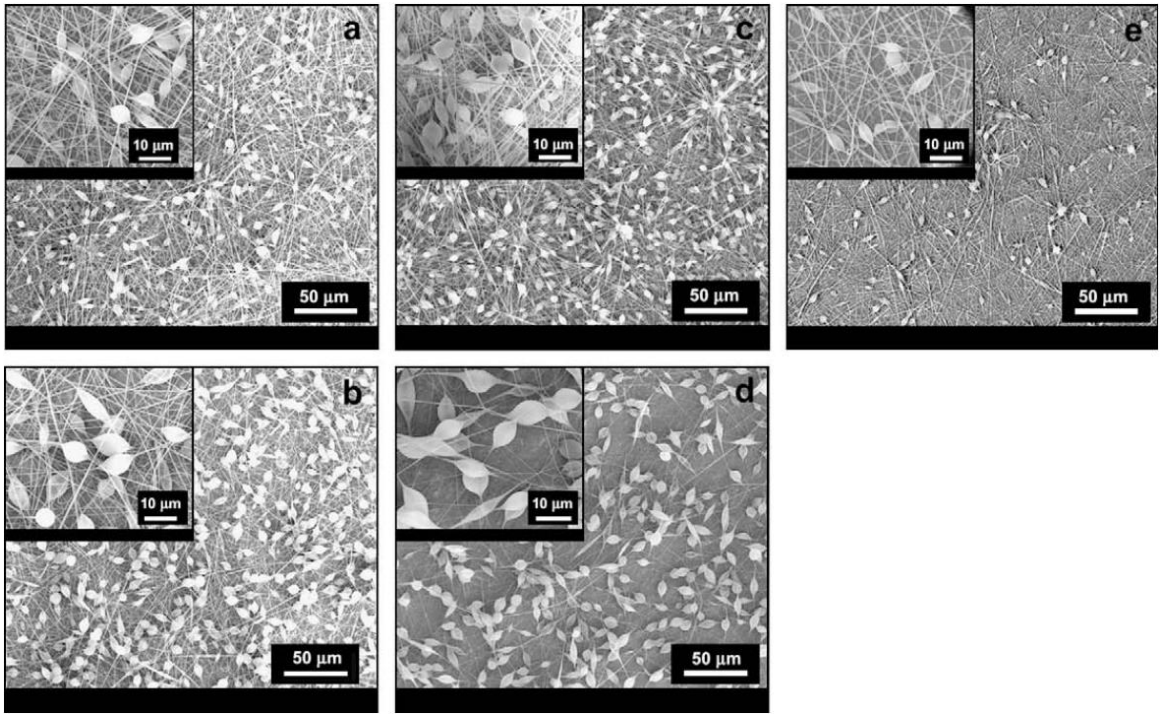


*Figure 2.8 Fibres produced from a 10 wt% PS solution with different suppliers and purities of DMF (a) DMF2-Aldrich 99%, (b) Sigma 99.8%, (c) Fluka 98%, (d) Fluka 99.8%, (e) DMF1-Aldrich 99%[24]*

Although each polymer-solvent interaction is unique, and for an accurate prediction of morphology, one should find research on the combination of these materials or experiment personally, some trends are common amongst multiple combinations. Wannatong et al. found that when creating a solution of polystyrene (PS) with various solvents (acetic acid, acetonitrile, m-cresol, toluene, tetrahydrofuran (THF and DMF), fibre diameters decreased with increasing density and boiling point of the solvents. An increasing difference between the solubility parameters of PS and the solvent led to a bead-on-string morphology [25].

#### *2.4.4 Additives*

In addition to the polymer and the solvent, or a combination of solvents, additives can be added to the solution to adjust specific properties and help with the solution's spinnability. There are three main additives in solution electrospinning: salts, surfactants, and hydrogen-bonding additives.

### *2.5 Solution Properties and Their Effect on Electrospun Fibres*

Specific properties of an electrospinning solution affect how or if fibres will be formed at the given parameters. The most critical solution properties are viscosity, conductivity, surface tension, and polymer chain length.

#### *2.5.1 Volatility*

Solvent volatility, how readily a substance vaporizes, can also contribute to fibre morphology. Generally, solvents with high volatility yield larger diameter fibres due to the fibre drying earlier in the electrospinning process and spending less time in the whipping/elongating step of electrospinning [26]. However, in some studies, such as those shown by Naumcharoen et al., when adding volatile solvents (Acetone, tetrahydrofuran, methyl acetate, ethyl acetate, propyl acetate, butyl acetate, ethanol, methanol, chloroform, and hexane) to a solution of poly(vinylidenefluoride) (PVDF) and DMF the resulting fibres increased in fibre diameter. In some cases, as the more volatile solvent concentrations increased, the fibre diameter decreased after the initial increase, or the solution was no longer spinnable [27].

### *2.5.2 Viscosity*

Viscosity and surface tension are the critical parameters to whether a solution can be electrospun and the morphology of the fibre itself [28, 29, 30]. These properties can be controlled by selecting the polymer and solution mixture, the polymer concentration, the solution ratio of more than one solvent, and the use of surfactants. The viscosity and surface tension have a range where the solution can be electrospun, depending on the electrospinning parameters [31, 32]. If the viscosity is too low, the solution will not form fibres, and electrospray will occur; if the solution viscosity is too high, the solution will not extrude at all [33]. There is a noticeable change in the morphology of the fibres as the viscosity increases, which also shows how uniform fibres are formed. Electrospray occurs at very low viscosities, and thin fibres with beads are observed when the viscosity is at the low end of the spinnable solution. As the viscosity increases, these beads slowly elongate. The beads disappear after a critical viscosity that differs with each solution, creating uniform fibres. It is thought that the beads eventually stretch out during the whipping phase to be evenly distributed amongst the uniform fibre. Generally, for each solution, the viscosity and surface tension range is specific to the mixture. However, the academic journals that comment on the viscosity range from 1-40 poise, and they have a surface tension around 35-55 dyn/cm2; other viscosities and surface tensions have been successfully electrospun; however, this range is more common [33, 34, 35].

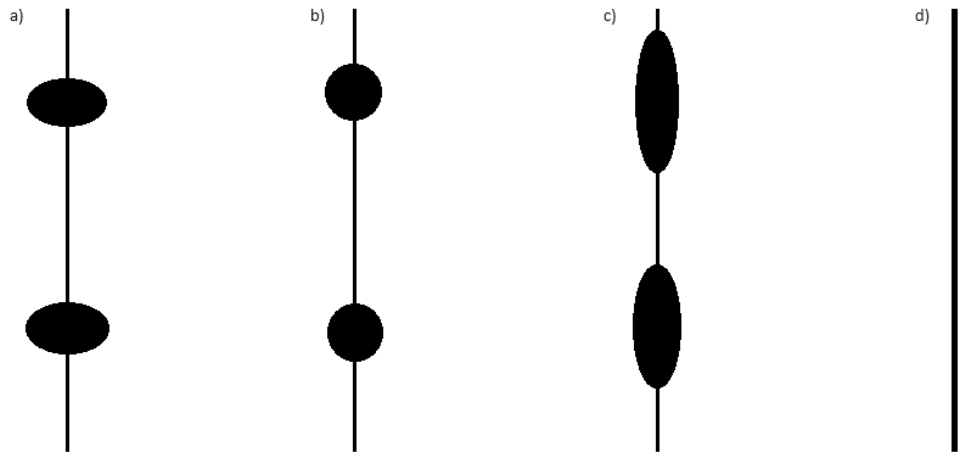


*Figure 2.9 A visualization of how fibres change from a bead-on-a-string type of fibre into a uniform fibre that occurs with increased viscosity.*

### *2.5.3 Surface Tension*

Even if the viscosity is within the range for electrospinning, the surface tension controls the upper and lower end of the electric field, which is required to begin fibre creation [33]. The polymer jet that extracts the fibres from the solution only occurs when the electric charges overcome the surface tension of the solution. Surface tension directly influences the diameter of the polymer jet, which occurs when the electric field is applied to the spinneret tip. This further translates to the final diameter of the fibre [36]. This means that if the surface tension is too high, regardless of the other properties, the solution will only yield fibres if a large enough electric field is applied. However, a low surface tension directly relates to a spinnable solution.

### *2.5.4 Conductivity*

The electrospinning process fundamentally requires a transfer of charge to produce fibres from a solution. This requires the solution to be within a range of conductivity, which means that non-conductive solutions cannot be electrospun. The polymer and solvent of the solution play the most significant role in the conductivity of the final product; however, when additives are included in the solution, they increase the number of impurities present, which typically increases the conductivity [37]. Increasing the polymer content in the solution often results in a conductivity decrease, but if the polymer has ionic capabilities, such as a polyelectrolyte, the conductivity of the solution will be higher, and an increased concentration of the polymer will not be as relevant as with other solutions [33].

## *2.6 Electrospinning in Air Filtration*

Electrospinning and nanofibres have been studied for use in air filtration for many years, often showing favourable results; the only downside to these facemasks is the production volume, as these setups cannot produce at the rate of current mass fibre production methods [38]. The most common air filters are fibreglass filters and meltblown filters. Of these two types, melt-blown filters can be heavily enhanced by electrospinning technology. Without changing the structure or material of the meltblown masks but using electrospinning to create smaller diameter fibres, the filtration efficiency of the filter increases [39]. Not only does the filtration efficiency of the air filter increase, but electrospun nanofibre filters or

face masks, also have a better reusability rate as one study showed that cleaning a melt-blown face mask after a single use reduces its filtration efficiency to 64% compared to a new mask. In contrast, in an electrospun nanofibre facemask, after the same amount of use and an identical cleaning protocol, the facemask remained almost unchanged at 97-99% efficiency [40]. The efficiency of electrospun facemasks can be further enhanced beyond the fibre size changes by using the other aspects available, such as anti-bacterial/anti-viral polymers or inclusions.

### *2.6.1 Air Filtration Materials and Inclusions*

Typically, many air filters are made of melt-blown polylactic acid (PLA), polypropylene (PP), and polyethylene (PE) fibres due to their strength, durability, and chemical resistance [41, 42, 43]. However, with the degree of customization available in electrospinning, air filters created with this process can use materials unsuitable for melt-blowing and have other properties, such as antibacterial/antiviral polymers, additives, or inclusions. Materials such as chitosan, silk, licorice root extracts, cinnamon oil, silver, zinc, titanium, and many other types of materials can be electrospun or included in the solution to enhance the availability of the fibres [44, 45, 46, 47]. These materials are either the primary polymer in the electrospinning solution, such as chitosan, gelatin, or guanidine-based polymers [48, 49, 50], or additives in the solutions, such as silver, copper, or titanium nanoparticles (NP) and nanotubes (NTs), aloe vera, and some salts [51, 52, 53].

Chitosan, gelatin, and other such antimicrobial materials are derived from organic compounds found in nature. Chitosan is derived from chitin, which is a compound found in shellfish exoskeletons, green algae, or the cell walls of fungi; gelatin originates in the skin and bones of animals, and guanidine-based polymers are derived from guanidino groups found in plants like rice hulls and animals like mussels or earthworms. The main drawback of these materials is that they cannot easily be electrospun on their own and are often mixed with different polymers to fabricate nanofibres [48, 54]. Of the three materials mentioned, chitosan is the most popular for creating antimicrobial fibres. It has been studied for use in wound dressing, drug delivery, air filtration, and face masks, to name a few [55, 56, 57]. When used in face mask fabrication, it is often combined with various other polymers such as polyvinylidene fluoride (PVDF), its derivatives such as

Poly(vinylidene fluoride-hexafluoropropylene) (PVDF-HFP), graphene, etc. [58, 59]. These polymers are used for the structure of the facemask and not necessarily for its filtering and antimicrobial properties. Since a facemask is required to maintain its properties in all ordinary conditions, hydrophobic polymers like those mentioned above are used most often as the outer layer to prevent water from penetrating the filter and compromising the filter if hydrophilic or water-dissolving materials are used [58]. Face masks typically comprise three, five, or seven layers. These layers allow the facemask to fulfill various requirements. Unsurprisingly, a more significant amount of the filtration material results in higher filtration of particles. However, as the filtration media thickens, the pressure drop across the filter also increases. A filter's efficiency is calculated by taking into account the filtration of particles and pressure drop [20]. The following formula is

$$QF=(-\ln(1-\eta))/\Delta P \qquad (2.1)$$

used to find the quality factor of a given filter, where QF is the quality factor, $\Delta P$ is the pressure drop across the filtration media, and $\eta$ is the filtration efficiency. Many studies have shown that using multiple thin layers of a nonwoven fibre mat is more efficient than using the same mat mass in a single layer. This efficiency comes mainly from the reduced pressure drop when using multiple layers [20]. There are other ways to affect the pressure drop across a filter; it has been demonstrated by Iman Azarian Borojeni et al. that incorporating a beaded fibre structure into a filter decreases pressure drop across the filter, similarly to a layered structure, when compared to uniform fibres of the same polymer composition.

#### *2.6.1.1 Inclusions*

Inclusions can be used in electrospun fibres to customize the fibres to excel further at their use. Inclusions such as silver, copper, zinc, etc. nanoparticles (NPs) can be mixed into the polymer solutions to enhance fibres anti-microbial properties [20].

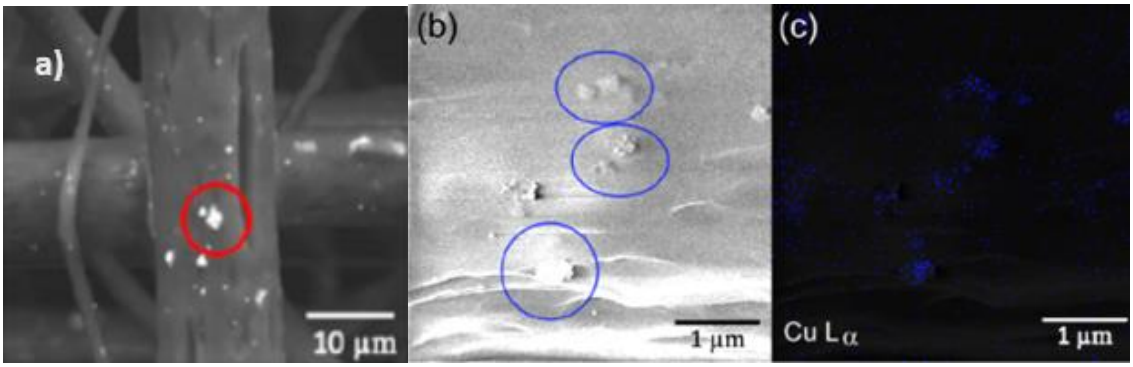


*Figure 2.10 a) SEM image of copper NPs embedded in an electrospun fibre, b) SEM image of the surface of a fibre with copper NP agglomerates, c) EDS map to show the copper locations in the fibre [60].*

#### *2.6.1.2 Nanoparticles*

Silver and copper nanoparticles and their compounds are renowned for their antibacterial and antiviral properties [61]. The antibacterial effect of silver, known since ancient times, is significantly enhanced when silver is in the nano-range. Silver nanoparticles can disrupt bacterial cell membranes and interfere with DNA and proteins, with their size and shape influencing their effectiveness. Truncated triangular silver nanoplates, for example, show higher antibacterial activity than other shapes [62]. Silver nanoparticles are also effective in viral disinfection, evidenced by their application in air filters. However, concerns about silver nanoparticle toxicity, including argyria and negative environmental impacts, have been raised [62, 63].

Copper, like silver, is effective against viruses and bacteria and can be integrated into micro/nanofibres [64, 65]. It disrupts protein structures in microorganisms and damages their cell membranes and DNA. While copper is essential for bodily functions, overexposure can lead to significant health issues, including copper toxicity affecting various organs [66].

Metal oxide nanoparticles like zinc oxide (ZnO) and titanium dioxide (TiO2) are essential antimicrobial agents. ZnO is effective against various bacteria and fungi and has low toxicity, making it suitable for various industries [67, 68]. Its antimicrobial action is attributed to generating reactive oxygen species that damage bacterial cell membranes. ZnO is also used in combating SARS-CoV-2, causing oxidative stress to the virus [69, 70].

However, the use of nanoparticles in this context is still under investigation, and their long-term effects are yet to be fully understood.

## *2.7 Mechanisms of Air Filtration*

In air filtration, there are five mechanisms by which particles are filtered from the air. These mechanisms are interception, inertial impaction, Brownian diffusion, electrostatic, and gravity effect. However, for very fine particles, the effect of gravity can be ignored for particles 500nm and smaller [57, 71].

### *2.7.1 Interception Mechanism*

Van der Waals attraction occurs between the particles passing through the filter and the filter fibres. If the particles are close enough to the fibres, they are attracted to and captured by them. This mechanism is usually adequate for 0.1 to 1 µm particles and is further enhanced by increasing the specific surface area of the fibres [72].

### *2.7.2 Inertial Impaction*

When airflow passes through the filter, streamlines are formed and influenced by the presence of fibres. Particles that are 0.3µm or more cannot adjust their direction as easily as smaller particles and will be intercepted by the fibres. Increasing airflow velocity and the packing density of the filter improves the effects of inertial impaction [57].

### *2.7.3 Brownian Diffusion*

Brownian diffusion randomly deviates the particle's motion due to its interaction with other tiny, fast-moving particles. Temperature and small particle size, less than 0.1 micrometre, further enhance this effect [73, 74].

### *2.7.4 Electrostatic Deposition Mechanism*

The interaction between the particle's charge and the charge of the filtration media is the driving force for this mechanism. If they have opposite charges, the particles are attracted to the filtration fibres and deposited on the surface of said fibres [75].

### *2.7.5 Gravity Effect Mechanism*

For large particles, specifically those with a diameter of 0.5 µm or greater, gravity will deviate the particle's path through the airstream and cause interactions between the particles and filtration media [57].

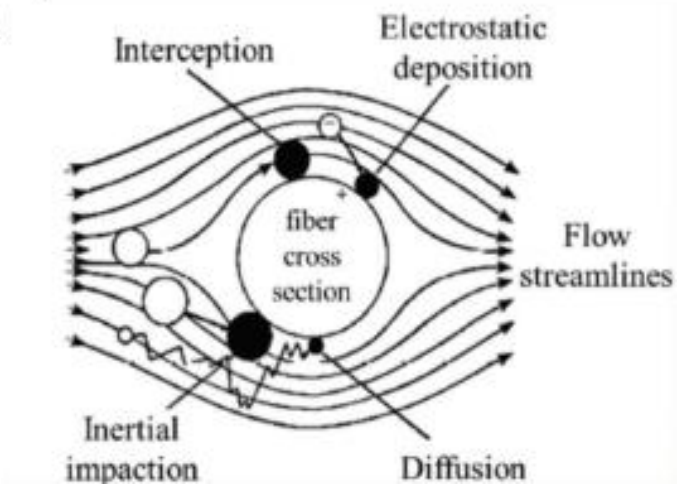


*Figure 2.11 Air filtration mechanisms for small particles [57].*

## *2.8 Coaxial Electrospun Fibres and their Applications*

Coaxial electrospun fibres are used in just as many industries as single-solution fibres. They offer the same benefits as single-solution fibres but with the added ability to better tailor them to a specific use. This tailoring can take the form of self-healing fibres, increased mechanical strength, increased thermal properties, better drug delivery, the creation of carbon nanotubes, etc. [76, 77, 78, 79].

Coaxial electrospun fibres, with their ability to spin previously non-spinnable materials through encapsulation or create hollow fibres, represent a significant innovation in the field. These fibres are utilized in a wider range of applications than single-solution fibres [80]. However, to successfully fabricate these fibres, the two solutions must be immiscible [81, 82]. If the solutions are miscible, they can create a single fibre of varying polymer concentrations or react with each other at the spinneret tip, leading to gelatinization or even solidification [83].

With their encapsulating properties, coaxial electrospun fibres find practical applications in various industries such as energy, biomedical, drug delivery, and textile [84]. The materials encapsulated in these fibres are not limited to polymers but extend to nanoparticles, macromolecules (proteins and drugs), and various structures like aerogels [7, 76] For instance, in lithium-ion batteries, using coaxial electrospun fibres containing nanoparticles of various metals, where the core polymer is dissolved in post-processing, provides a supportive outer shell that helps reduce metal degradation. During the lithiation process, as the nanoparticles increase in volume, the sheath provides good volume buffering capacity, with some studies suggesting reversible specific capacities after 400-500 cycles [7]. Furthermore, in multiple tests, the release of a drug was slowed down from 18 hours to 72 hours with coaxial fibres, making the fabricated fibres four times more effective at their application [85, 86]. These fibres can also be used for textile applications with excellent thermal management [84]. However, the fabrication process of a successful coaxial fibre with an aerogel-like internal structure can be complex.

### *2.9 Nanofibre Morphology*

Due to the parameters discussed earlier, the morphology of the fibre changes in many ways. Each polymer solution differs depending on these parameters, but there are trends and plenty of research on specific materials. Synthetic and natural polymers have been electrospun for various uses, and each does not necessarily benefit from uniform nanofibres. Some applications might benefit from beaded fibres, such as drug delivery or air/water filtration [87], and other applications benefit from electrospraying these polymers, such as food coatings [88].

It is essential to delve into a comprehensive review of the parameters that influence fibre morphology. This in-depth analysis will provide a richer understanding of the electrospinning process and its diverse applications.

### *2.10 Single Solution Fibre*

There is much more research on various polymers and the parameters that affect the morphology of single-solution fibres. Even though every polymer solution is different, there are general trends that most electrospinnable polymers follow, as seen in Figure 2.12.

| | *Effect on fiber morphology* |
|---|---|
| **Processing parameters** | |
| Applied voltage | Increasing applied voltage can result in<br>Increased beading[27–31]<br>Decreased fiber diameter[29,32–35] |
| Distance to collector | Increasing distance to collector can result in<br>Decreased fiber diameter[35,36]<br>Decreased fiber wetness[33,34] |
| Flow rate | Increasing flow rate can result in<br>Increased fiber wetness[37]<br>Increased bead formation[30,36–40] |
| **Solution parameters** | |
| Polymer molecular weight | Increasing molecular weight can result in decreased beading[29,41–43] |
| Polymer concentration | Increasing concentration can result in<br>Decreased beading[27–30,32–38,42–54]<br>Increased fiber diameter[28,31,38,41,42,45–48,51,53,55,56] |
| Solution conductivity | Increasing conductivity through the addition of salt can result in<br>Defect-free fibers[27,39,50,57]<br>Smaller diameter fibers[45,47] |
| Solvent dielectric constant | Increasing dielectric constant can result in decreased bead formation[40,49,58] |

*Figure 2.12 Electrospinning and solution parameters effect on fibre morphology [89].*

### *2.11 Processing Parameters*

The process parameters that affect fibre morphology are relative humidity, temperature, applied voltage, distance to the collector, and solution flow rate. Humidity affects almost all properties of the obtained fibres, including but not limited to crystallinity, mechanical properties, morphology, wetting properties, and fibre diameter [90]. One of the most notable changes RH affects is the smoothness of fibres. At lower RH values, fibres are often more wrinkled with little to no porosity; as the RH increases, the fibre smoothens, and eventually, pores start forming on the fibre [90]. However, with this porosity comes changes to other properties, such as mechanical strength. Bead-on string morphology can

be a result of a delay in solidification and jet undergoing thinning [91]. However, bead formation caused by RH needs to be taken individually for each polymer-solvent system as it was proven that the resulting morphology is dependent on the wetting properties of the polymer and solvent evaporation rate [92].

### *2.11.1 Humidity*

Furthermore, humidity also affects the fibre's diameter. Depending on the polymer and solvent combination, increasing the RH can retard the evaporation of the solvent from the fibre elongating the whipping stage, or the higher humidity can interact with the polymer and solvents, causing the polymer to precipitate and decreasing the time the fibre has in the whipping stage [93]. Vapour-induced phase separation (VIPS) is a standard method for creating porous membranes by introducing a nonsolvent vapor, water, into a polymer solution. This process involves the slow diffusion of the vapour into the solution, and pore formation can be controlled by reducing the polymer concentration and increasing pore formation with higher RH or lower polymer concentrations [94].

### *2.11.2 Temperature*

Regarding temperature, a balancing act is at play to predict the fibre morphology. Generally, the temperature affects the fibre diameter the most [95]. At lower temperatures, the evaporation rate of the solvent from the polymer solution decreases, leaving more time for the fibre ejected from the Taylor cone to whip and elongate; as the temperature increases, the fibre diameter increases as well. However, with some solutions, the fibre diameters again decrease after a specific temperature. This is due to the decrease in the viscoelastic forces of the solution. As mentioned previously, the stretching of electrospun fibres is opposed by viscous forces and surface tension; as the temperature increases, the solution viscosity decreases, and the polymer chains can move more quickly and be stretched at a much faster rate [96].

### *2.11.3 Applied Voltage*

Applied voltage has returned mixed results for its effect on fibre morphology. This is likely due to the polymer solution and how its parameters are affected by the applied voltage. Some research states that applied voltage increases fibre diameter [97, 98], others claim that higher voltages decrease fibre diameter [99], and others yield inconclusive results [100]. However, in all studies, the fibre diameters had more size variation, and the polymer draw from the spinneret tip increased as the applied voltage increased. A consensus is reached that increasing applied voltage decreases fibre diameters; however, in the few cases where the fibre diameter increases, it may be due to the properties of the solution. Noor et al. explain that their research used a polystyrene and DMF solution; during the stretching/whipping phase, the polymer jet becomes segmented early into the process. These segments do not undergo elongation after separation and land on the collection as thicker fibres. This phenomenon occurs at higher applied voltages due to the ejected fibres repelling each other after formation due to their charges [97].

### *2.11.4 Polymer Jets*

Polymer jets manifest modes or regimes depending on the testing parameters, with applied voltage being one of the significant affecting parameters. These regimes do not have official names, but some studies have named them as such: dripping, cone-jet, rotational, and multi-jet [101].

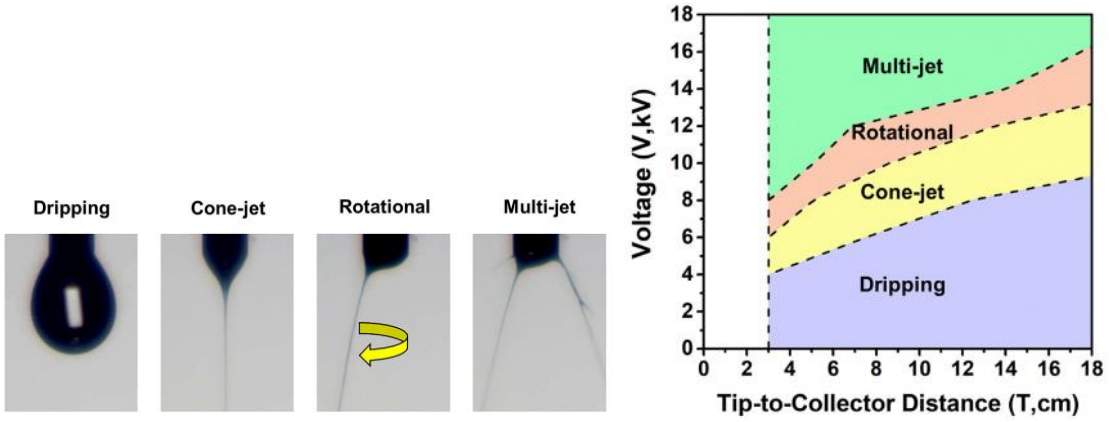


*Figure 2.13 (left) visual representation of the regimes in electrospinning, (right) Operating regime map of electrospinning regimes based on voltage and tip to collector distance [101].*

In the dripping regime, the electric field is not strong enough to overcome the viscoelastic forces, no jet forms, and the polymer solution drips off the spinnerette tip. The cone-jet regime is a stable regime where a single jet is expelled from the polymer solution at the apex of the droplet forming at the spinnerette tip. The rotational regime at higher applied voltages is a transitional regime between the cone-jet and multi-jet regimes. It is a non-steady jet that rotates around the edge of the spinnerette tip. Lastly, the multi-jet regime occurs at the highest voltages used for electrospinning. In this regime, multiple jets are ejected from the polymer solution, often propagating from the edges of the spinnerette. These regimes often deplete the polymer solution so quickly that the jet appears to begin on the edge of the spinnerette rather than from a solution droplet.

### *2.11.5 Tip-to-Collector-Distance*

The tip-to-collector distance has a straightforward effect on fibre morphology. The effects are essential since the tip-to-collector distance only influences when the ejected jet stream is away from a solid surface. If the tip-to-collector distance is too short, the jet does not have time to elongate thoroughly and dry, leaving the resultant morphology thick, wet, and heavily beaded fibres [102]. As the tip-to-collector distance grows, the resulting morphology is thinner, and the fibres are dry with fewer beads. Studies have demonstrated that the quality of the jet expelled from the solution droplet is affected by the applied voltage and the tip-to-collector distance [101]. As mentioned in the applied voltage section, the tip-to-collector distance also affects the electrospinning Taylor cone regimes. As the collector moves closer to the spinnerette tip, the electric field is affected, and it is possible to create a Taylor cone and eject solution in one of these regimes at lower voltages. However, fibres created this way are often subpar in shape and wetness. When deposited on the collector, wet fibres often crosslink and form a very different morphology compared to individual fibres. Typical tip-to-collector distances range from 10-20 cm. However, these distances can range from 3 cm to distances greater than 25 cm. It would also be wise to keep in mind that in horizontal setups, the effect of gravity can begin to affect fibre collection at distances of 10 cm or greater; these fibres can be poorly distributed on the collector, grouped at the bottom or even collected below the collector [103]. However, these setbacks have been overcome by utilizing a spinning collector that will more evenly

collect the fibres on the entirety of its surface at even greater distances. On top of overcoming these setbacks, a rotating drum collector allows the collection of aligned fibres, with the alignment being linked to the speed at which the collector rotates [104].

#### *2.11.6 Solution Flow Rate*

The solution flow rate is a crucial parameter of electrospinning. In many cases, the flow rate dictates the quality of the fibres. If the flow rate is too low, there will not be enough polymer solution at the spinnerette tip to make a solution droplet where a Taylor cone can form, leading to intermittent fibre creation, reducing both the continuousness of the fibres, the number of fibres produced within the set time, and a more comprehensive range of fibre diameters. The flow rate is not a constant parameter; it must be adjusted for each process. The parameter that affects the flow rate the most is the applied voltage. As the voltage increases, the electric field it creates can eject more of the polymer solution, meaning a more significant flow rate is needed. At lower flow rates, the only central point of note in fibre morphology is that the fibres have a larger diameter variation due to creating an unstable Taylor cone [105]. However, more deviations occur in the fibre morphology at higher than necessary flow rates. Large beads and more imperfections appear on fibres when a high flow rate is used. This is due to the excess of available solutions to be ejected. Along with deformed fibres, a large amount of solution can be electrosprayed during spinning. Increasing flow rate also caused wet fibres to be collected due to insufficient solvent evaporation, leading to branched, splitting fibres, blobs, and flattened web-like structures [105].

### *2.12 Solution Parameters*

The polymer solution, with its myriad of characteristics, presents a fascinating complexity that directly influences the fibre morphology. Even the slightest alteration to the solution, be it the choice of solvent, the polymer concentration, the polymer type, or the presence of additives, can significantly modify the solution properties and, consequently, the final fabricated fibre.

### *2.12.1 Polymer Concentration*

As mentioned, increasing polymer concentration and solution viscosity produces more uniform fibres and larger fibre diameters. This is due to the lower concentration polymers not having the viscoelastic forces to suppress droplet breakup entirely but not a small enough force to facilitate electrospraying [89]. Increased polymer molecular weight has a similar effect to the electrospun fibre. These two parameters are the same as the polymer solution. A higher polymer molecular weight means that the polymer that is being dissolved in the solution has a higher number of chain entanglements in the polymer solution at a lower concentration [106]. However, if there is a lower molecular weight polymer but at a higher concentration, the polymer solution chain entanglements also increase.

### *2.12.2 Solution Conductivity*

Solution conductivity is a parameter that can heavily influence fibre stretching [107]. A solution with high conductivity, enriched with electrical charges, facilitates the extension of the polymer jet when subjected to an electric field. This process contributes to the reduction in fibre diameter through elongation. The manipulation of solution conductivity by adding salts opens up new avenues for understanding and controlling the electrospinning process. Research by Angammana et al. [108] indicates that as the conductivity of the solution increases, the initial average jet current rises before slightly decreasing. Simultaneously, the average fibre diameter exhibits a power law relationship, decreasing with increasing solution conductivity. These trends can be explained by considering the surface charge distribution around the electrospun jet and variations in the tangential electric field on the fluid's surface. Polymer solutions with very low conductivity fail to electrospin due to insufficient surface charge. In contrast, highly conductive solutions do not form a Taylor cone due to a diminished tangential electric field. Increased conductivity can also lead to the formation of multijets and fibre protrusions from the fluid droplet.

### *2.12.3 Dielectric Constant*

The dielectric constant measures how well a solution can allow electric field lines to pass through it. It indicates how an applied electric field can polarize the solution. A high dielectric constant means the solution can be easily polarized, while a low dielectric constant resists polarization [109]. The dielectric constant depends on the solvent used to dissolve the polymer. Wu et al. (2018) [110] found that the number of jets ejecting from the droplet increases as the dielectric constant increases. However, when the dielectric constant is lowered to single digits, no matter how high the applied voltage rises, only stable single jets are formed [110].

## *2.13 Coaxial Fibre Morphology*

Understanding how solution and electrospinning parameters influence single-solution fibre morphology is complex. It is reasonable to assume that some of these effects transfer onto coaxial spun fibres. However, since the core solution is not exposed to ambient conditions, it would likely not be affected by parameters such as humidity and ambient temperature in terms of solvent evaporation. Solvent volatility will also likely be less prominent for the core solution. This complexity underscores the crucial need for our research on solution miscibility in coaxial electrospinning, which will significantly contribute to the field.

### *2.13.1 Solution Miscibility*

However, the effect of solution miscibility and the resulting solution mixing on the morphology of co-electrospun products remains largely unexplored. Our research, therefore, aims to fill this gap and provide a comprehensive understanding of this crucial aspect of coaxial electrospinning. It has been widely proven that a highly electrospinnable shell solution can carry out the non-electrospinnable core polymer solution or even non-polymeric liquid to form core-shell nanofibres. This means that the effect of the core fluid is modest [111].

Solution miscibility is the only aspect of coaxial electrospinning that can not be represented or extrapolated by studying single-solution fibre fabrication. Since the two solutions used in coaxial electrospinning can range from fully miscible to not at all miscible, there is expected to be some degree of fibre morphology effect from the interaction between the

solutions. Only some studies focus on the miscibility of polymer solutions for coaxial electrospinning, and of the few that exist, there are various approaches to acquiring results. Some research has suggested that similar or even identical solutions can successfully create a core/shell structure [112, 113]. One study says this is because the electrospinning process is much faster than the boundary diffusion between the two solutions (~1ms and 0.01-1s, respectively). It has also been stated that a highly electrospinnable shell solution facilitates the creation of a core/shell fibre structure. This is demonstrated in studies that show that either a solvent or solvent-rich air flow is used as a core "solution" to create core/shell fibres [114, 115]. Yan et al. compared multiple solutions, those created from cellulose acetate (CA), that were highly miscible with each other; however, the solution labeled CA-A (cellulose acetate and Acetone) was electrospinnable.

In contrast, the solution labelled CA-D (cellulose acetate and DMAc) could only be electrosprayed. A combination of the two solutions labelled CA-AD (cellulose acetate with different ratios of Acetone and DMAc), which can be electrospun, and the last solution made from Poly (lactic-co-glycolic acid) (PGLA) with the solvents being dimethylacetamide (DMAc) and Acetone, that has low miscibility with the CA solutions [111]. If two solutions yield similar single-solution fibre results, the coaxial fibre can be expected to keep the same or similar morphology. However, the differences showed when an electrospinnable shell and electrosprayable core were tested together. For the highly miscible CA-A and CA-AD21 (2:1 ratio of Acetone to DMAc), Yan et al. adjusted the flow rate to show the difference in morphology between the fibres. It was found that when adjusting the ratios of the spinnable shell and sprayable core, the solution with the larger flow rate had a larger impact on the final morphology. As the core:shell ratios changed from 1:6 to 1:1, the resultant fibres became thinner, and beads appeared, eventually turning into spheroids. Electrospray resulted when the core solution overtook the shell solution at a flow rate ratio of 1:0.2 only.

In order to see whether or not these solutions were mixed during electrospinning, silver nanoparticles (Ag-NPs) were mixed into the core solution. Using TEM and fluorescent microscopy were used to analyze the resulting fibres. The fluorescent microscopy showed that both solutions are continuous throughout the fibres. However, Ag-NPs were found to

have sections of different behaviours. In some sections, Ag-NPs were found only in the center of the fibre, showing little to no solution mixing. However, Ag-NPs were also found randomly scattered in other sections of the fibres and accumulated in the marginal area or near the outside edge. This means that fibres fabricated from miscible solutions can mix at random intervals, and the morphology is not constant throughout the fibre. When electrospinning the PGLA as the core and CA-AD21 as the shell, the same conclusion was reached regarding the flow rate ratios and final fibre morphology. The solution with the higher flow rate controls the shape of the fibre. The fibres were uniform fibres when the shell had a higher flow rate, and when flow rates were equivalent, beads-on-a-string fibres were created. Switching the miscible solutions to make the electrosprayable solution as the shell and the electrospinnable solution as the core, previous studies have shown that this configuration has worked in creating a core/shell fibre by using the electrospinnability of the core to carry the shell solution to form the fibre [116]. However, when the core solution had a higher flow rate, the electrosprayable shell solution was pulled along to make a fibre morphology, but the shell was cracked and not continuous.

### *2.13.2 Solution Viscosity*

Since the typical setup for a coaxial fibre has a higher flow rate for the shell over the core, the shell solution viscosity is much more important than the core. The shell solution tends to drive the inner liquid into fibre formation. The shell solution viscosity needs to be high enough to overcome the surface tension between the two solutions, allowing the formation of a compound Taylor cone [117]. In this case, the viscosity is critical in the way that the shell solution itself should be able to be electrospun. In this case, the viscosity and electrospinnability of the core solution are not critical or necessary for the formation of core/shell fibres [118]. However, as was mentioned in the miscibility section, an electrospinnable core can also carry the shell to form the core/shell fibre, in which case the requirements of the shell formula mentioned would be applied to the core solution.

The research conducted by Masha et al. (2020) provides valuable insights into the relationship between viscosity and core/shell fibre diameter. Their results suggest that as the core or shell solution viscosity increases, the core/shell fibre diameter also increases

[119]. The study also reveals that as the ratio of viscosities of the core:shell solution increases, the likelihood of forming a core/shell structure decreases. For instance, when the polystyrene (PS) shell solution was set to a constant 20 wt% and the (PVP) poly(vinyl pyrrolidone) solution was mixed at three concentrations (5 wt%, 20 wt%, and 35 wt%), a core/shell structure was formed at core concentrations of 5 wt% and 20 wt%. However, at a core concentration of 35 wt%, the fibre could not be classified as a core/shell structure. At best, a very thin layer of the PS solution was coating the PVP fibre. This lack of a core/shell structure for the 35 wt% PVP core solution was attributed to the relationship between the volatilization of the shell solution and the diffusion speed of the solvent of the core solution as it travelled outwards through the shell solution [119].

#### *2.13.3 Solution Flow Rate*

As mentioned earlier, the solution flow rate plays a role in determining the shape of the fibre. However, increasing the shell solution flow rate increased the diameter of the fabricated core/shell fibre. In this study, when the core and shell solutions were spun as single solution fibres, the shell solution yielded larger fibres, measuring up to 700 nm. In contrast, the core solution did not show the same diameter increase, with the largest fibres measuring 400 nm [120]. This suggests that the solution flow rate, particularly of the shell solution, can significantly influence the core/shell fibre size.

### *2.14 Preceding Research (Face Masks)*

The figure below shows that the 2:3 DMF: Acetone ratio creates uniform fibres with a large fibre diameter distribution. The 1:1 ratio also shows uniform fibres but with a more narrow fibre diameter distribution. As the DMF:Acetone ratio increases, more beads appear in the fibres, and the fibre diameters reduce accordingly.

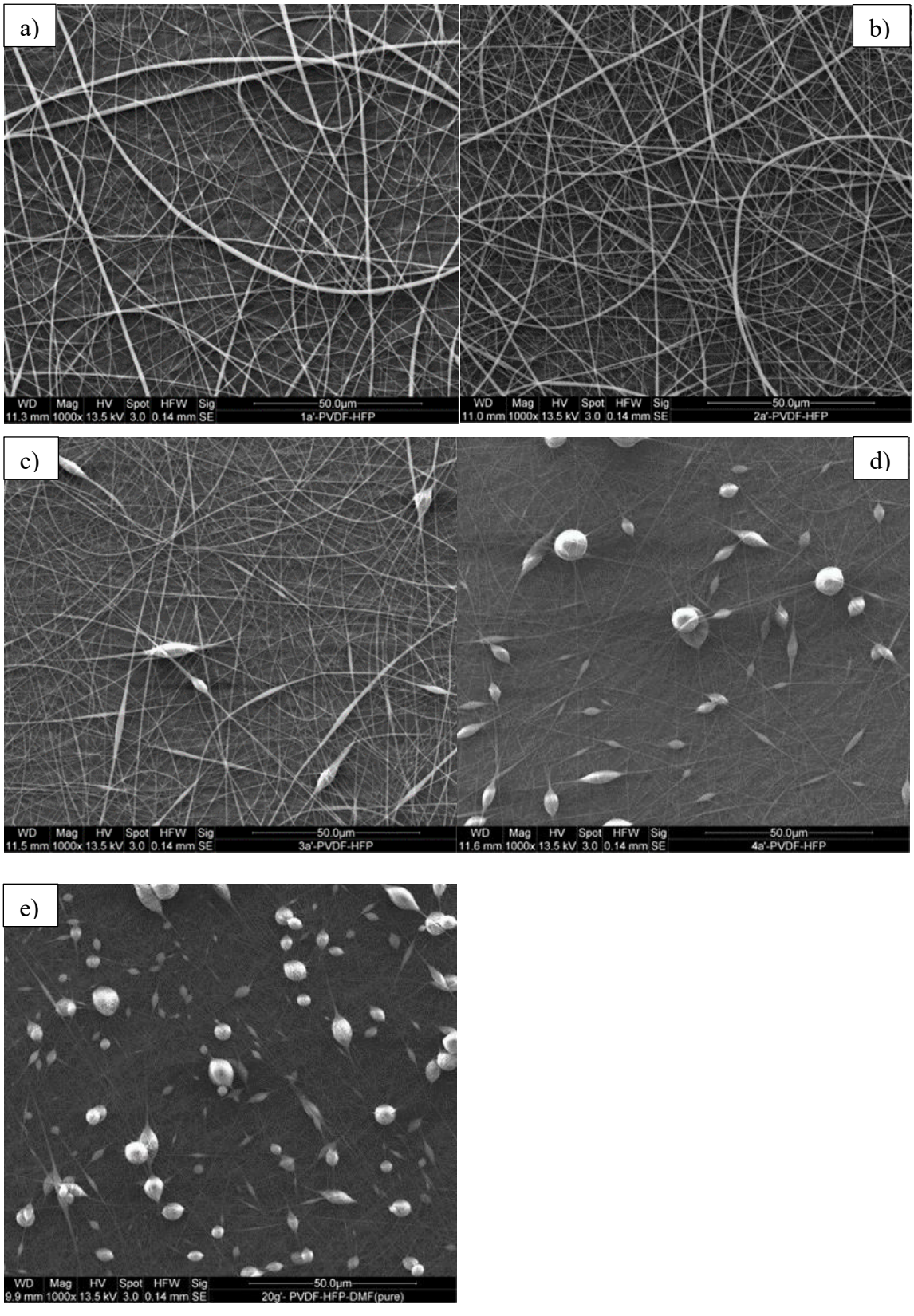


*Figure 2.14 All solutions are 20 wt% PVDF-HFP with a) 2:3 DMF: Acetone ratio, b) 1:1 DMF:Acetone ratio, c) 3:2 DMF:Acetone ratio, d) 4:1 DMF:Acetone ratio, and e) 1:0 DMF:Acetone ratio [20]*

The fibre diameter distribution was calculated, and it was found that the fibre diameter distribution had more variance with higher Acetone content. As expected, the fibre diameters also decreased with the volume of Acetone in the solution; this was due to the development of beads in the fibres.

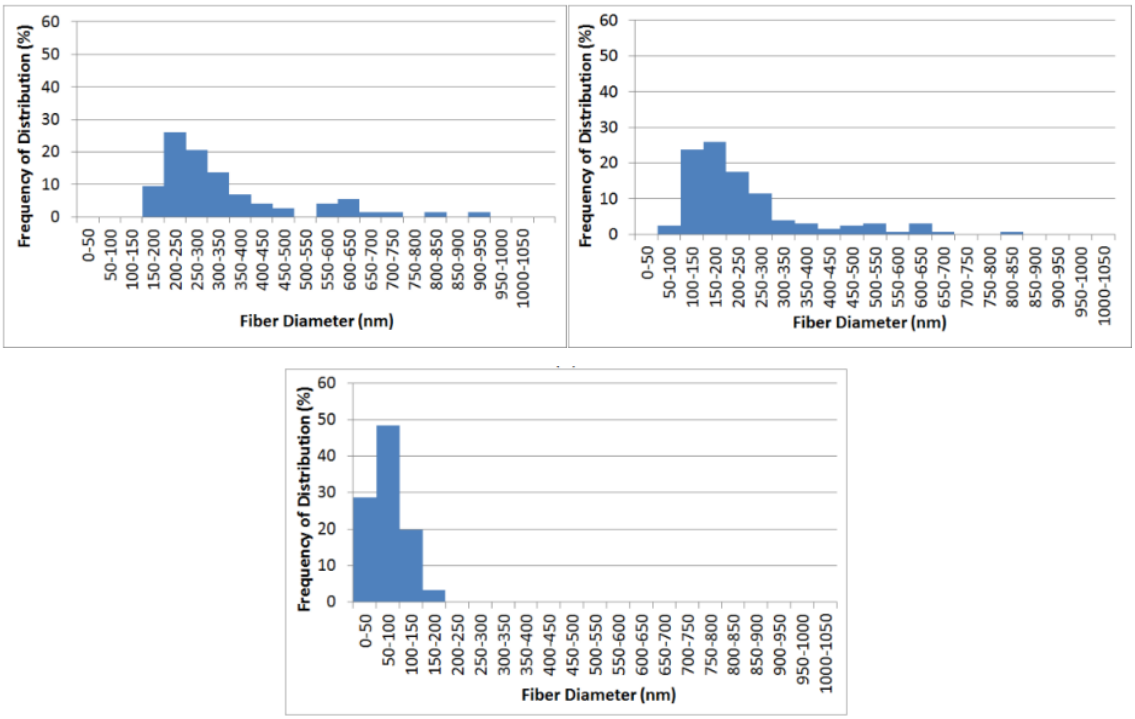


*Figure 2.15 Fibre diameter size distribution based on DMF:Acetone solvent ratio top left: 2:3, top right: 3:2, bottom center: 1:0 [20]*

These fibre mats were tested for filtration capabilities and pressure drop to see which nonwoven mats were ideal for continued testing—first, the 3:2 and 4:1 DMF:Acetone ratio solutions were tested. The uniform fibres were not tested as the needle clogged less than 15 minutes into the process, not allowing enough fibres to accumulate on the PP spunbond layer to test for filtration capabilities. The beaded fibres displayed good filtration capabilities, and the pressure drop decreased as the number of beads in the microstructure increased. This was interesting as most research dismisses beaded fibres and focuses on uniform fibres. On top of the two samples, which will be referred to as PLB for the low beaded structure, the 3:2 DMF:Acetone ratio, PHB for the high beaded structure, the 4:1 DMF:Acetone ratio, and PUB for the ultra-high beaded structure, or the pure DMF solution. The samples that were sent had two forms of macrostructure. First, both PLB and PHB fibrous mats were prepared as a single mat that was spun for 39 minutes between

layers of the PP spunbond that it was collected on, and one sample of the PLB microstructure was prepared in three layers of fibrous mats that were spun for 13 minutes each, for a total of 39 minutes. The macrostructure of the latter is as follows: PP-PLB-PP-PLB-PP-PLB-PP (Figure 2.16) to see what effect this layer will have on the filtration efficiency.

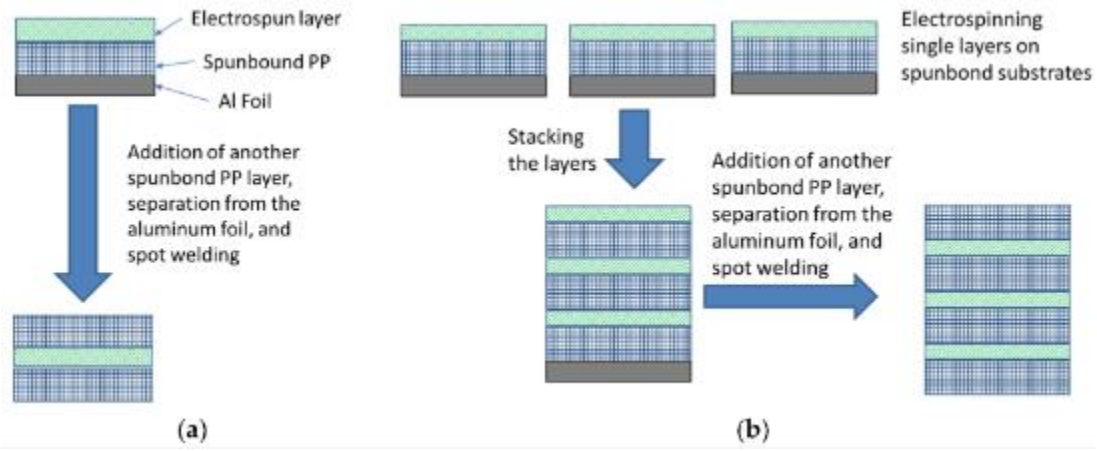


*Figure 2.16 macrostructure of the filtration assemblies (a) single-layer and (b) multi-layer filters*

As seen in Table 2.1, the multilayered sample had a similar efficiency with a slightly lower pressure drop. This shows that the microstructure is more important to the final quality factor rather than the layered structure of the fibrous mats.

*Table 2.1 The filtering parameters (pressure drop, initial filtration efficiency, efficiency at Most Penetrating Particle Size, and quality factor) of PLB-13-3L, PLB-39, PHB-39, the Spunbond layer(P0), and an N95 mask. [20]*

| Sample | Pressure Drop (Pa) | Initial Filtration Efficiency (%) | Efficiency at MPPS (%) | Quality Factor (Pa^-1) |
|---|---|---|---|---|
| PLB-13-3L | 117.3 | 96.54 | 95.17 | 28.7*10^-3 |
| PLB-39 | 148.6 | 79.56 | 76.5 | 10.7*10^-3 |
| PHB-39 | 40 | 77.37 | 73.86 | 37.1*10^-3 |
| P0 | 8 | 12.97 | 7.26 | 17.4*10^-3 |
| N95 | 159 | 97.74 | 96.28 | 23.9*10^-3 |

The N95 masks are the primary masks used as PPE, and although they have a filtration efficiency of at least 95%, these filtration efficiencies are not up to par. The most direct way to increase filtration efficiency is to increase the number of fibres per fibrous mat.

Mats were fabricated at 90 minutes for the PLB, 90 and 150 minutes for the PUB, and 90, 120, and 150 minutes for the PHB. Since there exists an inverse relationship between the pressure drop and the number of beads in the fibrous mat, the PLB was expected to underperform when comparing it to the PHB and PUB for the 90-minute samples but was tested to prove this theory. Beyond that, the PHB and PUB samples were the main points of interest. Table 2.2 shows that the theory for PLB was correct through comparing the pressure drop. With PHB-120 outperforming the PLB-39 (Table 2.1) in pressure drop the beads are shown to have a significant impact, and pressure drop is heavily represented in the quality factor calculations. There is a point where the PHB fibres outperform the PUB.

*Table 2.2 The filtering parameters (pressure drop, initial filtration efficiency, efficiency at Most Penetrating Particle Size, and quality factor) of N95 PUB-90/150, PHB-120/150air filters. [20]*

| Sample | Pressure Drop (Pa) | Initial Filtration Efficiency (%) | Efficiency at MPPS (%) | Quality Factor (Pa^-1) |
|---|---|---|---|---|
| N95 | 117.3 | 96.54 | 95.17 | 28.7*10^-3 |
| PUB-90 | 169.3 | 99.32 | 98.91 | 29.5*10^-3 |
| PUB-150 | 192 | 97.56 | 95.87 | 19.3*10^-3 |
| PHB-120 | 146.6 | 98.25 | 97.47 | 27.6*10^-3 |
| PHB-150 | 206.6 | 99.61 | 99.36 | 26.9*10^-3 |

As seen above, the PUB-90 has the highest quality factor, exceeding that of the N95 mask. The three beaded solutions were also tested for hydrophobicity using a contact angle.

Figure 2.17 shows the results from the water contact angle test.

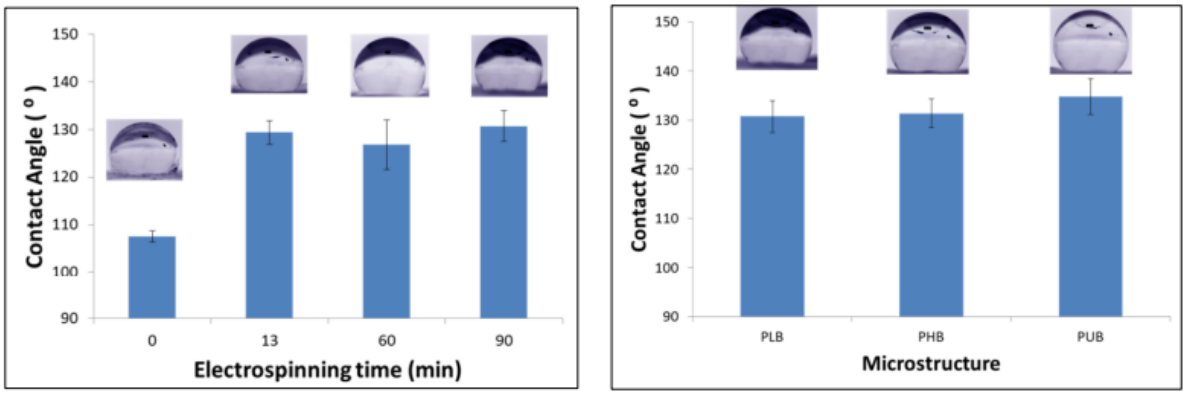


*Figure 2.17 (left) effect of electrospinning time of PLB fibres on contact angle (0 means only the PP spunbond layer) and (right) effect of microstructure on contact angle (90 minutes electrospinning time) [20]*

Figure 2.17 shows a drastic change in contact angle even at minimal fibre fabrication and minimal change from the 13-minute fibrous mat to the 90-minute fibrous mat with all three tests resting near 130 degrees. The microstructure's bead density does affect the fibrous mat's hydrophobicity, but the effect is less than 10%.

One final test was done to test repeatability, and a double N95 mask was used for comparisons in extreme situations where these masks are recommended to be doubled up. Because the PHB-90-minute mask has the lowest pressure drop, a PHB-150 non-woven mat was fabricated to try to increase the filtration efficiency to compete with the N95 while having the best-case scenario for a low-pressure drop. As shown in Table 2.3, the N95 mask still has the best quality factor of all tests.

*Table 2.3 Filtration tests for PLB, PHB, PUB filters fabricated for 90 minutes, and a PHB filter fabricated for 150 minutes, compared to the medical standard N95 mask as well as two N95 masks layered on top of each other. [20]*

| Sample | Pressure Drop (Pa) | Initial Filtration Efficiency (%) | Efficiency at MPPS (%) | Quality Factor (Pa^-1) |
|---|---|---|---|---|
| N95 | 117.3 | 96.54 | 95.17 | 28.7*10^-3 |
| 2*N95 | 388 | 99.86 | 99.65 | 16.9*10^-3 |
| PHB-90 | 110.7 | 92.26 | 90.5 | 21.3*10^-3 |
| PLB-90 | 170.6 | 94.21 | 92.5 | 15.2*10^-3 |
| PUB-90 | 169.3 | 99.33 | 98.91 | 27.6*10^-3 |
| PHB-150 | 206.6 | 99.61 | 99.36 | 26.9*10^-3 |

However, the PUB-90 and PHB-150 both have a similar quality factor while achieving similar filtration efficiencies to the double-layered N95 mask. They also have a 57% and 47% decrease in pressure drop across the filter compared to the 2XN95.

During the electrospinning process for the solutions with 2:3 and 1:1 DMF:Acetone, the spinneret clogged after 10-15 minutes. This is likely due to the evaporation rate of Acetone, as when the ratio of DMF:Acetone increased, the clogging stopped. With a boiling point of 56 degrees Celsius, room temperature facilitates a much faster evaporation rate than DMF, which has a boiling point of 153 degrees Celsius. Other reasons for the needle clogging are the humidity, spinnerette size, or feed rate. The humidity would affect the clogging of the spinnerette tip because of the solution's interaction with the water in the atmosphere. When the solution meets water, the PVDF-HFP molecules polymerize into long chains, forming solids [121]. The feed rate and spinnerette size also influence the volume of the solution exposed to the atmosphere. With a low feed rate or a tiny spinnerette opening, tiny amounts of solution are exposed to the ambient parameters. With smaller amounts of the solution exposed, a low amount of Acetone must evaporate to force the solution to be unbalanced, as the solubility of PVDF-HFP in Acetone and DMF is limited to approximately 25% at the higher end [122]. Since these solutions were mixed at a 20% PVDF-HFP concentration, they will begin to solidify if too much Acetone evaporates from the solution.

The formation of beads on the fibres was not ideal as most research shows beads as undesired; however, with the formation of fibres, the non-woven mats for the 3:2 and 4:1 DMF:Acetone ratios were chosen to test the filtration efficiency and pressure drop. It was surprising to see that the beads caused a minimal drop in filtration efficiency, ~2.5%, but a vast improvement in the pressure drop across the filter, ~73%, when compared to the layered filter, ~22.6%, which has been a proven form of reducing pressure drop without negatively impacting the efficiency of the filter [123, 124]. This is due to the larger beads in the PHB fibres reducing the packing density throughout the filter. As beads appeared in the fibres the fibre diameters shrunk noticeably. This change in fibre diameter and bead content allows air to pass through more efficiently, reducing the size of the fibre while increasing the bead size more effectively separated the fibres, making it easier for the air

to pass through, but the same surface area is taken up for filtration. At the same time, in the multilayered sample, the PP spunbond layers could only reduce the packing density at the interface between the layers of the PLB fibres. In some studies, the beads have been studied for their use in reducing the pressure drop, as layering and beaded fibres have been proven to reduce the filter's packing density [125, 126]. However, a consensus has yet to be reached regarding which method is more effective. In this situation, the beaded fibres have a higher impact on the final breathability of the filter. Although the filtration efficiency decreased slightly because of the significant improvement of the pressure drop, the quality factor increased from $10.7*10^{-3}$ $Pa^{-1}$ (PLB-39) up to $37.1*10^{-3}$ $Pa^{-1}$ (PHB-39).

# CHAPTER 3 – Materials and Methods

### *3.1 Materials and Methods*

Polyacrylonitrile (PAN) (Mw = 150,000) and Poly(vinylidene fluoride-co-hexa-fluoropropylene) (PVDF-HFP), (Mw= ~455,000, average Mn= ~110,000 pellets) were both acquired from Sigma Aldrich. N, N-Dimethylformamide, 99.8% (DMF) was acquired from Sigma-Aldrich, and Acetone was sourced from the University of Windsor labs.

### *3.2 Sample Preparation*

Polymer solutions were prepared under ambient conditions using magnetic stirring. All solutions were mixed based on weight percentage and stirred for 24 hours before use in the electrospinning process.

### *3.3 Preliminary Solutions*

The following experiments were done with a chitosan, polyethylene oxide, and Triton x-100, dissolved in an acetic acid and water solution. The composition of the solution was 4% wt. Chitosan and polyethylene oxide, 1% wt. Triton x-100, and 95% wt. were the acetic acid and water solvent. The only variable in the tests was the solvent. Eight solutions were made with 0.5%, 1%, 2.5%, 5%, 10%, 20%, 50%, and 90% acetic acid solution. The concentration of acetic acid was changed to see how it affected the spinnability of the chitosan solution.

PAN solutions were prepared using 8 wt% and 10 wt% PAN and 92 wt% and 90 wt % DMF, respectively. PVDF-HFP solutions were prepared using 20 wt% PVDF-HFP. The solvents used were Dimethylformamide (DMF, 99.8%) and Acetone, at the following ratios of DMF:Acetone: 2:3, 1:1, 3:2, 4:1, and 1:0. Of these solutions, the ones that were able to fabricate the most uniform fibres were chosen for coaxial testing.

### *3.3.1 Core Solution*

The chosen core solution was the 10 wt% PAN dissolved in a pure DMF solution.

### *3.3.2 Shell Solutions*

The PVDF-HFP solution that created the most uniform fibres and was used in the coaxial fibre fabrication was the solution where the solvent ratio of DMF: Acetone was 1:1. Solutions used in the preliminary single solution tests have the ratios 2:3, 3:2, and 4:1. Multiple polymer concentrations were needed for the tests so four solutions were tested. These solutions comprised 15 wt%, 17.5 wt%, 20 wt%, 22.5 wt%, and 25 wt%. Solutions were placed on the magnetic stirrers for 24 hours before use to ensure full homogenization of polymers and solvents. Under these conditions, the first three concentrations, 15%, 17.5%, and 20%, were the solutions used for coaxial fibre fabrication, and the 20 wt% was used for face mask filtration, as the 22.5 wt% and 25 wt% PVDF-HFP solution were not consistently fully dissolved after 24 hours and was removed from the testing parameters.

## *3.4 Electrospinning*

A plexiglass enclosure was set up to isolate the electrospinning experiments from outside variables. The homogenous solutions were loaded into 12 mL plastic syringes. The syringes were connected to a coaxial spinneret via a Polytetrafluoroethylene (PTFE) tube and pressure fittings. The syringes were mounted on separate syringe pumps (NE-1002X from New Era Pump Systems Inc.) during the electrospinning process to control each solution flow rate independently of the other (From 10 - 75 microlitres/minute). For consistency and to help ensure the coaxial structure of the fibres, the shell solution was fed through the tubing and spinnerette first to create a droplet at the tip of the spinnerette. After the droplet has formed, the core solution is fed through its tubing to ensure a complex droplet is formed at the spinnerette tip. The coaxial needle was passed through a fixture in a horizontal orientation and connected to a power supply (Gamma High Voltage Research, ES50P) to charge the solutions by applying 15 kV, 20 kV, or 25 kV, depending on testing requirements. For the single solution set up the same basic set up was used as the coaxial fibres but a single spinnerette was used and voltages up to 35 kV were applied. For the dual

spun mats, two separate spinnerettes were set up to be collected on the same drum using the same electric field.

An aluminum drum (D=100 mm) rotated at 100-150 rpm was used to collect the non-woven fibre mats. For the coaxial fibres research, the drum was wrapped with a 14 x 30.5 cm sheet of either aluminum foil and a glass slide for optical microscopy, secured using plastic tape, and used as the collector, for the single solution tests for the high-efficiency mask research, a polypropylene (PP) spunbond layer was secured on top of the aluminum sheet to collect the fibres. The drum rotated between 100 and 150 rpm, within the range necessary to not force aligned fibres. The working distance for all experiments was 200 mm. Sensors were used to monitor the temperature and humidity inside the enclosure. The humidity was controlled by the sensor and a line of compressed air that would be turned on and off to keep the relative humidity at 30% +/- 2% during experimentation for coaxial fibres and 35% +/- 2% for the high-efficiency masks single solution fibres. All tests were run between 22 and 24 degrees Celsius. Tests for the mats were run at various timestamps for the filtration fibres, for coaxial fibres the tests were run for 30 minutes to allow for enough fibre fabrication to create samples for scanning electron microscopy (SEM). The shell concentration applied voltage, and feed rate ratio of core:shell (2:3, 1:2, and 1:3) were the only adjusted parameters throughout the coaxial tests.

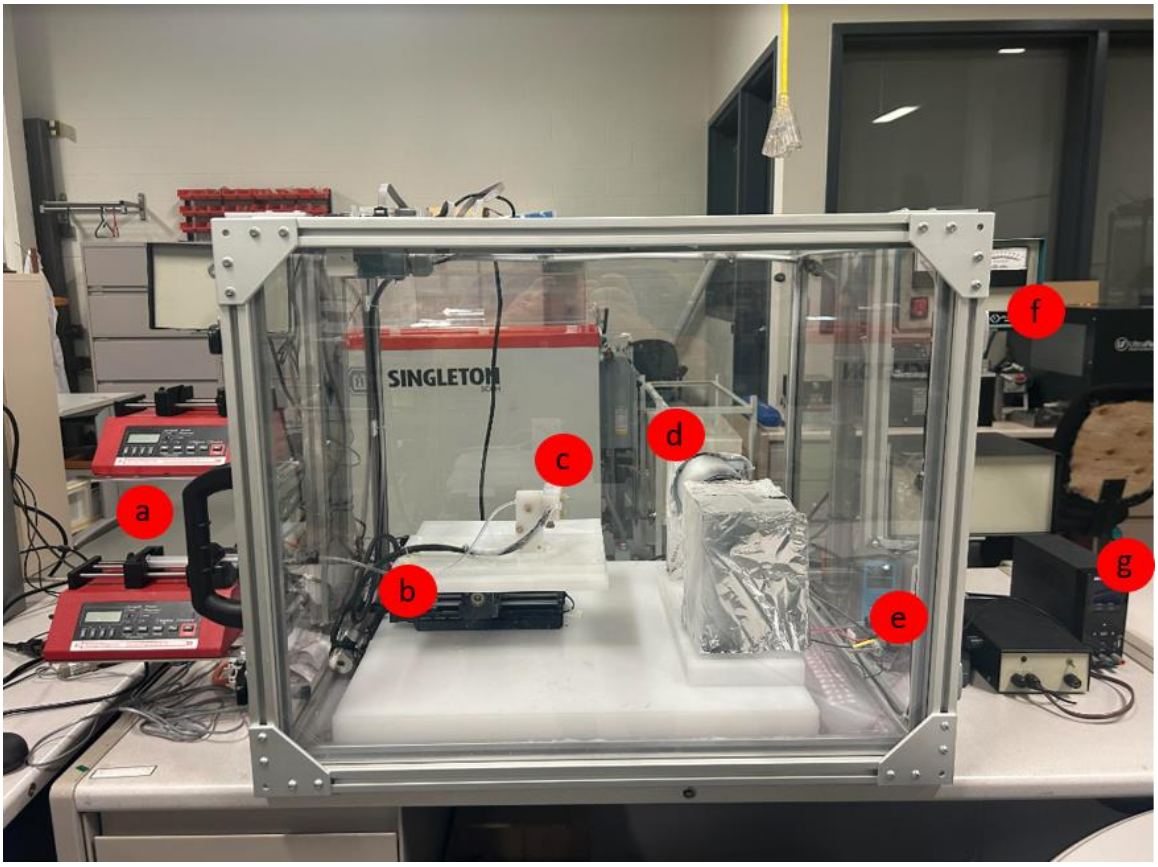


*Figure 3.1 The electrospinning set up (a)syringe pumps, (b)PTFE tubing, (c) spinneret insert, (d) collector, (e) humidity and temperature readings to ensure proper conditions, (f) voltage control, (g) collector rotation speed controller.*

### *3.5 Sample Preparation for Filtration Fibres*

The samples were prepared for the single solution PVDF-HFP and Chitosan fibres for air filtration by placing a second layer of PP spunbond fibres on top of the fabricated fibres. These layers were bonded using hot spot welding exceeding the melting point of the PP spunbond layer, the PVDF-HFP, and Chitosan fabricated fibres (160, 140, and 102.5 degrees Celsius, respectively). For the layered samples, the overall test time of all the fabricated layers was equivalent to the full test time of the single layer samples they were compared to. The stacking consisted of alternating the PP spunbond layers and the fabricated PVDF-HFP, sandwiching the Chitosan fibres, or dual spinning PVDF-HFP and Chitosan fibres into one non-woven mat, then topping it with a PP spunbond layer before hot spot welding the layers together. For the optical microscopy images, a glass plate is attached to the collector and the fibres are collected at the same time as the fibres used for

the filter. As the electrospinning process is underway the fibres collect the most densely in the middle of the collector. For both the filtration tests and microscopy the fibres used are from the center of the nonwoven mat fabricated.

### *3.6 Sample Preparation for Coaxial Fibres*

For optical microscopy, the samples used were prepared in the same way as for the filtration fibre optical microscopy, from the center, or most fibre dense area, of the glass slide. Samples for the SEM were taken from the center of the aluminum foil sheet that the fibres were collected on.

Samples were prepared for the SEM using a two-part epoxy to coat fibre samples retrieved from the fibres deposited on the aluminum sheets. The two-part epoxy was mixed according to the instructions on the bottle. A 1:1 ratio by weight was prepared and mixed for the time instructed. A thin layer of the mixed two-part epoxy was laid down onto a non-stick surface. The fibre samples were pressed onto the epoxy, ensuring no air pockets were created, and then covered with another thin layer of epoxy. These samples were pressed with wax paper to create a thinner sample. The samples were left for 24 hours to cure fully, according to the manufacturer. The samples were then collected and labelled accordingly. Two methods were used to break the samples into small enough pieces for use with the SEM. Due to the glass transition temperature of the PAN being 95 degrees Celsius and PVDF-HFP being -35 degrees Celsius, the first set of samples was cooled with liquid nitrogen and then swiftly broken over a sharp edge to ensure a clean edge to view the cross-section of the coaxial fibres. The subsequent samples were prepared much in the same way; however, instead of cooling in liquid nitrogen, freezing the samples in a chest freezer to approximately -5 degrees Celsius was found to be sufficient, with the glass transition temperature of the two-part epoxy being 50 degrees Celsius. Both methods allowed for the cross-section viewing of the coaxial fibres. The chosen samples were then mounted onto their respective platforms and gold coated using a 3 Target Plasma Sputtering Coater from MTI corporation (Type: GSL1000X-SPC16-3) and stored in a desiccator.

### *3.7 Characterization*

Fibres were characterized using the following methods. Optical microscopy for fibre uniformity and diameter sizes, SEM for cross-sectional imagery and changes to core/shell morphology, and the filtration samples were sent to Delhaouse University to undergo pressure drop and filtration efficiency testing.

### *3.8 Optical Microscopy*

An optical microscope was used to visualize the fibres along their lengths. Their size, uniformity, and interaction with one another were observed at magnifications of 100x, 400x, and 1000x.

### *3.9 Scanning Electron Microscopy (SEM)*

The scanning electron microscope was used to obtain cross-sectional images of the fibres. These images were used to identify the ratio of core:shell fibre morphology and any other phenomena that occurred and were not apparent through optical microscopy. A current of 12-14 kV was used to generate high-definition images without damaging the samples.

### *3.10 Image Processing (Image J)*

Image J was used for fibre measurements and analysis. The scale bars for both the optical microscopy and SEM images were first measured in pixels to calibrate the length/pixel for each respective image. Twenty fibres were randomly selected from each optical microscopy image at the same magnification and measured by drawing a line perpendicularly to its axis. For the SEM images, the fibres are measured in two ways. Firstly, if the software cannot isolate the cross-sectional fibre area and the fibre is circular, they will be measured across the diameter of the fibre; these diameters will then be converted to their respective areas, assuming a circular cross-section, to compare. In the case where the shape of the fibre is irregular, or the software can isolate the cross-sectional areas, the overall area of the fibre will be calculated, followed by either the core or shell cross-sectional area, and they will be subtracted from one another to find the percentage of the core and shell.

### *3.11 Filtration and Pressure Drop Testing*

The evaluation of filtering performance and pressure drop for the produced air filters was performed at Dalhousie University's Department of Physics and Atmospheric Science. The filters were secured using a stainless steel holder (Pall 1209) that exposed a 25 mm diameter circular section to the NaCl aerosol stream. A NaCl aerosol flow was created, neutralized, and directed through the filter at a rate of 2.2 litres per minute. Filtering efficiency was assessed by sampling the aerosol upstream and downstream of the filter. These samples were analyzed using a Scanning Mobility Particle Size (SMPS) Spectrometer, which includes a Condensation Particle Counter (TSI-3772) and an Electrostatic Classifier (TSI-3082), to determine the size distribution of the NaCl particles. The range of particle sizes measured from 20 to 450 nm was used to evaluate the filtering capabilities of the samples. The filtering efficiency for specific particle sizes ($\eta s$) was calculated using the following formula:

$$\eta_s=((c_u-c_d)/c_u)\times 100\% \quad (3.1)$$

where $c_u$ and $c_d$ represent the concentrations of NaCl particles of specific sizes in the upstream and downstream flows, respectively.

To determine the overall efficiency, the concentration measurements for all particle sizes were aggregated to calculate the total particle concentration within the 20–450 nm range for both upstream and downstream flows. The overall efficiency, denoted as $\eta$, was then derived using the equation below:

$$\eta=((N_u-N_d)/N_u)\times 100\% \quad (3.2)$$

where $N_u$ and $N_d$ refer to the total particle concentrations in the 20–450 nm range in the upstream and downstream flows, respectively. The pressure drop ($\Delta P$) across the upstream and downstream flows was determined using a differential manometer (Model 223BD-AAU; MKS). The quality factor formula in the section “2.6.1 Air Filtration Materials and Inclusions” is then used to find the quality factor.

# CHAPTER 4 – Results and Discussions

### *4.1 Filtration Results*

The ideal result for electrospinning in this study is to create an unwoven net with uniform fibres. Uniform fibres are continuous fibres with little to no beading and a small variation in diameter. Another factor that is looked at is the resulting electrospray from the tests. Electrospray can cause issues by changing the uniformity of the fibres. Small drops of the solution are sprayed onto the collector and will bond with the nanofibre net that is being spun. Electrospray tends to occur when the bonds between the strands of polymers cannot adequately elongate due to a mismatch between the viscosity of the solution and the voltage applied. This can occur when the voltage applied is too high for the solution to be able to form fibres, or if the solution has a lower concentration of polymer, the charged jet will be destabilized in either situation and break down into spherical droplets. Outside of creating the unwoven net with uniform fibres, minimizing electrospray is another aspect looked at, to reduce solution waste and create a net that does not have defects outside of the spun fibres. Using SEM images, the fibres were inspected. For the acetic acid concentrations that were tested the 50 wt.% and 90 wt.% solutions did not yield enough fibres to be considered viable. In the first test, where the concentration of acetic acid is the only variable that is changed, there is electrospray in every test. At low magnifications, the scale of electrospray can be visualized as well as large fibres and fibres that were not able to fully dry before reaching the substrate on the collector.

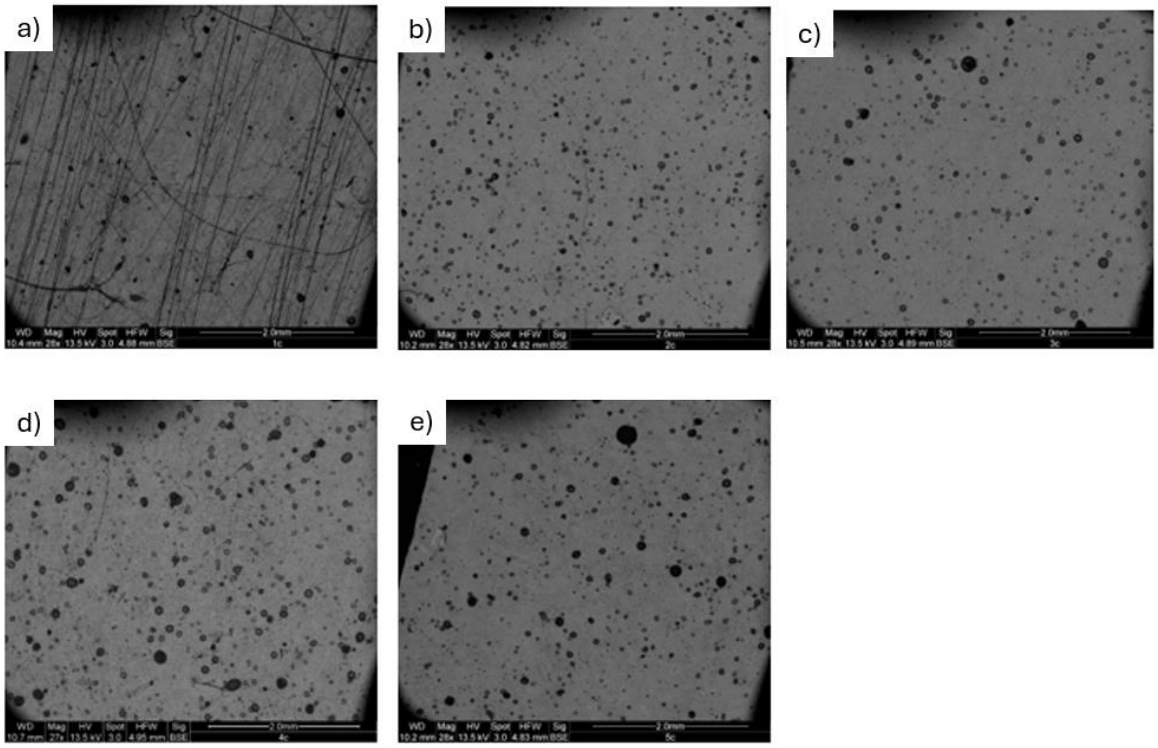


*Figure 4.1 SEM images of chitosan electrospun fibres (27x) at different concentrations of acetic acid (a) 0.5%, (b) 1.0%, (c) 2.5%, (d) 10%, (e) 20%*

The variation in fibre diameter is higher in the 0.5 wt.% and the 10 wt.% samples compared to the other samples. Larger fibres can be seen in these concentrations, figure 4.1 a-f. Figure 4.1 also shows how the fibre density changes with acetic acid concentration, showing that a low acetic acid concentration is needed to create enough nanofibres to cover the substrate over the elapsed time, but too low of an acetic acid concentration can reduce the fibre yield.

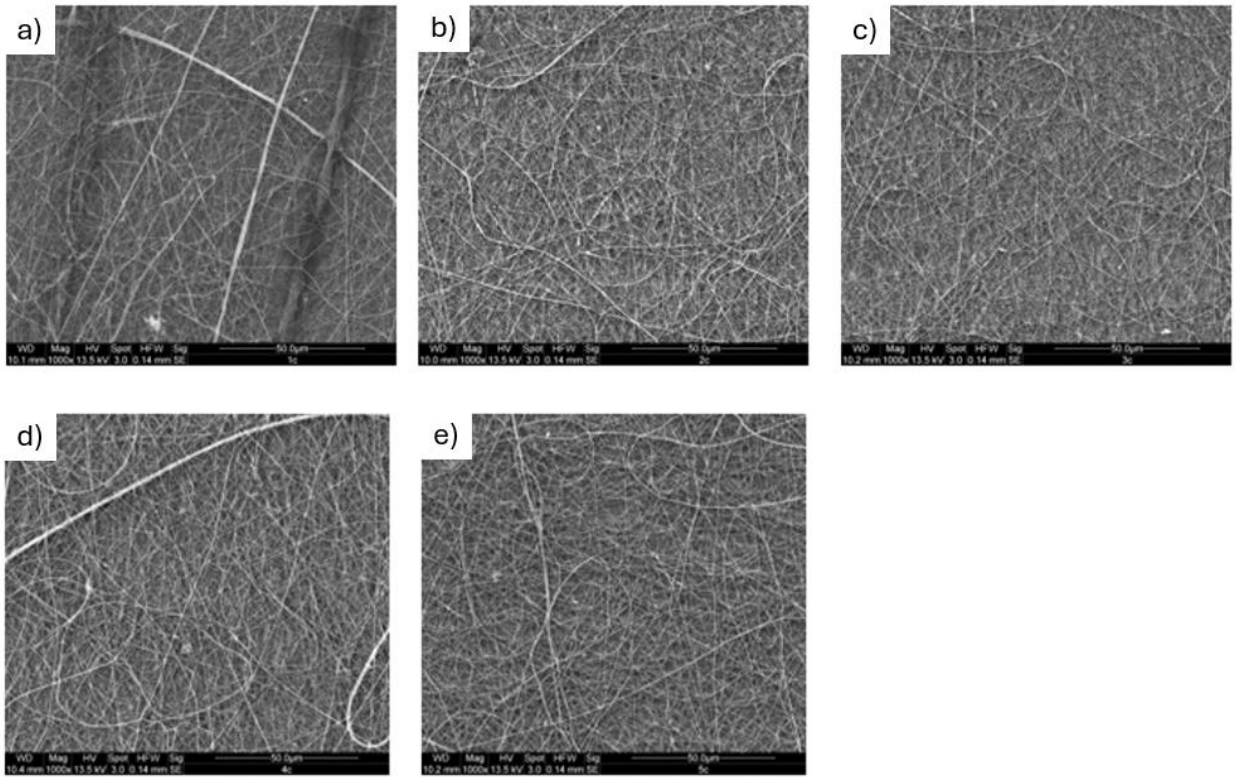


*Figure 4.2 SEM images of Chitosan electrospun fibres (1000x) with varying concentrations of acetic acid solution (a) 0.5%, (b) 1.0%, (c) 2.5%, (d) 10%, (e) 20%*

The high magnification images Figure 4.2 show that the fibres are highly uniform with no detectable beading occurring in the microstructure. The random fibre directions also shows that the collector rotation speed is low enough to allow the fibres to dry on the surface and create a non-woven mat, rather than forcing the alignment of the fibres. This helps create a stronger mat by letting the fibres interact with each other and create a random matrix, as well as a maze that increases filtration efficiency.

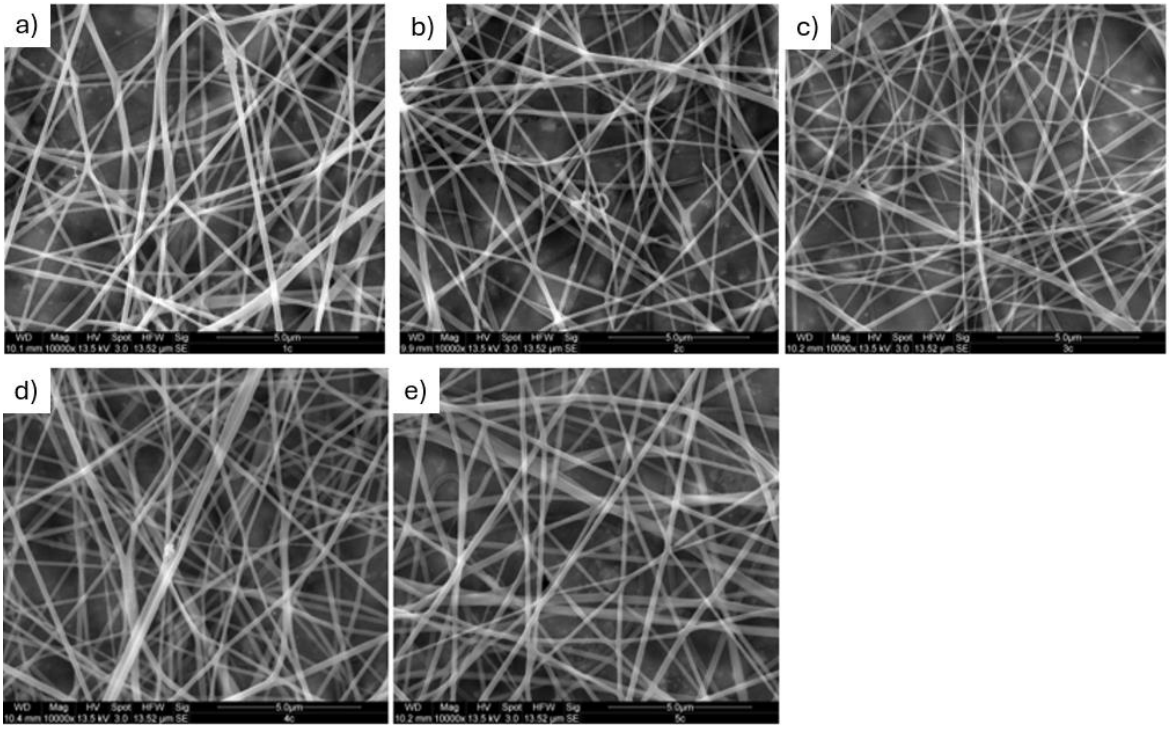


*Figure 4.3 SEM images of Chitosan electrospun fibres (10000x) with varying concentrations of acetic acid solution (a) 0.5%, (b) 1.0%, (c) 2.5%, (d) 10%, (e) 20%*

After the acetic acid solutions test was concluded the ratio of PEO to CS was explored as an option to reduce the amounts of unspun droplets produced. Ratios of 3, 3.5, 4, 5, and 7 parts PEO to 1 part CS were tested, as well as a pure PEO and a pure CS solution. Increasing the amount of PEO to CS improved the spinability of the solutions. It is obvious that the higher the ratio of PEO to CS the fewer droplets are formed. The ratio of 4:1 is the lowest ratio, where the amount and size of unspun droplets can be considered negligible.

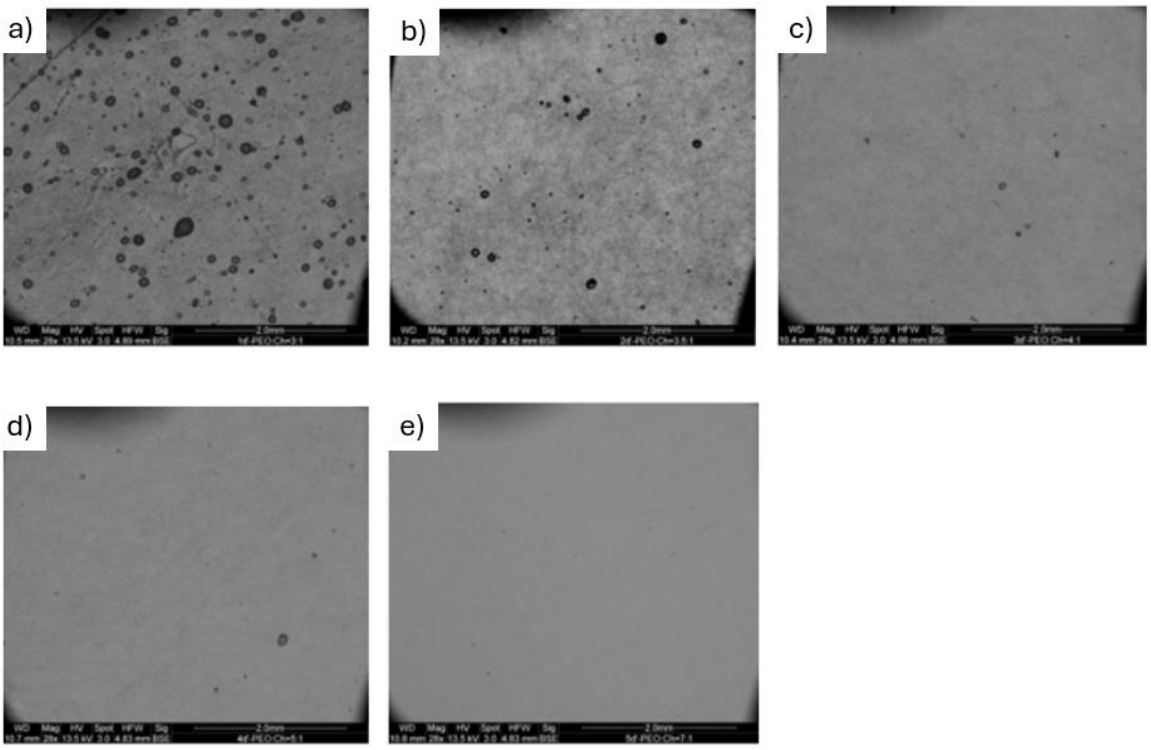


*Figure 4.4 SEM images of Chitosan electrospun fibres (28x) with varying concentrations of PEO as a stabilizer (PEO:Chitosan) (a)3:1 ,(b) 3.5:1, (c) 4:1,(d) 5:1, (e) 7:1*

The increase in PEO to CS ratio also shows a decrease in fibres. Although not obvious in the lower ratios, higher ratios make this much more obvious. All ratios show similar fibre diameter distribution and uniformity, with no beads. There are little to no defects in the fibres and the fibre diameter is around 100 nm.

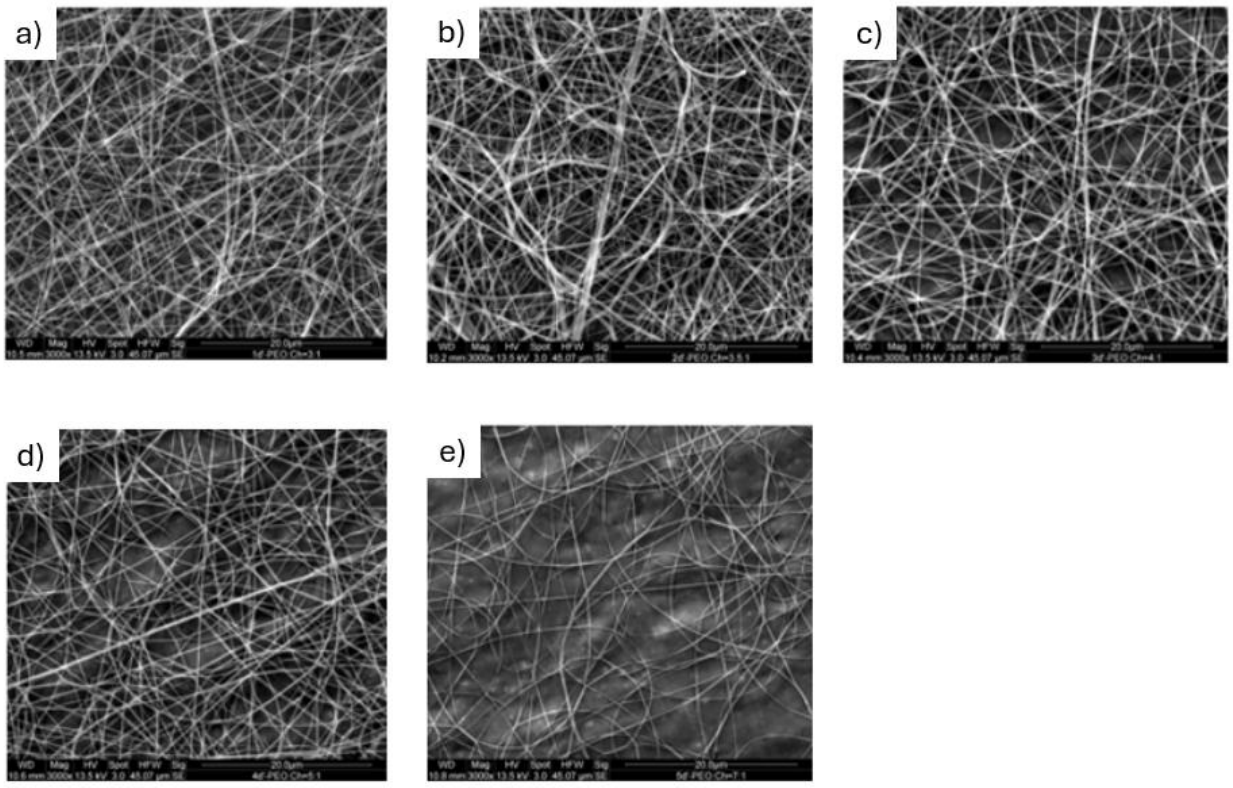


*Figure 4.5 SEM images of Chitosan electrospun fibres (3000x) with varying concentrations of PEO as a stabilizer (PEO:Chitosan) (a)3:1 ,(b) 3.5:1, (c) 4:1,(d) 5:1, (e) 7:1*

The preceding research showed that a high filtration rate can be achieved with PVDF-HFP with a beaded microstructure [20]. However, PVDF-HFP, on its own, has no other mechanisms for protection beyond filtration. Using Chitosan, which is anti-microbial in nature and can contribute to making a safer, more effective filtration system. Tests were run with two filter macrostructures. The layered and dual spun structures in Figure 4.5 used the same PHB and PUB structures that were outlined in the preceding research [20].

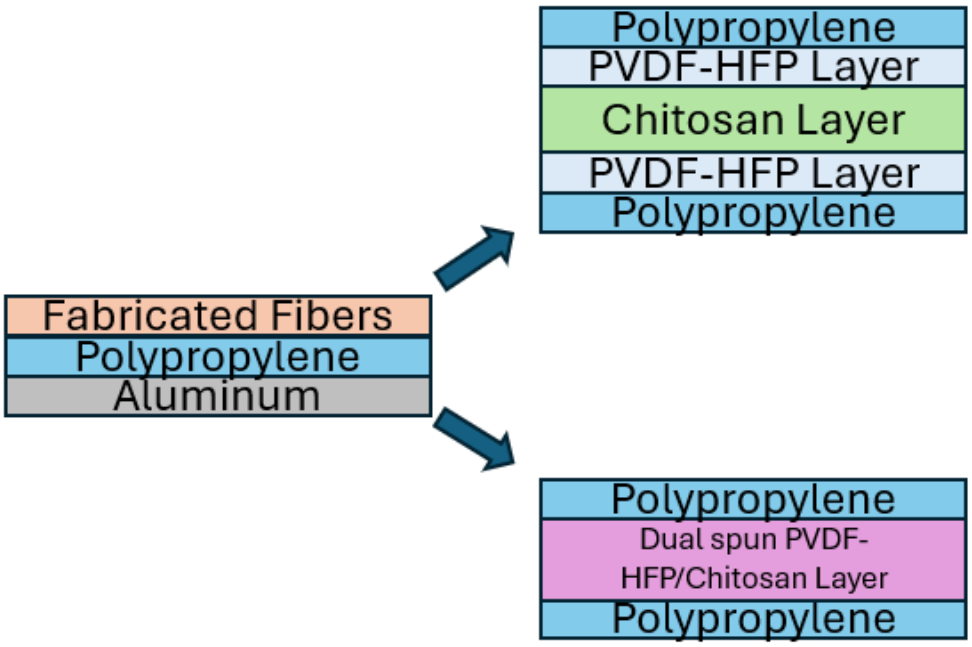


*Figure 4.6 macrostructure of PVDF-HFP/Chitosan filters. (top) sandwiching a layer of Chitosan spun for 120 minutes between 2 layers of PVDF-HFP (PHB) spun for 60 minutes each. (bottom) a single layer of dual spun PVDF-HFP and Chitosan into the same woven mat between two layers of spunbond polypropylene.*

Table 4.1 shows that the multi layered structure has the lowest pressure drop out of all three fabricated filtration mediums, and the filtration efficiency rises with the pressure drop. However, the difference in filtration efficiency is negligible at the initial filtration has even less difference at the most penetrating particle size. All three tests pass the maximum standard limit for inhalation resistance for face masks, which is 343 Pa. Due to the quality factor equation using the natural logarithm in its calculations, the small changes in the filtration efficiency give the PUB/CS-120 sample a larger quality factor that nears the performance of the N95 face masks.

*Table 4.1 comparison between multi-layered PVDF-HFP/Chitosan and dual spun PVDF-HFP/Chitosan filters.*

| Sample | Pressure Drop (Pa) | Initial Filtration Efficiency (%) | Efficiency at MPPS (%) | Quality Factor (Pa^-1) |
|---|---|---|---|---|
| N95 | 117.3 | 96.54 | 95.17 | 28.7*10^-3 |
| 3L-PHB2-CS1-120 | 237.31 | 99.04 | 98.53 | 19.6*10^-3 |
| PHB/CS-120 | 275.97 | 99.21 | 98.76 | 17.5*10^-3 |
| PUB/CS-120 | 293.3 | 99.93 | 98.76 | 24.8*10^-3 |

### *4.2 Face Masks Discussion*

The quality of fibre, and whether droplets form is influenced by the surface tension when other variables and concentrations are held constant [127]. When no other additives were added to the solution, a chitosan concentration of about 7–7.5% of 106,000 g/mol molecular weight along with 90 wt% acetic acid, created continuous fibres. Showing that Triton x-100 and PEO are used as stabilizers to reduce the amount of acetic acid needed for continuous uniform fibres. Although some tests have had success with electrospinning 90% acetic acid chitosan solution [127], with added PEO and Triton x-100 large concentrations of acetic acid are not needed and can hinder the spinning process, since even a 50% acetic acid solution did not yield many fibres. Of all tests the 2.5% acetic acid concentration has the most uniform and fine fibres. The density of fibres in the SEM images may not be reliable due to a slight time difference in tests or the sample is taken from a part of the substrate that did not have as many fibres.

In many studies, electrospray has occurred but is not always reported. There are many reasons why electrospray is used, and they vary depending on setup. The horizontal setup was used in these experiments so droplets falling from the spinneret due to low, high flow rate and/or low electric field were not an issue. However, droplets being sputtered on the collector from the spinneret due to a low viscosity and/or a powerful electric field that dissolves and disrupts the homogeneity of the spun fibres [128] have been found across

multiple papers. Studies focusing on electrospray droplet size and pattern have found that the droplets depend on flowrate, voltage, and viscosity [129]. The most common result is that at higher voltages the spray pattern created has smaller droplets in a smaller distribution [130]. Other studies focusing on chitosan and PEO with varying concentrations of the acetic acid solution, usually on the higher end (>50 wt%), have had success in creating effectively defect free nano fibres of different diameters, some as small as 63 nm, but most have all shown evidence of unspun droplets that may influence the final structure of the nanofibre mat. If the flow rate and electric field are not matched up properly, droplets will form, at lower electrical fields, the flow rate will be too much for the field, and droplets will drop from the spinneret onto the surface below or be propelled onto the collector in front periodically. However, if the electric field is too high, small unspun droplets will be propelled onto the collector, which will affect the homogeneity of the fibre mat. However. There is evidence to show that higher voltages can create finer nanofibres [128], so a balance must be found. Furthermore, using a higher voltage can improve broken fibres to become continuous and decrease junctions of fibres resulting in more uniform fibres [131]. The surface tension factors  determine how quickly or slowly this phenomenon happens. The only other way to fix the unspun droplets issue would be by changing the concentration of the additives to find the proper surface tension and viscosity or to adjust the flow rate to see if it is possible to reduce or eliminate the droplets at the current solution concentration.

The quality factor shows that small changes in filtration efficiency can change the quality of the face mask drastically; a 0.7% increase in filtration efficiency from the PHB to the PUB filters increased the quality factor by ~41.7%, even with a 6.2% increase in pressure drop (which negatively impacts the quality factor). However, with the filtration efficiency being so close to 100% most of the improvement left in this realm of study is through changing the materials to help with more effective anti-microbial properties, the ability to hold its charge for longer periods of time, and decreasing the pressure drop of the filter. Lastly, mechanical strength was mentioned in the literature review but was not tested. This is due to the strength of the fibres easily exceeding their needed strength. For this research, mechanical strength was only needed to survive the assembly of the filter and the filtration tests. None of the samples failed in this regard, so no tests were required.

### *4.3 Coaxial Electrospinning Results*

The first set of fibres created for coaxial electrospinning were single-solution PVDF-HFP and PAN fibres. The previous mask research showed that a 1:1 DMF:acetone solvent made uniform fibres with minimal diameter variation. Both PVDF-HFP and PAN solutions were electrospun at the ambient conditions previously mentioned. Fibres were formed at all concentrations, and the fibres had minimal defects. Figure 4.7 shows the optical microscopy of the single solution PAN fibres. Initially, two tests were trialled with PAN fibres to see how easily they are electrospinnable. Both 10 wt% and 12 wt% PAN solutions could easily create fibres with minimal defects. Both sets of fibres were spun for 30 minutes; the 10 wt% PAN solution produced a more significant number of fibres that appeared almost entirely uniform. The 12 wt% PAN solution also produced many uniform fibres. With minimal differences between the two sets of fibres, the 10 wt% PAN solution was chosen as the core solution to save on materials.

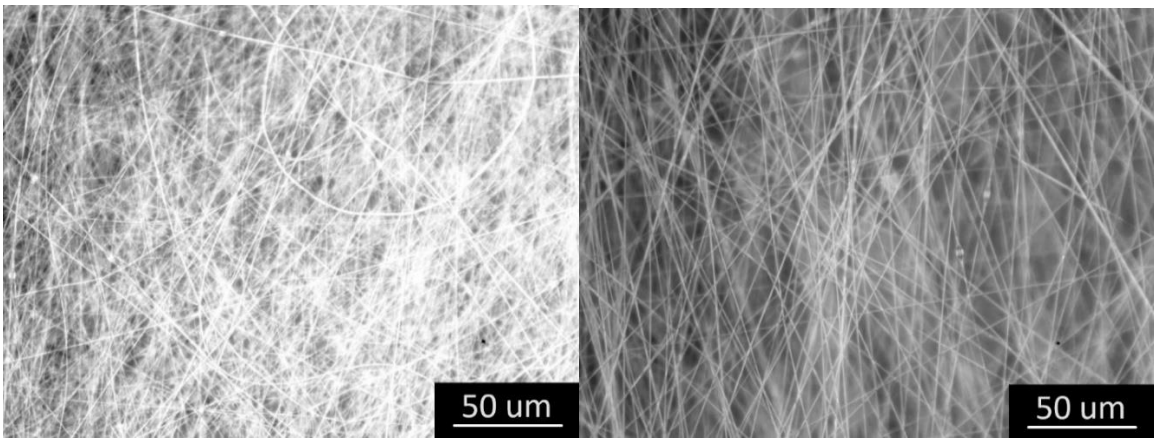


*Figure 4.7 Optical microscopy of PAN fibres (left) 10 wt% PAN dissolved in DMF, and (right) 12 wt% PAN dissolved in DMF*

The PVDF-HFP solutions were used as the shell for coaxial electrospinning, and the PAN solution was the core. For a proof of concept, the first set of experiments was tested at different voltages, 15 kV, 20 kV, and 25 kV, and different polymer shell concentrations, 15 wt%, 20 wt%, and 25 wt%, at a feed rate ratio of 2:3, core:shell. Of these tests, the fibres that appeared the most uniform and likely to have yielded core-shell fibres were chosen for SEM imaging. Figure 4.8 below shows the first coaxial spun fibres. These first experiments yielded fibres easily viewed in the optical microscope. Through the transparent fibres, there

appears to be an internal translucent line that follows some of the fibres. This is likely due to the material change from PVDF-HFP to the PAN core. However, it does not guarantee that this core-shell structure exists in a significant number of the fibres, or if this fibre has that structure, it could be a defect of the fibre that is refracting the light in a way that appears as a core. The other coaxial fibres in Figure 4.8 were chosen based on this similar optical distinction. For reference, the surface tension of DMF is measured to be 37.1 mN/m, whereas the surface tension of Acetone is 23 mN/m, which can affect both electrospinning and light refraction [132, 133].

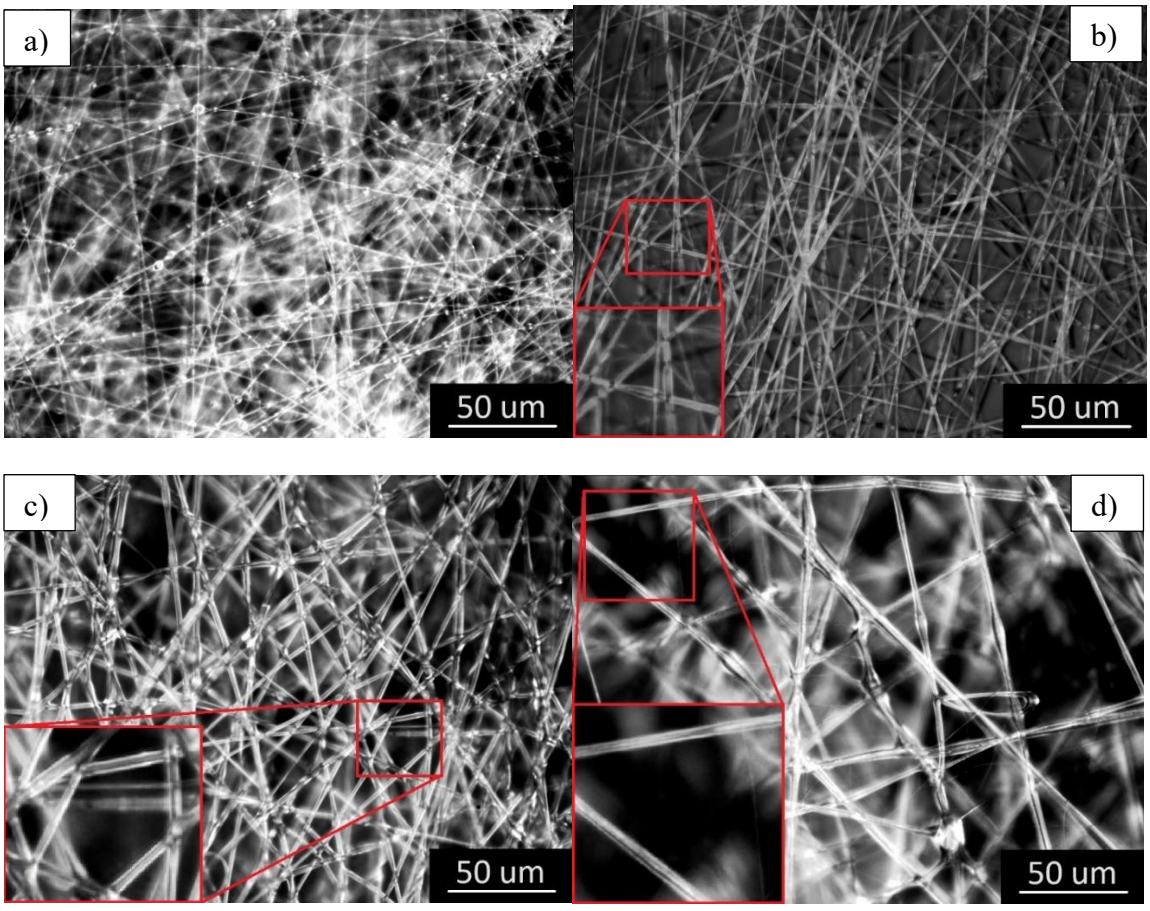

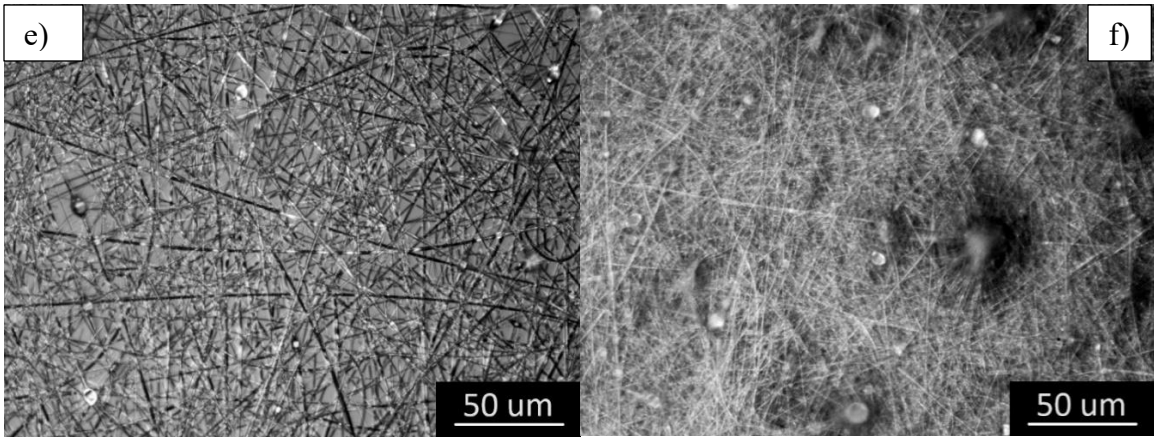


*Figure 4.8 Coaxial fibres with a 10% PAN core solution and a) (D9) 15 wt% PVDF-HFP shell solution in DMF, b) (D11) 25 wt% PVDF-HFP shell solution in DMF, c) (D15) 15 wt% PVDF-HFP shell solution in 1:1 DMF:Acetone, d) (D18) 20 wt% PVDF-HFP shell solution in 1:1 DMF:Acetone e) 15 wt% PVDF-HFP in 1:2 DMF:Acetone, f) 20 wt% PVDF-HFP in 1:2 DMF:Acetone*

The difference of solvent in the polymer solutions from DMF to equal parts DMF and Acetone and 1:2 DMF:Acetone is displayed in Figure 4.8. It is plain to see that the 15 wt% pure DMF solution creates highly beaded fibres with very thin diameters. Due to the fibres' size, no characteristics display whether these fibres might contain the core-shell structure. Both solutions that contain equal parts DMF and Acetone Figure 4.8 (c, d) created thicker, more uniform fibres with a visible core-shell structure. Both solutions display more fused fibres as well. This is ideal for non-woven fibre mats as it will create more connections and greater strength among the mat, but a disadvantage if the goal of fibre fabrication is to create individual fibres, as it will not allow the fibres to be separated, and in some cases, like aligned fibres it may even fully fuse multiple fibres to create one thick fibre after it is dry. As mentioned previously, the surface tension is one of the parameters that directly influences the electrospun fibre morphology. The resultant fibre diameters decrease when the surface tension decreases [134]. This is shown in Figures 4.8 (e) and f, the fibres created from the 1:2 DMF:Acetone ratio solvent, increasing the amount of Acetone decreases the overall surface tension, allowing the solution to be more easily electrospinnable by lowering the electric field threshold to eject solution and create a Taylor cone but also creating finer fibres. Unlike the pure DMF solution, these fine fibres are much more uniform. Although some beads are formed, their concentration is much smaller.

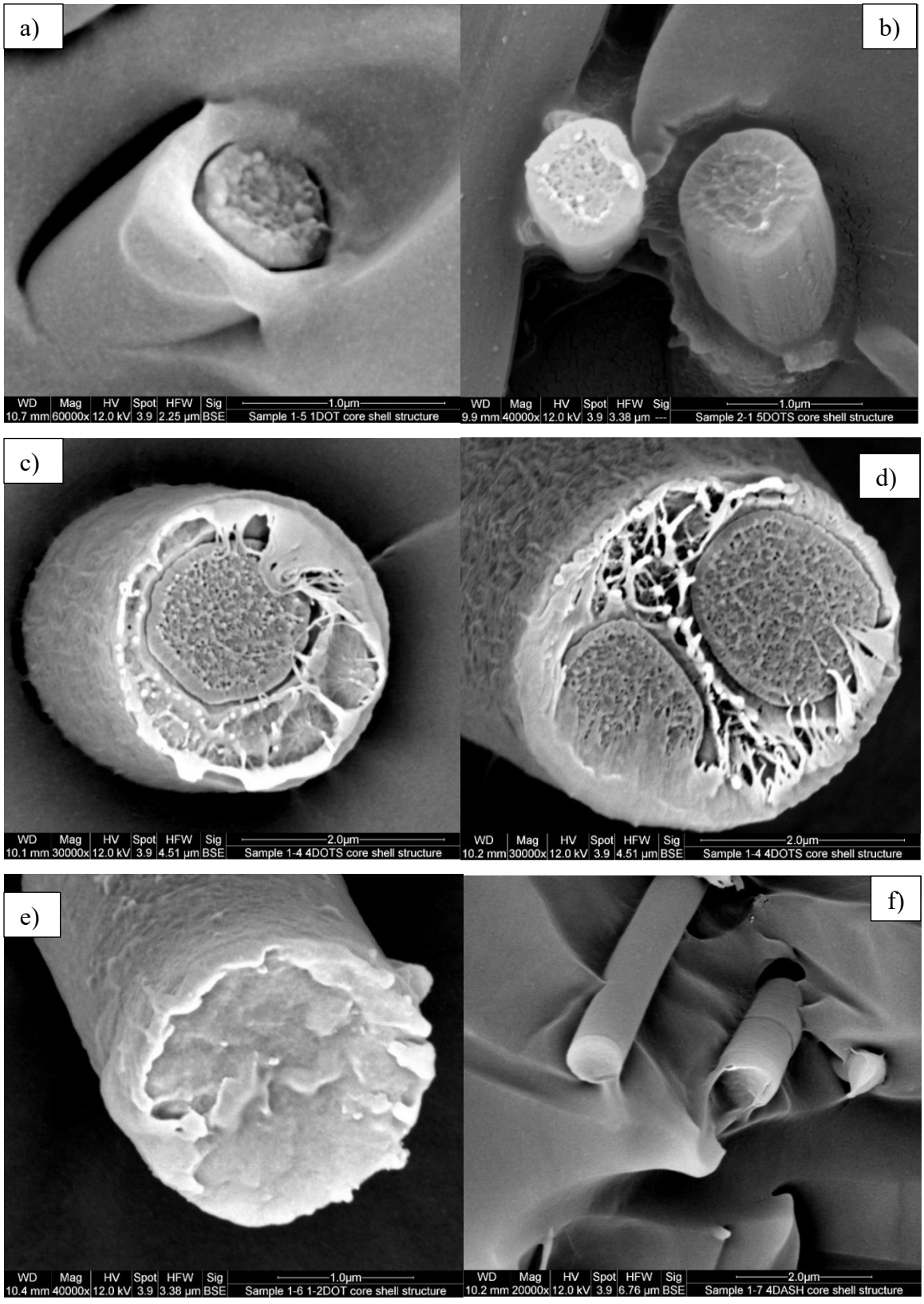


*Figure 4.9 SEM images of the cross-sectional area of the following samples a) D11, b) D15, c) D18, d) D18 (dual core), e) D23, f) D24. (naming convention found in Table 4.1)*

The SEM images in Figure 4.9 show that the core-shell fibre structure was achieved using the parameters chosen for this research. For most of the fibres, the core-shell structure is apparent; however, for solutions with a 1:2 DMF:Acetone solvent ratio, the fibre appears to have a substantial core and a very thin shell, or the fibre does not have the core-shell structure. The shell is essentially a film that is only visible because of its higher glass transition temperature, allowing the PVDF-HFP to have a more ductile break, differentiating it from the PAN core. Figure 4.9 (e) shows an inconclusive result for a core-shell fibre, as there is more of a ductile break on the far edge of the fibre. However, it needs to be more consistent, and there is no separation between the two solutions.

Meanwhile, Figure 4.9 (f) shows a much more apparent thin film on the outside of the fibre, and the film appears as a very thin veil that drapes over the core. The samples with equal parts DMF and Acetone in Figure 4.9 (a, b, c, and d) show more obvious signs of a core-shell structure. The two solutions have varying degrees of separation, and Figure 4.9(b) has the most connected core and shell. All the images from this sample had the same break pattern of an outer brittle breaking surface, transitioning into a ductile border with significant and noticeable necking followed by a dimpled break surface. This dimpled surface is seen in the other images as the core surface. It can also be seen that in one of the samples, Figure 4.9 (d), some of the thicker fibres contain multiple cores. These multiple cores are most likely not due to two Taylor cones forming and creating a unique fibre or to the ejected solution having two cores. This phenomenon was only seen occasionally throughout the sample.

*Table 4.2 The calculation of the core, shell and empty space percentages in the sample fibres*

| Sample ID | Core Percentage | Shell Percentage | Empty Space Percentage | Shell Solution Concentration | Solvent Ratio (DMF:Acetone) | Voltage (kV) |
|---|---|---|---|---|---|---|
| D11 | 29.26 | 59.88 | 10.86 | 25 | 1:0 | 20 |
| D12 | 33.47 | 66.53 | 0 | 25 | 1:0 | 25 |
| D15 | 37.43 | 62.57 | 0 | 15 | 1:1 | 15 |
| D18 | 42.6 | 56.31 | 1.09 | 20 | 1:1 | 20 |
| D23 | 86.9 | 13.1 | 0 | 20 | 1:2 | 15 |
| D24 | 90.03 | 9.97 | 0 | 20 | 1:2 | 20 |

Table 4.2 shows the difference in the percentage of core:shell ratios in the SEM cross-sectional images.

For all initial samples examined in Figure 4.9 (SEM imagery), the feed rate was 3:2, with shell solution:core solution. D11 and D15, the samples with only DMF as their solvent, have the smallest core size, with the core size increasing as the voltage used during fabrication increases the core size. The core size also increases with increasing Acetone in the solvent for the shell solution. Two fabricated fibres, D11 and D18, also had some visible spacing between the fibre's core and shell. The other samples either had an established border or, in some cases, the core and shell appeared to be fused, with the fracture surface being the identifying factor of the structure.

After the conceptual fibres were created, a few refinements were made to the process. The 25 wt% PVDF-HFP solution did not regularly fully dissolve in the solvent, leaving its results uncertain and not reproducible. For future experiments, 15 wt%, 17.5 wt%, and 20 wt% PVDF-HFP solutions were used as they were more consistent in their mixing. These three solutions were paired with a 10 wt% PAN core solution for all tests, and three distinct feed rate ratios, 2:3, 1:2, and 1:3 core:shell, were used to see if the feed rate ratio affected the core-shell structure. Optical microscopy images were taken of all fabricated fibres. Figure 4.10 shows some optical microscopy fibre images from the 27 tests. Table 4.3 also shows that the shell shrunk with the addition of Acetone to the solvent in the shell solution. The voltage and polymer concentration did not influence the core-shell structure.

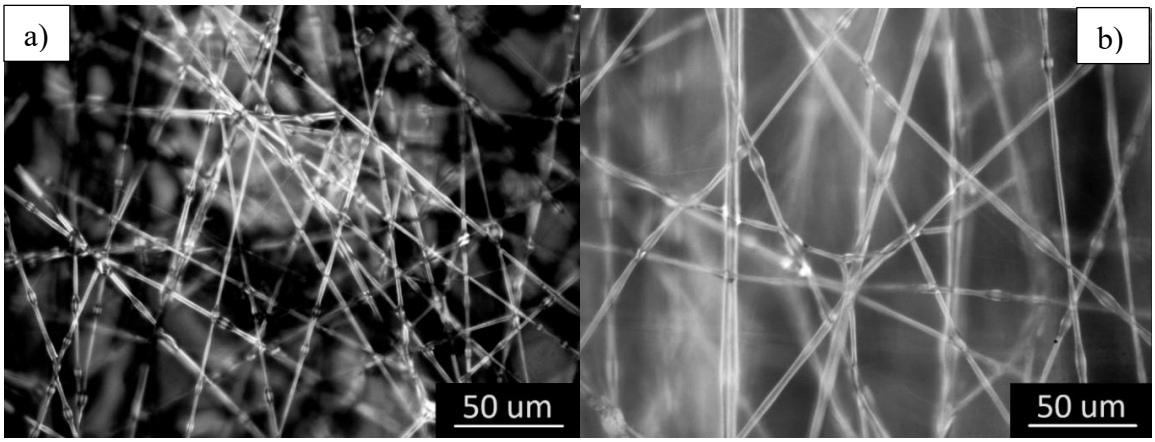

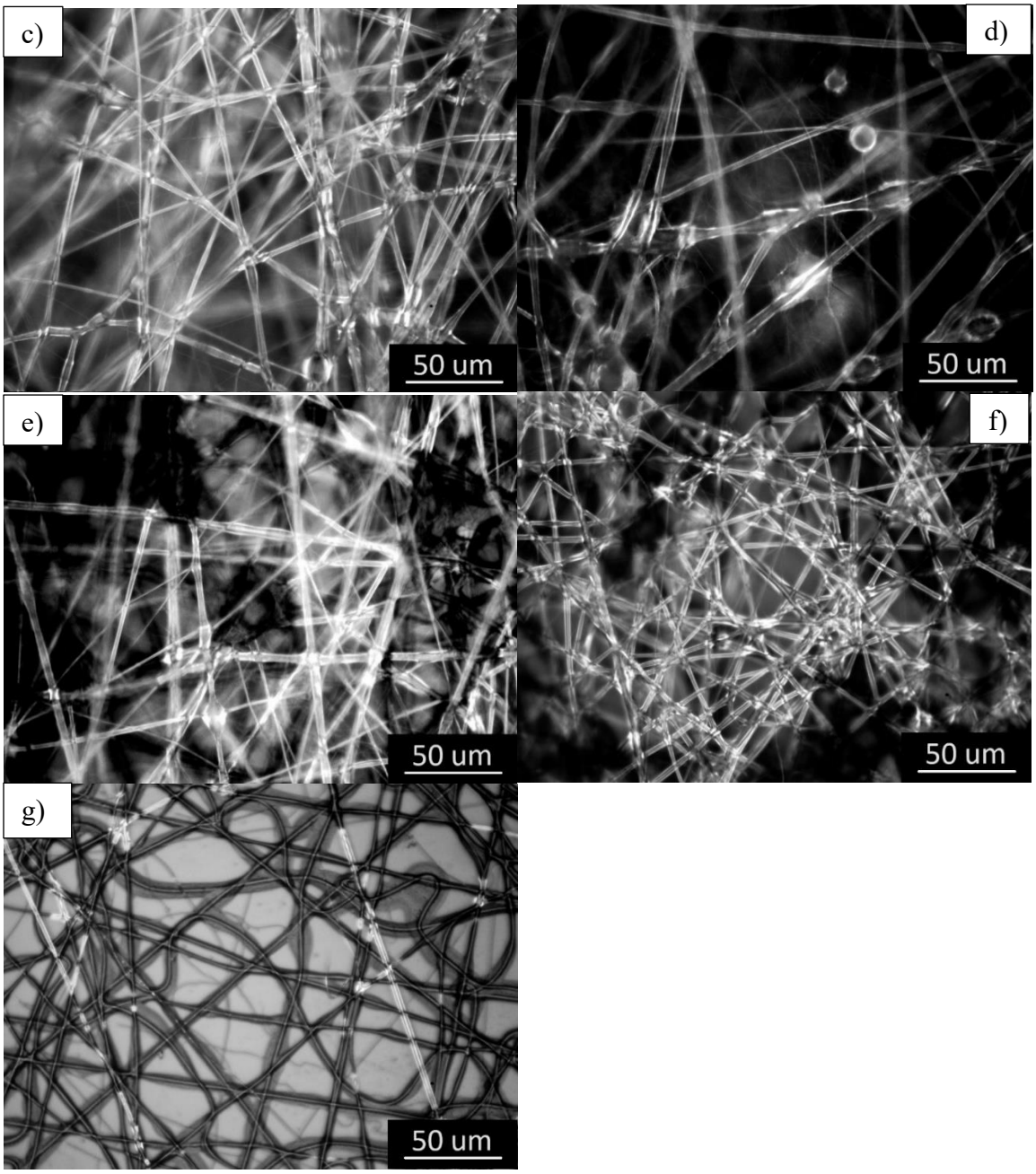


*Figure 4.10 Optical microscopy of fibres created from solutions a) F8B, b) F20B, c) F23B, d) F26B, e) F40, f) F41B, g) F42B. (Naming conventions found in Table 4.2).*

The images in Figure 4.10 show the optical microscopy of the final fibres. None of the fibres fabricated are fully uniform; however, the beads formed are visibly in the transition from beaded fibre to uniform fibres, which could be manipulated to form uniform fibres with a change in the tip-to-collector distance. Throughout all the images, some fibres show a change in transparency in the center of the fibre, suggesting the existence of a core-shell structure. Figure 4.10 (g) shows both light and dark grey fibres. The dark grey fibres are

fibres that did not finish drying before reaching the collector, landing on the collector, and the fibre slightly spread out before they dried; the lighter coloured fibres are the fibres that did not make contact with the collector and were able to dry while still suspended in the air, allowing the fibres to keep their shape. Table 4.2 shows the parameters under which each image was fabricated.

*Table 4.3 Fabrication parameters of final coaxial fibre solutions*

| Sample ID | Shell Solution (PVDF-HFP) | Shell Solution Feed Rate (uL/min) | Core Solution | Core Solution Feed Rate (uL/min) | Voltage (kV) | Temperature (C) |
|---|---|---|---|---|---|---|
| F8-B | 15% | 27 | 10% | 13.5 | 15 | 22.5 |
| F20-B | 17.50% | 36 | 10% | 18 | 15 | 21.9 |
| F23-B | 17.50% | 37 | 10% | 18.5 | 20 | 22.4 |
| F26-B | 17.50% | 39 | 10% | 19.5 | 25 | 22.9 |
| F40-B | 20% | 36 | 10% | 24 | 15 | 22.2 |
| F41-B | 20% | 41 | 10% | 20.5 | 15 | 23.1 |
| F42-B | 20% | 45 | 10% | 15 | 15 | 23 |

All samples were fabricated within a range of 1.2 degrees Celsius of each other, allowing for minimal effects on the fibres. Some trends that can be seen are that as the polymer concentration increases, the overall feed rate is also mirrored with increasing voltage. Even with changing the feed rate ratio of shell:core solutions, the overall total feed rate has little to no change.

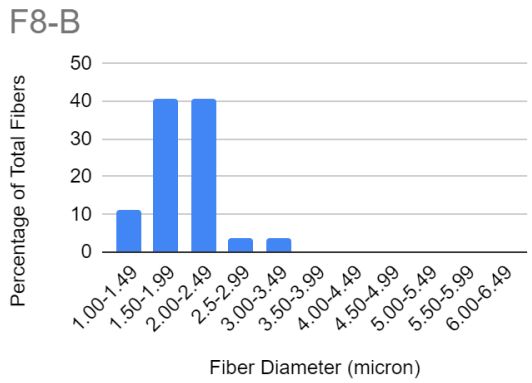


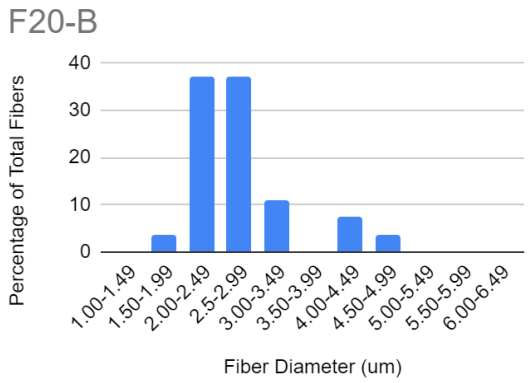

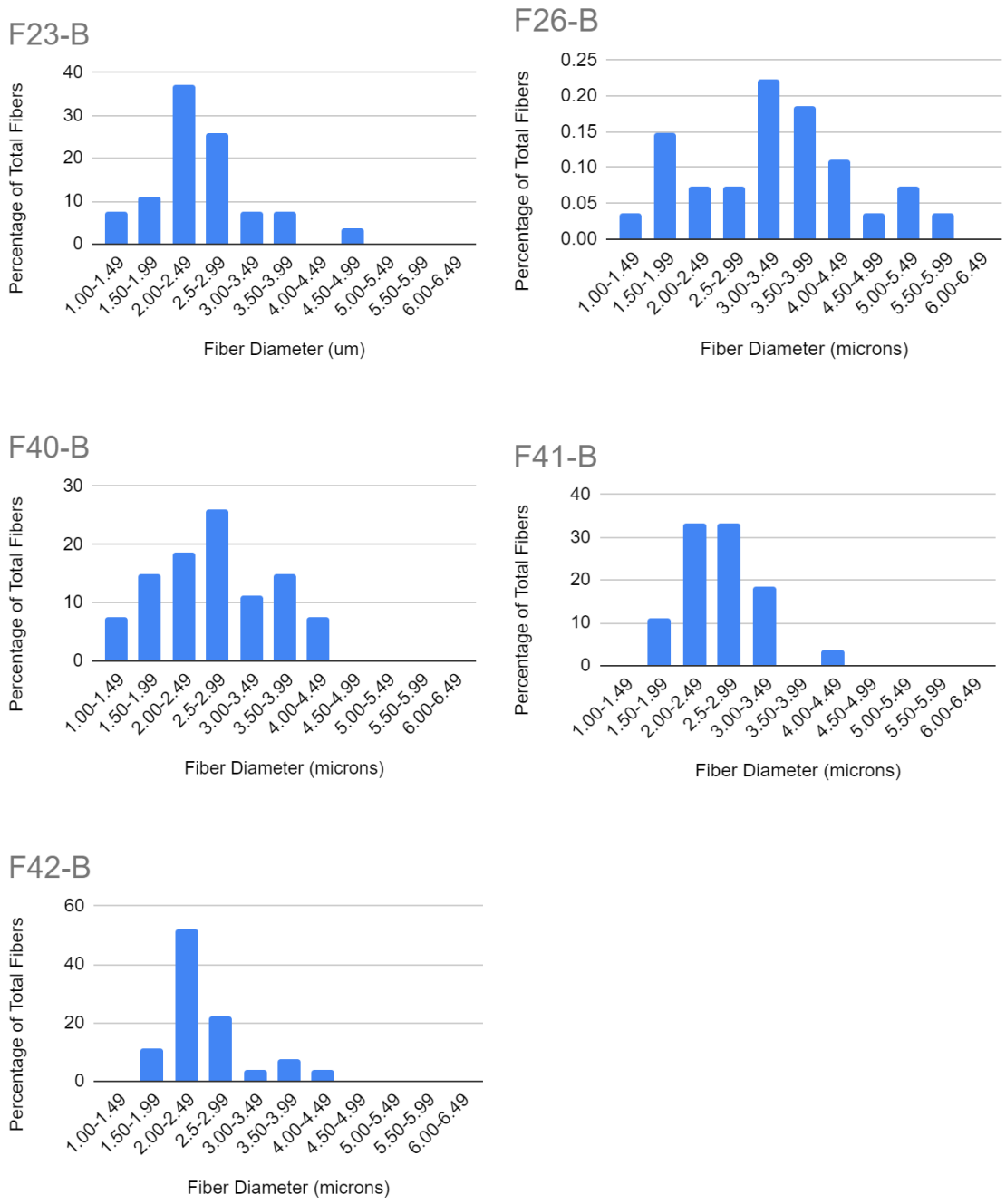


*Figure 4.11 Fibre diameter distribution of the final coaxial fibres*

*Table 4.4 Viscosity of the four solutions (three shell and one core) used in the fabrication of coaxial fibres.*

| Solution | Viscosity | Standard Deviation (+/-) |
|---|---|---|
| 15% PVDF-HFP | 251.50 | 9.07 |
| 17.5% PVDF-HFP | 322.83 | 13.78 |
| 20% PVDF-HFP | 1097.83 | 30.50 |
| | | |
| 10% PAN | 694.50 | 11.73 |

Table 4.4 shows the viscosity of the solutions used in the coaxial fibre fabrication; as expected, the higher the concentration of polymer, the greater the viscosity. Keeping this in mind Figure 4.11 shows that F8-B, F20-B, and F40-B, which have the same parameters except for the concentration of the shell solution polymer, have a greater diameter distribution the higher the polymer concentration in the shell solution. This distribution is due to the large number of polymer chains within the solution; these chains get entangled and can cause the fabrication of larger fibres. As the chains are ejected from the Taylor cone, they pull other chains along with them; this basic principle changes electrospray into electrospinning. These chains have a critical mass (or polymer concentration) where they no longer create uniform fibres. Instead, it inhibits the flow of the polymer solution and can clog the spinnerette tip or cause beaded fibres to be formed [135]. However, this fibre diameter distribution does not appear to carry through to F41-B and F42-B. The darker pools outlining the dried portion of the fibres show that these fibres were partially dry before coming into contact with the collector. For the F41-B fibres, many of the fibres are interlinking. This structure allowed many fibres to support each other from falling onto the collector while still wet.

The final testing occurred with samples F8B, F20B, F23B, F26B, F40B, F41B, and F42B. These samples were chosen to span the various parameters that were tested. F8, F20, and F40 span the polymer concentration changes while all other parameters remain constant. F20, F23, and F26 have only the voltage changing throughout the tests, and F40, F41, and F42 have the shell:core feed rate ratios spanning 3:2, 2:1, and 3:1, respectively. This will give a good idea of if or how these parameters will affect the fibre morphology.

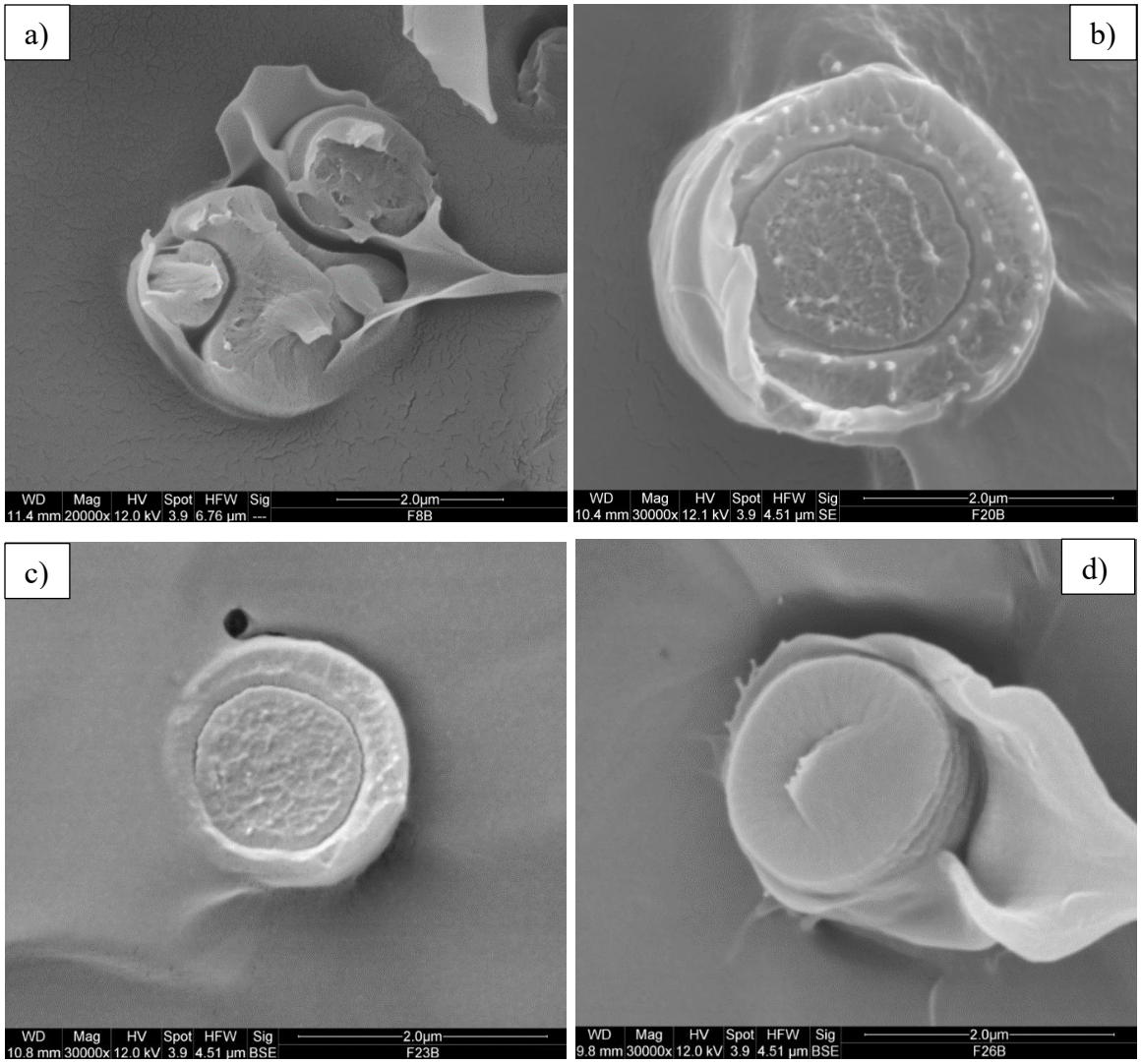
a)
WD Mag HV Spot HFW Sig
11.4 mm 20000x 12.0 kV 3.9 6.76 µm ---
2.0µm
F8B
b)
WD Mag HV Spot HFW Sig
10.4 mm 30000x 12.1 kV 3.9 4.51 µm SE
2.0µm
F20B
c)
WD Mag HV Spot HFW Sig
10.8 mm 30000x 12.0 kV 3.9 4.51 µm BSE
2.0µm
F23B
d)
WD Mag HV Spot HFW Sig
9.8 mm 30000x 12.0 kV 3.9 4.51 µm BSE
2.0µm
F26B

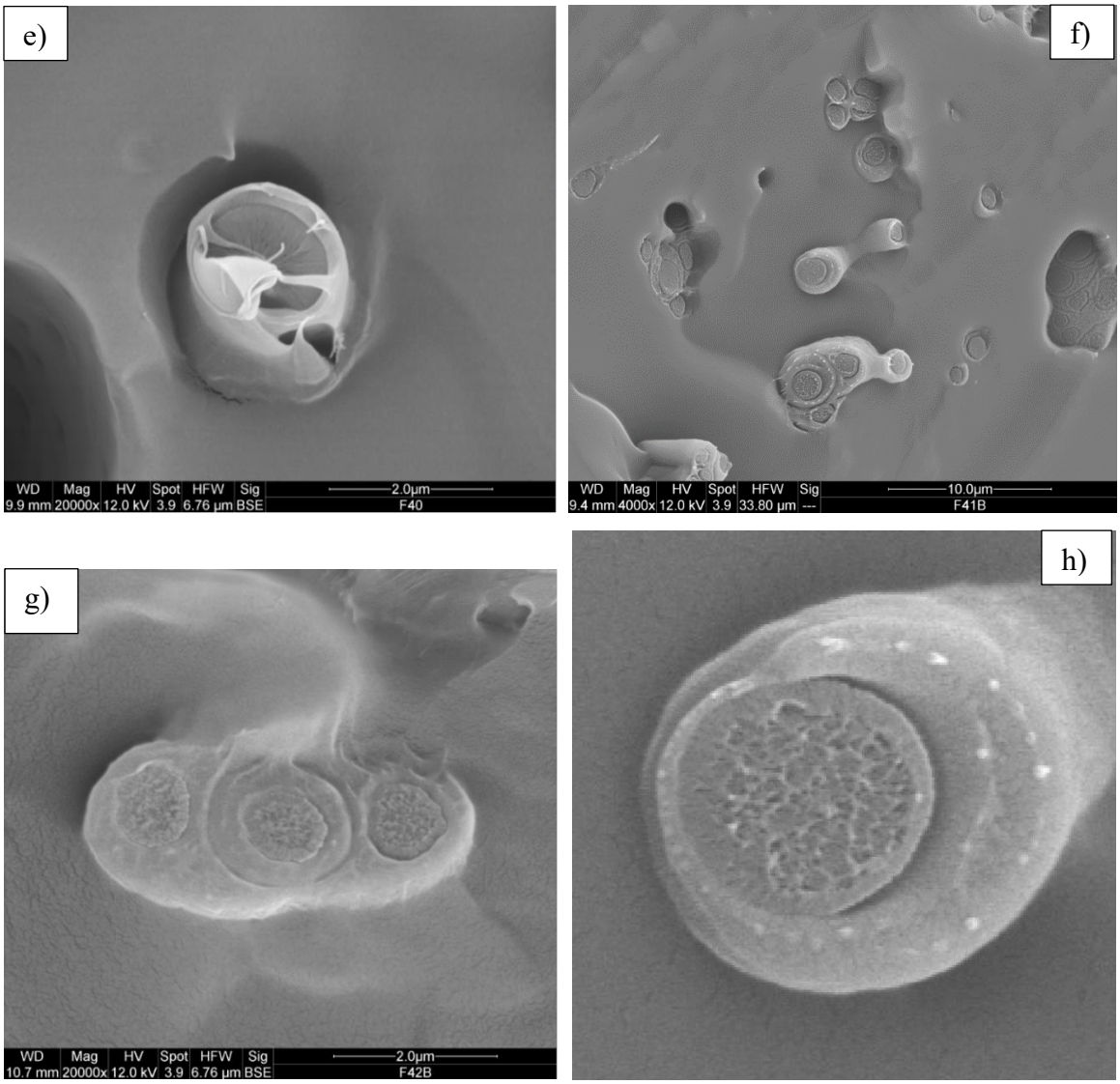


*Figure 4.12 SEM images of coaxial fibres a) F8B, b) F20B, c) F23B, d) F26B, e) F40B, f) F41B, g) F42B, h) F41B-zoom*

These SEM images show the cross-sectional microstructure of the previously chosen solution combinations. All the samples show round single fibres with some variation regarding fibres with multiple cores Figure 4.12. These fibres with multiple cores further the possibility that the fibre variation is largely due to collisions during the stretching phase. Even though all of the samples have the core-shell structure, F8B, F26B, and F40B have a thin shell. These samples have the feed rate ratios of shell:core at 2:1, 2:1, and 3:2. These samples do not have any overlap of a shared parameter, and the fibres appear very different when the fibres are fused to create a multi-core fibre in the cases of F26B and F40B.

*Table 4.5 The calculation of the core and shell percentages in the coaxial fibres*

| Sample ID | Core Percentage | Shell Percentage | Shell Solution Concentration | Feed rate Ratio (Shell:Core) | Voltage (kV) |
|---|---|---|---|---|---|
| F8-B | Shell underwent major plastic deformation, could not properly calculate | | 15% | 3:2 | 15 |
| F20-B | 37.05 | 62.95 | 17.50% | 3:2 | 15 |
| F23-B | 40.23 | 59.77 | 17.50% | 3:2 | 20 |
| F26-B | 62.62 | 37.38 | 17.50% | 3:2 | 25 |
| F40-B | 55.82 | 44.18 | 20% | 3:2 | 15 |
| F41-B | 46.51 | 53.49 | 20% | 2:1 | 15 |
| F42-B | No single core fibers were created in this sample due to fiber wetness upon collection | | 20% | 3:1 | 15 |

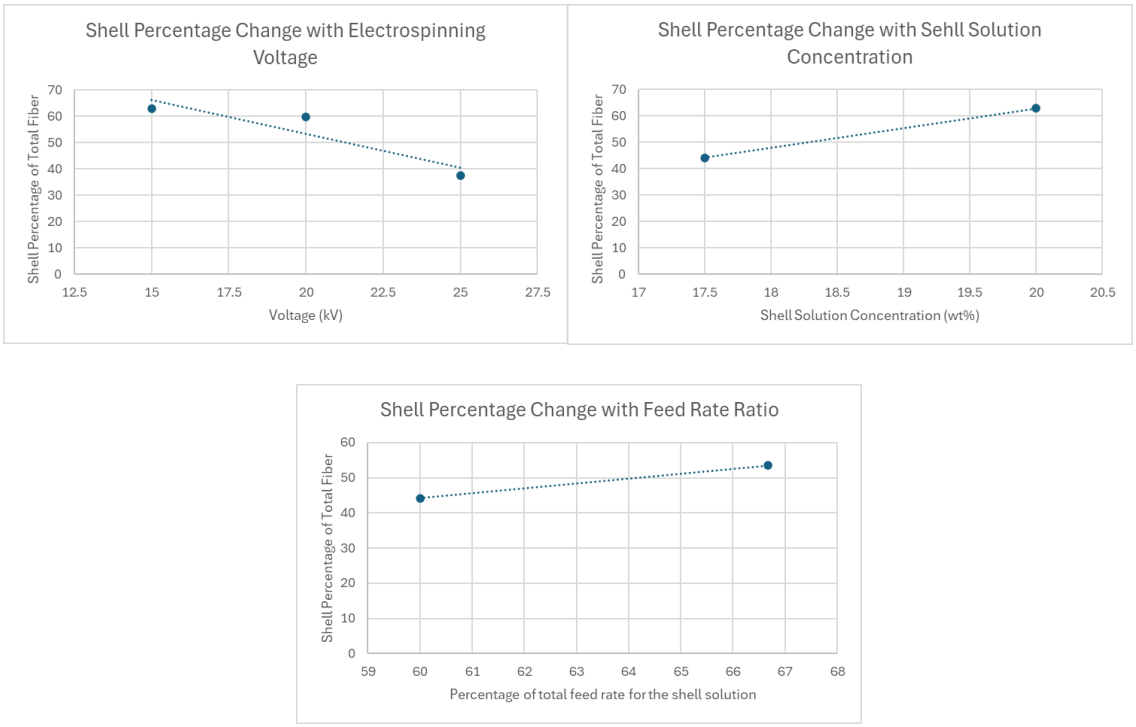


*Figure 4.13 Visualization of Table 4.5, the change in shell percentage of a coaxial fibre with a change in (top left) voltage, (top right) shell solution concentration, (bottom) feed rate ratio*

Due to the change in SEM sample preparation, changing from liquid nitrogen cooling to a conventional chest freezer to freeze the samples before breaking. With the glass transition temperature of PVDF-HFP being well below the temperatures reached in the chest freezer, this allowed the shell to deform and reduced the number of fibres that kept their shape and proportions for viewing as can be seen in Figure 4.12 (a), (d), and (e). Figure 4.13 shows the visualization of Table 4.5 data grouping the changed parameters together. The found data suggests that as the feed rate ratio changed from 3:2, to 2:1, and likely to 3:1

(shell:core) the shell percentage increased. Contrary to the feed rate, the fabricated fibres do not show the same proportions as the feed rate, F40-B should have 60% shell percentage, but in actuality, it is 44.18%. Voltage also appears to have an influence over the shell:core ratio. As can be seen with samples F20-B, F23-B, and F26-B, their concentrations and feed rate ratios are constant, but the processing voltage ranged from 15-25 kV. With a small change in shell percentage of 3.18%, but a significantly larger change in shell percentage of 22.39% with having fibres within similar fibre diameter distributions. The shrinkage or growth of the shell is not either good or bad on its own. This research is focused on how the parameters of the experiment change the final result. Depending on the application of the fibres a thicker shell may be more favourable. For example, in medicine delivery, a thicker shell may assist in a slower release or larger gap before the medicine is released. However, if the end goal were to have very thin hollow carbon tubes, a thinner shell would be more desirable. The trends shown in Figure 4.13 can be used as a guide to better tailor the expected fibres in the direction wanted for a given application.

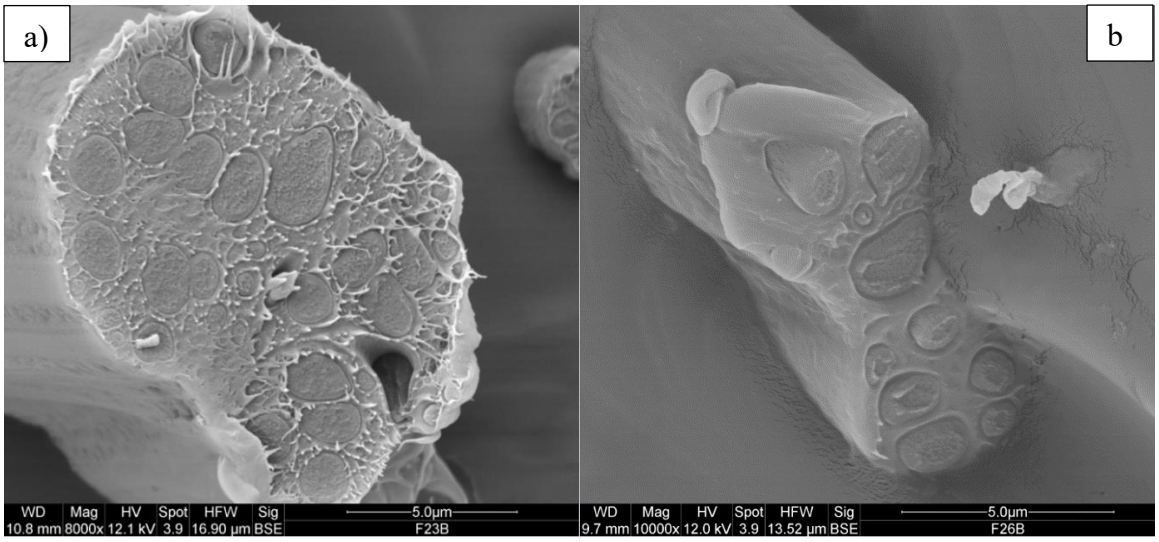

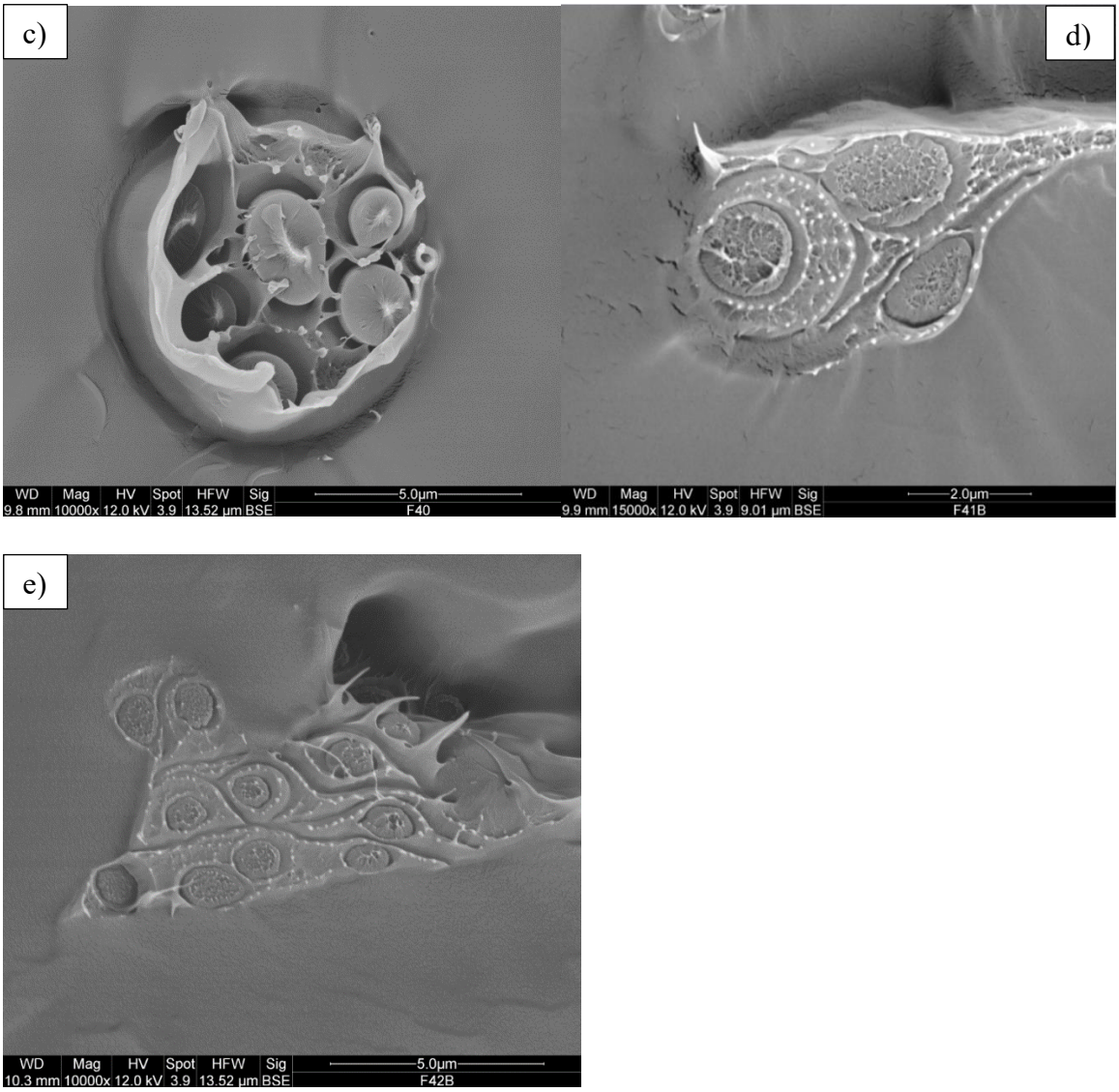


*Figure 4.14 SEM images of the samples that have multiple core fibres. a)F23B, b)F26B, c)F40B, d)F41B, and e)F42*

The above samples showed multiple instances of fibres fusing together to create multi-core fibres. F42B, the sample with a 3:1 shell:core ratio, showed the greatest fibre fusion. This is likely due to the fibres being wet upon contact with the collector, as shown in the optical microscopy images in Figure 4.10. However, it is not only the shell:core feed rate ratio that influences the fusion of fibres; this is because sample F40B, which has a shell:core feed rate ratio of 3:2, has examples of fused fibres, while samples F8B and F20B are almost entirely made up of single-core fibres and they have a shell:core feed rate ratios of 2:1.

The shell volume of samples F26B and F40B, which have thinner shells when they are single-core fibres, appears much thicker when fused into multi-core fibres. F8B did not

have any obvious multi-core fibres formed within the sample; however, as seen in Figure 4.12(a), some fibres appear nearly fused. Other than F42B, which has a very high rate of multi-core fibres due to the wet fibres upon collector contact, F23B and F26B have multi-core fibres with the highest number of cores per fibre. This multi-core fibre formation is likely related to the voltage at which the fibres were fabricated. Previously, higher voltages were thought to create a larger variety of fibre diameters due to the instability of the Taylor cone [136]. However, with the core-shell structure, it can be seen that these fibres likely have much less variation per fibre created from the Taylor cone but that the variation occurs during the whipping phase, where the fibres may collide. Suppose the parameters allowed rapid drying during fibre fabrication, likely through low humidity and higher temperatures. In that case, the fibres likely dry before fusing, and a much more uniform fibre size and a very dense fibre matrix may be created.

### *4.4 Coaxial Electrospinning Discussion*

Figure 4.10 (b, c, and d) all have thicker fibres, allowing a possible visualization of the structure of these fibres. In the enlarged area, there appears to be some change in the material in the center of the fibres. This change in visualization can be a change in material showing the core-shell structure, but more data is needed to conclude. The fusion of fibres in Figure 4.10 (c and d) may be due to the addition of Acetone to the solution. Although Acetone has a faster rate of evaporation than DMF, as it evaporates from the solution, it cools the rest of the solution and fibres, allowing the DMF to stay in the formed fibre, preventing it from drying completely for a longer amount of time, allowing for the fibres to fuse upon initial contact. The droplets in Figure 4.10 (f) are likely not due to fibre formation but some solution being ejected as a droplet from the spinneret and landing on the fibres. The earlier droplets fuse with the fibres and create dark spots, similar to how the fibres appear darker in Figure 4.10 (e), but after the fibres have been formed, the solution rests on top of the fibres as they are hydrophobic.

For the SEM images, the chances of one of the cross sections existing in one of the beads are minuscule, due to the low occurrence of beaded areas, in optical microscopy images, and even with a highly beaded structure, the fibres still have a vastly larger amount of

fibres. In some instances, there appear to be holes in the resin that coincide with the surrounding fibre diameters. Leading to believe that even with reaching the glass transition temperature the fibres do not necessarily break on the same plane as the epoxy. This means that the cross sections for all SEM images can be assumed to be located in the smallest part of the fibres, showing common uniformity.

In Figure 4.9 (f), the thin veil is likely the PVDF-HFP (shell) material because the breaking mode is very ductile, where both the epoxy encasing the fibre and the core PAN solution has a much higher glass transition temperature leading to a very brittle breaking surface at the conditions at breaking the sample for SEM imaging, this has been documented before, Yan et al. has shown that in some cases the solutions mix heavily leaving only an "ultrathin shell" that can be seen in their TEM imagery, Figure 4.15 [111].

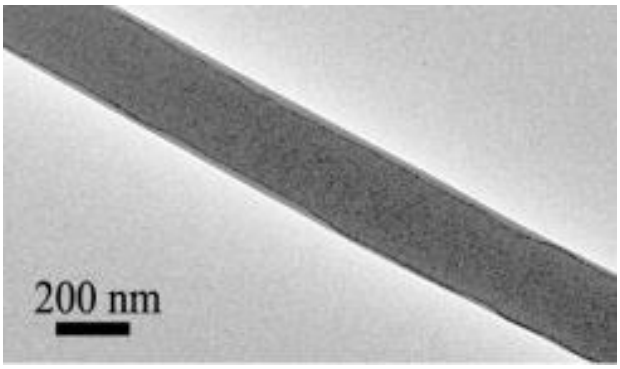


*Figure 4.15 TEM imagery of a coaxially spun fibre where the core and shell solutions showed mixing, leaving an ultrathin shell [111]*

The dual-core occurrence in Figure 4.9 (d) is likely linked to the whipping/stretching phase of the fibre fabrication process. At higher voltages, this sample being fabricated at 20 kV, the whipping/stretching stage is more dynamic; during this stage, it is possible that two or more fibres could collide and fuse, creating a single thicker fibre with two cores. However, this phenomenon has only appeared in this sample, so more instances of this should appear in future fibres to give significance to this outcome.

The slightly beaded structure in Figure 4.10 is likely due to the spinneret tip-to-collector distance. Whereas for single-solution fibres, these solutions at this tip-to-collector distance did not produce beaded fibres, the addition of a core solution and the resultant fibres being

much thicker than their single-solution counterparts are all factors that could contribute to this morphology.

For F42-B (Figure 4.10 (g)), the fibre diameter distribution (Figure 4.11) is likely due to the wet fibres. The smaller, lighter fibres were able to avoid contacting the collector before they dried. The wet fibres were likely larger than they appeared in the image. As these fibres made contact with the glass slide, the solution spread out onto the surface. Since these fibres were wet on contact, they likely shrunk due to this solution distribution. If in a drier environment, the size of these fibres was likely larger than what is shown.

Some reasons for the test in Figure 4.10 (g) yielding wet fibres could be the increased volume of water from the increase in temperature between tests, approximately 0.6 degrees Celsius. This seemingly small increase in temperature increased the relative humidity by 4%. This, paired with the larger fibre diameters and the amount of solution ejected during fabrication, could be the difference between wet and dry fibres on the collector.

In Figure 4.10, the interlinking fibres could be due to the fibres still being wet when they come into contact. If they are wet, they will fuse, creating this interlinking pattern. During this contact, if they are not dried enough, they may transfer some of the solutions to one another, evening out the fibre diameters, likely seen in Figure 4.10 f (41-B), especially with the minuscule distances the fluid would travel. Another possibility is that when the fibres are wet, they may combine or consume the smaller fibres, not allowing the fabricated fibre diameters to be viewed, but rather the viewed fibres underwent some transformation on the collector before drying.

The thin veil shell may be the morphology of the fibres. However, it may also involve preparing the sample for SEM viewing. The shell, made of PVDF-HFP, has a glass transition temperature of -35 Celsius. It has greater ductility, allowing it to stretch more during the breaking process and appear as a thin shell when the shell undergoes significant plastic deformation until failure to appear thin. This theory is showcased in Figure 4.14 (c) with the F40B multi-core fibre since it shows signs of significant plastic deformation with large spaces between the cores. However, the shell appears thin with the single fibre in Figure 4.12 (e), but at a closer glance, there is a circular edge to the resin around the fibre,

showing some form of fibre that was in that negative space but deformed into a thin shell during the fibre's breaking.

The multi-core fibres are a phenomenon that has not been regularly reported on for either being unwanted in the research or rarely found depending on the electrospinning parameters. The multi-core fibres grants a different perspective on the trends of increasing voltage and its effects on fibre diameter. With single solution electrospinning at higher voltages it is reported that fibre diameters vary to a higher degree than with lower voltages (actual voltages depend on the polymers used). However, the multi-core fibres show that these fibres may all begin similar in size. The cores found in the multi-core fibres are very similar in size, but it appears that during the stretching/whipping phase they collide with other fibres, fuse, and dry before reaching the collector. This behaviour is viewed at higher voltages, likely due to the higher energy that is used to extract the fibres from the solution. This energy then translates into a more intense stretching phase, which is seen as the fibre diameter reduces initially with increased voltage. This more violent whipping stage increases the likelihood that two or more fibres come into contact, and if they are not yet dry, they will fuse together. This is impossible to distinguish with single solution fibres as these fused fibres are homogeneous, but the multiple cores show this fusion occurs. This fusion is neither bad nor good in general, but like shell shrinkage, its usefulness depends on its application. Multichannel electrospinning has been studied previously but is not a common form of electrospinning, however if its end goal is to create multi-core fibres coaxial electrospinning at higher voltages may be able to create fibres that serve the same purpose. Although in this case not all the multi-core fibres are continuous with themselves, there are some precautions that could be taken to create a more continuous multi-core fibre. A rotating collector has previously been used to create fibres that are much more aligned than the nonwoven fibre mat that was created in these experiments. Furthermore, if conditions could be found that would discourage the fibres from fusing with each other finer fibres may be able to be created than previously possible. It appears that the multi-core fibres do not have the same tendency to form cylindrical fibres as the single core and single solution fibres do. However, there appears to be a trend where the lower voltages lead to fibres with a more cylindrical shape. In Figure 4.14, F23B, although not cylindrical, has a more cylindrical shape than the fibre created in sample F26B, and the same goes for

F40B, with a near perfect cylindrical shape and F41B has a much more irregular shape. When comparing across the shell solution concentrations, F40B has a much more cylindrical shape than F23B. This could also be due to the shell solution taking longer to dry, allowing the fibre to be shaped more in the stretching/whipping stage of electrospinning. More experimentation is needed to see if there are parameters that affect the uniformity of the multi-core fibres, but it is possible that these fibres may be able to be better predicted and controlled as well.

# CHAPTER 5 – Conclusions and Future Work

### *5.1 Conclusion*

This thesis investigated the fabrication and characterization of electrospun polyvinylidene fluoride-hexafluoropropylene (PVDF-HFP) and Chitosan nanofibres for application in high-efficiency face masks and the exploration of coaxial electrospinning techniques to understand the impact of various parameters on fibre morphology. The study began with reviewing the results from the preceding research that explored producing single-solution PVDF-HFP fibres optimized for uniformity and fibre diameter by adjusting the dimethylformamide DMF:Acetone solvent ratios. It was determined that a 1:1 DMF:Acetone ratio yielded the most uniform fibres, a crucial attribute for both mask efficacy and as a precursor to coaxial electrospinning experiments. This was then compounded with finding the ratios of acetic acid and PEO to find the best yield of Chitosan fibres.

The study also explored the layering of fibrous mats and its impact on filtration efficiency, revealing that microstructure plays a more critical role than the layered configuration in determining the overall quality factor of the fibrous mats.

The coaxial electrospinning segment extended this research by experimenting with core-shell fibre structures, aiming to leverage the identified optimal solvent ratios and electrospinning parameters for creating fibres with potentially superior properties. The investigation into coaxial fibres focused on optimizing the core-shell ratios, solvent compositions, and electrospinning parameters to achieve fibres with desired morphological characteristics. SEM analysis confirmed the successful fabrication of core-shell structures, with variations in fibre morphology significantly influenced by the solvent composition and electrospinning conditions.

1. High Filtration face masks were achieved, with a higher filtration efficiency than N95 masks. With the N95 mask MPPS efficiency being 95.17% an MPPS

efficiency of 98.76 was achieved with the PVDF-HFP and Chitosan fibres with both the high beaded and ultra high beaded structures.

2. Using a multi-layered and dual-spun structures showed differences in the pressure drop of the face mask. The multi-layered approach did decrease the pressure drop of the mask by nearly 40 Pa, however, the overall quality factor of all created face masks did not reach that of the N95 face mask (28.7*10^-3) with the dual spun PUB structure and chitosan fibres reaching 24.8*10^-3.

3. Coaxial fibres were successfully produced, and working solutions were found with the shell solution being in the range of 15-20 wt.% PVDF-HFP in 1:1 DMF:Acetone and a core solution of 10% PAN in DMF.

4. All parameters in this study created various core:shell fibres. The uniformity and fibre diameter distribution of these fibres changed as the voltage, shell solution concentration, and shell:core feed rate ratio changed. The most uniform fibres with the smallest fibre distribution would likely be created with a 15 wt% shell concentration, electrospun at 15 kV with a 3:1 shell:core federate ratio.

5. It was visible that many fibres collide and fuse the higher the applied voltage is for electrospinning. What was previously seen as just a diameter variation is due to the collision and fusion of fibres in the stretching/whipping stage.

6. The ratio of core to shell changed depending on the shell solution, voltage, and feed rate ratios. As Acetone was added to the shell solution, the shell shrunk, this can be seen in the SEM images when comparing the 1:1 to the 1:2 DMF:Acetone fibres. This could be due to the effect that Acetone had on the solution's surface tension or the mixing of the core and shell fibres. Increasing voltage has also been shown to shrink the shell percentage of the fibre from 62.95% for a 17.50 shell solution fibre fabricated at 15 kV to 37.38% at 25 kV for the same solution combination, a reduction of approximately 40%. However, increasing the feed rate ratio of the shell:core solutions increased the overall shell percentage of the fibres, with a change from 44.18% to 53.49% when the feed rate ratio changed from 3:2 to 2:1.

### *5.2 Future Work*

This study contributes to the broader understanding of electrospun nanofibre applications in protective face masks and the potential of coaxial electrospinning to create fibres with tailored properties. The findings suggest that creating a face mask/filter with a better filtration efficiency than an N95 mask is very possible, the area of improvement is reducing the pressure drop across the mask. Furthermore, the successful fabrication of core-shell fibres opens avenues for developing advanced materials with customizable properties for various applications beyond face masks, including filtration, drug delivery systems, and composite materials.

Future research should explore the anti-microbial properties of the chitosan/PEO fibres or explore other sterile possibilities for facemasks to combat the transmission of viruses as well as other routes to decrease the pressure drop across a filter without a large negative effect on the filtration efficiency. Additionally, further investigation into the coaxial electrospinning process, focusing on refining core-shell ratios and understanding the impact of various polymers and solvents, as well as the effect of tip-to-collector distance, could show new insights into which parameters such as viscosity, surface tension, conductivity, etc. influence the formation of core-shell structure and if it is applicable across different polymers. Exploring environmental conditions, such as humidity and temperature, on the electrospinning process and the resultant fibre morphology represents another critical area for future studies to enhance the reproducibility and quality of electrospun fibres.

# REFERENCES/BIBLIOGRAPHY


[1] I. Partheniadis, I. Nikolakakis, I. Laidmäe, and J. Heinämäki, "A Mini-Review: Needleless Electrospinning of Nanofibers for Pharmaceutical and Biomedical Applications," *Processes*, vol. 8, no. 6, p. 673, Jun. 2020, doi: 10.3390/pr8060673.

[2] Shepa, I., Mudra, E. and Dusza, J. 'Electrospinning through the prism of Time', Materials Today Chemistry, 21, p. 100543, Aug. 2021, doi:10.1016/j.mtchem.2021.100543.

[3] L. Vysloužilová *et al.*, "Needleless coaxial electrospinning: A novel approach to mass production of coaxial nanofibers," *Int J Pharm*, vol. 516, no. 1–2, pp. 293–300, Jan. 2017, doi: 10.1016/j.ijpharm.2016.11.034.

[4] X. Shi *et al.*, "Electrospinning of Nanofibers and Their Applications for Energy Devices," *J Nanomater*, vol. 2015, pp. 1–20, 2015, doi: 10.1155/2015/140716.

[5] J. Xue, T. Wu, Y. Dai, and Y. Xia, "Electrospinning and Electrospun Nanofibers: Methods, Materials, and Applications," *Chem Rev*, vol. 119, no. 8, pp. 5298–5415, Apr. 2019, doi: 10.1021/acs.chemrev.8b00593.

[6] L. Zeng, H. Xi, X. Liu, and C. Zhang, "Coaxial Electrospinning Construction Si@C Core–Shell Nanofibers for Advanced Flexible Lithium-Ion Batteries," *Nanomaterials*, vol. 11, no. 12, p. 3454, Dec. 2021, doi: 10.3390/nano11123454.

[7] D. Han and A. J. Steckl, "Coaxial Electrospinning Formation of Complex Polymer Fibers and their Applications," *Chempluschem*, vol. 84, no. 10, pp. 1453–1497, Oct. 2019, doi: 10.1002/cplu.201900281.

[8] K. Ghosal *et al.*, "Novel drug delivery systems based on triaxial electrospinning based nanofibers," *React Funct Polym*, vol. 163, p. 104895, Jun. 2021, doi: 10.1016/j.reactfunctpolym.2021.104895.

[9] W. Liu, C. Ni, D. B. Chase, and J. F. Rabolt, "Preparation of Multilayer Biodegradable Nanofibers by Triaxial Electrospinning," *ACS Macro Lett*, vol. 2, no. 6, pp. 466–468, Jun. 2013, doi: 10.1021/mz4000688.

[10] Bhattarai, Rajan, Rinda Bachu, Sai Boddu, and Sarit Bhaduri. "Biomedical Applications of Electrospun Nanofibers: Drug and Nanoparticle Delivery." Pharmaceutics 11, no. 1, Dec, 2018. https://doi.org/10.3390/pharmaceutics11010005.

[11] Y. Xu *et al.*, "Large-Scale Preparation of Polymer Nanofibers for Air Filtration by a New Multineedle Electrospinning Device," *J Nanomater*, vol. 2020, pp. 1–7, Apr. 2020, doi: 10.1155/2020/4965438.

[12] I. S. Chronakis, “Novel nanocomposites and nanoceramics based on polymer nanofibers using electrospinning process—A review,” *J Mater Process Technol*, vol. 167, no. 2–3, pp. 283–293, Aug. 2005, doi: 10.1016/j.jmatprotec.2005.06.053.

[13] Z.-M. Huang, Y.-Z. Zhang, M. Kotaki, and S. Ramakrishna, “A review on polymer nanofibers by electrospinning and their applications in nanocomposites,” *Compos Sci Technol*, vol. 63, no. 15, pp. 2223–2253, Nov. 2003, doi: 10.1016/S0266-3538(03)00178-7.

[14] N. Bhardwaj and S. C. Kundu, “Electrospinning: A fascinating fiber fabrication technique,” *Biotechnol Adv*, vol. 28, no. 3, pp. 325–347, May 2010, doi: 10.1016/j.biotechadv.2010.01.004.

[15] C. J. Luo, M. Nangrejo, and M. Edirisinghe, “A novel method of selecting solvents for polymer electrospinning,” *Polymer (Guildf)*, vol. 51, no. 7, pp. 1654–1662, Mar. 2010, doi: 10.1016/j.polymer.2010.01.031.

[16] J. Xue, T. Wu, Y. Dai, and Y. Xia, “Electrospinning and Electrospun Nanofibers: Methods, Materials, and Applications.,” *Chem Rev*, vol. 119, no. 8, pp. 5298–5415, Apr. 2019, doi: 10.1021/acs.chemrev.8b00593.

[17] Mohamed. A. Alnaqbi, A. G. Al Blooshi, and Y. E. Greish, “Polyethylene and Polyvinyl Chloride-Blended Polystyrene Nanofibrous Sorbents and Their Application in the Removal of Various Oil Spills,” *Advances in Polymer Technology*, vol. 2020, pp. 1–12, Apr. 2020, doi: 10.1155/2020/4097520.

[18] M. Bazgir *et al.*, “Degradation and Characterisation of Electrospun Polycaprolactone (PCL) and Poly(lactic-co-glycolic acid) (PLGA) Scaffolds for Vascular Tissue Engineering,” *Materials*, vol. 14, no. 17, p. 4773, Aug. 2021, doi: 10.3390/ma14174773.

[19] C. Bavatharani *et al.*, “Electrospinning technique for production of polyaniline nanocomposites/nanofibres for multi-functional applications: A review,” *Synth Met*, vol. 271, p. 116609, Jan. 2021, doi: 10.1016/j.synthmet.2020.116609.

[20] I. A. Borojeni, G. Gajewski, A. Jenab, M. Sanjari, C. Boudreault, and R. A. Riahi, “Fabrication of Ultra-High-Performance PVDF-HFP Air Filters by Electrospinning,” *Fibers*, vol. 11, no. 8, p. 71, Aug. 2023, doi: 10.3390/fib11080071.

[21] S. S. Ashraf, K. Parivar, N. Hayati Roodbari, S. Mashayekhan, and N. Amini, “Fabrication and characterization of biaxially electrospun collagen/alginate nanofibers, improved with Rhodotorula mucilaginosa sp. GUMS16 produced exopolysaccharides for wound healing applications,” *Int J Biol Macromol*, vol. 196, pp. 194–203, Jan. 2022, doi: 10.1016/j.ijbiomac.2021.11.132.

[22] S. L. Shenoy, W. D. Bates, H. L. Frisch, and G. E. Wnek, “Role of chain entanglements on fiber formation during electrospinning of polymer solutions: good

solvent, non-specific polymer–polymer interaction limit," *Polymer (Guildf)*, vol. 46, no. 10, pp. 3372–3384, Apr. 2005, doi: 10.1016/j.polymer.2005.03.011.

[23] J. Avossa, G. Herwig, C. Toncelli, F. Itel, and R. M. Rossi, "Electrospinning based on benign solvents: current definitions, implications and strategies," *Green Chemistry*, vol. 24, no. 6, pp. 2347–2375, 2022, doi: 10.1039/D1GC04252A.

[24] T. Uyar and F. Besenbacher, "Electrospinning of uniform polystyrene fibers: The effect of solvent conductivity," *Polymer (Guildf)*, vol. 49, no. 24, pp. 5336–5343, Nov. 2008, doi: 10.1016/j.polymer.2008.09.025.

[25] L. Wannatong, A. Sirivat, and P. Supaphol, "Effects of solvents on electrospun polymeric fibers: preliminary study on polystyrene," *Polym Int*, vol. 53, no. 11, pp. 1851–1859, Nov. 2004, doi: 10.1002/pi.1599.

[26] C. J. Cooper, A. K. Mohanty, and M. Misra, "Electrospinning Process and Structure Relationship of Biobased Poly(butylene succinate) for Nanoporous Fibers," *ACS Omega*, vol. 3, no. 5, pp. 5547–5557, May 2018, doi: 10.1021/acsomega.8b00332.

[27] P. Nuamcharoen, T. Kobayashi, and P. Potiyaraj, "Influence of volatile solvents and mixing ratios of binary solvent systems on morphology and performance of electrospun poly(vinylidene fluoride) nanofibers," *Polym Int*, vol. 70, no. 10, pp. 1465–1477, Oct. 2021, doi: 10.1002/pi.6218.

[28] A. Attout, S. Yunus, and P. Bertrand, "Electrospinning and alignment of polyaniline-based nanowires and nanotubes," *Polym Eng Sci*, vol. 48, no. 9, pp. 1661–1666, Sep. 2008, doi: 10.1002/pen.20969.

[29] P. Ginestra, E. Ceretti, and A. Fiorentino, "Electrospinning of Poly-caprolactone for Scaffold Manufacturing: Experimental Investigation on the Process Parameters Influence," *Procedia CIRP*, vol. 49, pp. 8–13, 2016, doi: 10.1016/j.procir.2015.07.020.

[30] M. M. Demir, I. Yilgor, E. Yilgor, and B. Erman, "Electrospinning of polyurethane fibers," *Polymer (Guildf)*, vol. 43, no. 11, pp. 3303–3309, May 2002, doi: 10.1016/S0032-3861(02)00136-2.

[31] A. Dodero, E. Brunengo, M. Alloisio, A. Sionkowska, S. Vicini, and M. Castellano, "Chitosan-based electrospun membranes: Effects of solution viscosity, coagulant and crosslinker," *Carbohydr Polym*, vol. 235, p. 115976, May 2020, doi: 10.1016/j.carbpol.2020.115976.

[32] E. Araújo, M. Nascimento, and H. de Oliveira, "Electrospinning of Polymeric Fibres: an Unconventional View on the Influence of Surface Tension on Fibre Diameter," *Fibres and Textiles in Eastern Europe*, vol. 24, no. 1(115), pp. 22–29, Jan. 2016, doi: 10.5604/12303666.1172083.

[33] N. Amariei, L. R. Manea, A. P. Bertea, A. Bertea, and A. Popa, “The Influence of Polymer Solution on the Properties of Electrospun 3D Nanostructures,” *IOP Conf Ser Mater Sci Eng*, vol. 209, p. 012092, Jun. 2017, doi: 10.1088/1757-899X/209/1/012092.

[34] Z. Li and C. Wang, “Effects of Working Parameters on Electrospinning,” in *One-Dimensional Nanostructures - Electrospinning Technique and Unique Nanofibers*, 2013, pp. 15–28. doi: 10.1007/978-3-642-36427-3_2.

[35] E. Ewaldz, J. Randrup, and B. Brettmann, “Solvent Effects on the Elasticity of Electrospinnable Polymer Solutions,” *ACS Polymers Au*, vol. 2, no. 2, pp. 108–117, Apr. 2022, doi: 10.1021/acspolymersau.1c00041.

[36] S. V. Fridrikh, J. H. Yu, M. P. Brenner, and G. C. Rutledge, “Controlling the Fiber Diameter during Electrospinning,” *Phys Rev Lett*, vol. 90, no. 14, p. 144502, Apr. 2003, doi: 10.1103/PhysRevLett.90.144502.

[37] P. Heikkila and A. Harlin, “Electrospinning of polyacrylonitrile (PAN) solution: Effect of conductive additive and filler on the process,” *Express Polym Lett*, vol. 3, no. 7, pp. 437–445, 2009, doi: 10.3144/expresspolymlett.2009.53.

[38] N. Wang, X. Mao, S. Zhang, J. Yu, and B. Ding, “Electrospun Nanofibers for Air Filtration,” 2014, pp. 299–323. doi: 10.1007/978-3-642-54160-5_12.

[39] F. N. H. Karabulut, G. Höfler, N. Ashok Chand, and G. W. Beckermann, “Electrospun Nanofibre Filtration Media to Protect against Biological or Nonbiological Airborne Particles,” *Polymers (Basel)*, vol. 13, no. 19, p. 3257, Sep. 2021, doi: 10.3390/polym13193257.

[40] S. Ullah *et al.*, “Reusability Comparison of Melt-Blown vs Nanofiber Face Mask Filters for Use in the Coronavirus Pandemic,” *ACS Appl Nano Mater*, vol. 3, no. 7, pp. 7231–7241, Jul. 2020, doi: 10.1021/acsanm.0c01562.

[41] M. Jafari, E. Shim, and A. Joijode, “Fabrication of Poly(lactic acid) filter media via the meltblowing process and their filtration performances: A comparative study with polypropylene meltblown,” *Sep Purif Technol*, vol. 260, p. 118185, Apr. 2021, doi: 10.1016/j.seppur.2020.118185.

[42] GregoryF. Ward, “Meltblown nanofibres for nonwoven filtration applications,” *Filtration & Separation*, vol. 38, no. 9, pp. 42–43, Nov. 2001, doi: 10.1016/S0015-1882(01)80540-1.

[43] Y. Xu, X. Zhang, X. Hao, D. Teng, T. Zhao, and Y. Zeng, “Micro/nanofibrous nonwovens with high filtration performance and radiative heat dissipation property for personal protective face mask,” *Chemical Engineering Journal*, vol. 423, p. 130175, Nov. 2021, doi: 10.1016/j.cej.2021.130175.

[44] J. Li, W. Wang, R. Jiang, and C. Guo, “Antiviral Electrospun Polymer Composites: Recent Advances and Opportunities for Tackling COVID-19,” *Front Mater*, vol. 8, Nov. 2021, doi: 10.3389/fmats.2021.773205.

[45] Z. Yue, J. Zhou, X. Du, L. Wu, J. Wang, and X. Wang, “Incorporating charged Ag@MOFs to boost the antibacterial and filtration properties of porous electrospinning polylactide films,” *Int J Biol Macromol*, vol. 250, p. 126223, Oct. 2023, doi: 10.1016/j.ijbiomac.2023.126223.

[46] A. Refate *et al.*, “Influence of electrospinning parameters on biopolymers nanofibers, with emphasis on cellulose & chitosan,” *Heliyon*, vol. 9, no. 6, p. e17051, Jun. 2023, doi: 10.1016/j.heliyon.2023.e17051.

[47] S. Mallakpour, E. Azadi, and C. M. Hussain, “Fabrication of air filters with advanced filtration performance for removal of viral aerosols and control the spread of COVID-19,” *Adv Colloid Interface Sci*, vol. 303, p. 102653, May 2022, doi: 10.1016/j.cis.2022.102653.

[48] H. Zhang *et al.*, “Electrospun Ribbon-Like Microfiber Films of a Novel Guanidine-Based ABA Triblock Copolymer: Fabrication, Antibacterial Activity, and Cytotoxicity,” *Macromol Chem Phys*, vol. 220, no. 13, Jul. 2019, doi: 10.1002/macp.201900138.

[49] T. Li, M. Sun, and S. Wu, “State-of-the-Art Review of Electrospun Gelatin-Based Nanofiber Dressings for Wound Healing Applications,” *Nanomaterials*, vol. 12, no. 5, p. 784, Feb. 2022, doi: 10.3390/nano12050784.

[50] I. Maliszewska and T. Czapka, “Electrospun Polymer Nanofibers with Antimicrobial Activity,” *Polymers (Basel)*, vol. 14, no. 9, p. 1661, Apr. 2022, doi: 10.3390/polym14091661.

[51] F. N. H. Karabulut, D. Fomra, G. Höfler, N. A. Chand, and G. W. Beckermann, “Virucidal and Bactericidal Filtration Media from Electrospun Polylactic Acid Nanofibres Capable of Protecting against COVID-19,” *Membranes (Basel)*, vol. 12, no. 6, p. 571, May 2022, doi: 10.3390/membranes12060571.

[52] C. López de Dicastillo, C. Patiño, M. Galotto, J. Palma, D. Alburquenque, and J. Escrig, “Novel Antimicrobial Titanium Dioxide Nanotubes Obtained through a Combination of Atomic Layer Deposition and Electrospinning Technologies,” *Nanomaterials*, vol. 8, no. 2, p. 128, Feb. 2018, doi: 10.3390/nano8020128.

[53] D. Kwaśniewska, Y.-L. Chen, and D. Wieczorek, “Biological Activity of Quaternary Ammonium Salts and Their Derivatives,” *Pathogens*, vol. 9, no. 6, p. 459, Jun. 2020, doi: 10.3390/pathogens9060459.

[54] H. Y. Chi *et al.*, “Fabrication of Gelatin Nanofibers by Electrospinning—Mixture of Gelatin and Polyvinyl Alcohol,” *Polymers (Basel)*, vol. 14, no. 13, p. 2610, Jun. 2022, doi: 10.3390/polym14132610.

[55] G. P. Tamilarasi, G. Sabarees, K. Manikandan, S. Gouthaman, V. Alagarsamy, and V. R. Solomon, “Advances in electrospun chitosan nanofiber biomaterials for biomedical applications,” *Mater Adv*, vol. 4, no. 15, pp. 3114–3139, 2023, doi: 10.1039/D3MA00010A.

[56] C. Cui, S. Sun, S. Wu, S. Chen, J. Ma, and F. Zhou, “Electrospun chitosan nanofibers for wound healing application,” *Engineered Regeneration*, vol. 2, pp. 82–90, 2021, doi: 10.1016/j.engreg.2021.08.001.

[57] I. A. Borojeni, G. Gajewski, and R. A. Riahi, “Application of Electrospun Nonwoven Fibers in Air Filters,” *Fibers*, vol. 10, no. 2, p. 15, Feb. 2022, doi: 10.3390/fib10020015.

[58] V. S. Naragund and P. K. Panda, “Electrospun nanofiber-based respiratory face masks—a review,” *Emergent Mater*, vol. 5, no. 2, pp. 261–278, Apr. 2022, doi: 10.1007/s42247-022-00350-6.

[59] Z. Lin, Z. Wang, X. Zhang, and D. Diao, “Superhydrophobic, photo-sterilize, and reusable mask based on graphene nanosheet-embedded carbon (GNEC) film,” *Nano Res*, vol. 14, no. 4, pp. 1110–1115, Apr. 2021, doi: 10.1007/s12274-020-3158-1.

[60] A. I. Quilez-Molina *et al.*, “Encapsulation of Copper Nanoparticles in Electrospun Nanofibers for Sustainable Removal of Pesticides,” *ACS Appl Mater Interfaces*, vol. 15, no. 16, pp. 20385–20397, Apr. 2023, doi: 10.1021/acsami.3c00849.

[61] A. A. I. A. S. Komaladewi, K. Khoiruddin, I. W. Surata, I. D. G. A. Subagia, and I. G. Wenten, “Recent advances in antimicrobial air filter,” *E3S Web of Conferences*, vol. 67, p. 03016, Nov. 2018, doi: 10.1051/e3sconf/20186703016.

[62] S. P. Deshmukh, S. M. Patil, S. B. Mullani, and S. D. Delekar, “Silver nanoparticles as an effective disinfectant: A review,” *Materials Science and Engineering: C*, vol. 97, pp. 954–965, Apr. 2019, doi: 10.1016/j.msec.2018.12.102.

[63] A. R. Gliga, S. Skoglund, I. Odnevall Wallinder, B. Fadeel, and H. L. Karlsson, “Size-dependent cytotoxicity of silver nanoparticles in human lung cells: the role of cellular uptake, agglomeration and Ag release,” *Part Fibre Toxicol*, vol. 11, no. 1, p. 11, Dec. 2014, doi: 10.1186/1743-8977-11-11.

[64] M.-W. Kim *et al.*, “Reusable and durable electrostatic air filter based on hybrid metallized microfibers decorated with metal–organic–framework nanocrystals,” *J Mater Sci Technol*, vol. 85, pp. 44–55, Sep. 2021, doi: 10.1016/j.jmst.2020.12.065.

[65] D. M. Mihut and A. Afshar, “Electrically assisted silver and copper coated filter papers with enhanced bactericidal effects,” *Colloids Surf A Physicochem Eng Asp*, vol. 606, p. 125428, Dec. 2020, doi: 10.1016/j.colsurfa.2020.125428.

[66] M. Hejazy, M. K. Koohi, A. B. M. Pour, and D. Najafi, “Toxicity of manufactured copper nanoparticles - A review,” *Nanomedicine Research Journal*, vol. 3, no. 1, pp. 1–9, Feb. 2018.

[67] C. Pokhum *et al.*, “A facile and cost-effective method for removal of indoor airborne psychrotrophic bacterial and fungal flora based on silver and zinc oxide nanoparticles decorated on fibrous air filter,” *Atmos Pollut Res*, vol. 9, no. 1, pp. 172–177, Jan. 2018, doi: 10.1016/j.apr.2017.08.005.

[68] Y. Cao, M. Naseri, Y. He, C. Xu, L. J. Walsh, and Z. M. Ziora, “Non-antibiotic antimicrobial agents to combat biofilm-forming bacteria,” *J Glob Antimicrob Resist*, vol. 21, pp. 445–451, Jun. 2020, doi: 10.1016/j.jgar.2019.11.012.

[69] S. M. El-Megharbel, M. Alsawat, F. A. Al-Salmi, and R. Z. Hamza, “Utilizing of (Zinc Oxide Nano-Spray) for Disinfection against ‘SARS-CoV-2’ and Testing Its Biological Effectiveness on Some Biochemical Parameters during (COVID-19 Pandemic)—”ZnO Nanoparticles Have Antiviral Activity against (SARS-CoV-2)”,” *Coatings*, vol. 11, no. 4, p. 388, Mar. 2021, doi: 10.3390/coatings11040388.

[70] S.-M. Ji, A. P. Tiwari, H. J. Oh, and H.-Y. Kim, “ZnO/Ag nanoparticles incorporated multifunctional parallel side by side nanofibers for air filtration with enhanced removing organic contaminants and antibacterial properties,” *Colloids Surf A Physicochem Eng Asp*, vol. 621, p. 126564, Jul. 2021, doi: 10.1016/j.colsurfa.2021.126564.

[71] F. Russo, R. Castro-Muñoz, S. Santoro, F. Galiano, and A. Figoli, “A review on electrospun membranes for potential air filtration application,” *J Environ Chem Eng*, vol. 10, no. 5, p. 108452, Oct. 2022, doi: 10.1016/j.jece.2022.108452.

[72] M. Zhu *et al.*, “Electrospun Nanofibers Membranes for Effective Air Filtration,” *Macromol Mater Eng*, vol. 302, no. 1, p. 1600353, Jan. 2017, doi: 10.1002/mame.201600353.

[73] B. V. Ramarao, C. Tien, and S. Mohan, “Calculation of single fiber efficiencies for interception and impaction with superposed brownian motion,” *J Aerosol Sci*, vol. 25, no. 2, pp. 295–313, Mar. 1994, doi: 10.1016/0021-8502(94)90081-7.

[74] S. K. Friedlander, “Theory of Aerosol Filtration,” *Ind Eng Chem*, vol. 50, no. 8, pp. 1161–1164, Aug. 1958, doi: 10.1021/ie50584a036.

[75] C. YANG, “Aerosol Filtration Application Using Fibrous Media—An Industrial Perspective,” *Chin J Chem Eng*, vol. 20, no. 1, pp. 1–9, Feb. 2012, doi: 10.1016/S1004-9541(12)60356-5.

[76] Y. Liu, X. Chen, Y. Liu, Y. Gao, and P. Liu, “Electrospun Coaxial Fibers to Optimize the Release of Poorly Water-Soluble Drug,” *Polymers (Basel)*, vol. 14, no. 3, p. 469, Jan. 2022, doi: 10.3390/polym14030469.

[77] P. Li *et al.*, "Coaxial electrospinning core-shell fibers for self-healing scratch on coatings," *Chinese Chemical Letters*, vol. 30, no. 1, pp. 157–159, Jan. 2019, doi: 10.1016/j.cclet.2018.01.037.

[78] P. McClellan and W. J. Landis, "Recent Applications of Coaxial and Emulsion Electrospinning Methods in the Field of Tissue Engineering," *Biores Open Access*, vol. 5, no. 1, pp. 212–227, May 2016, doi: 10.1089/biores.2016.0022.

[79] T. J. Longson, R. Bhowmick, C. Gu, and B. A. Cruden, "Core–Shell Interactions in Coaxial Electrospinning and Impact on Electrospun Multiwall Carbon Nanotube Core, Poly(methyl methacrylate) Shell Fibers," *The Journal of Physical Chemistry C*, vol. 115, no. 26, pp. 12742–12750, Jul. 2011, doi: 10.1021/jp201077p.

[80] P. Rathore and J. D. Schiffman, "Beyond the Single-Nozzle: Coaxial Electrospinning Enables Innovative Nanofiber Chemistries, Geometries, and Applications," *ACS Appl Mater Interfaces*, vol. 13, no. 1, pp. 48–66, Jan. 2021, doi: 10.1021/acsami.0c17706.

[81] D. Puppi and F. Chiellini, "Drug release kinetics of electrospun fibrous systems," in *Core-Shell Nanostructures for Drug Delivery and Theranostics*, Elsevier, 2018, pp. 349–374. doi: 10.1016/B978-0-08-102198-9.00012-0.

[82] B. S. Gupta and A. K. Moghe, "Nanofiber structures for medical biotextiles," in *Biotextiles as Medical Implants*, Elsevier, 2013, pp. 48–90. doi: 10.1533/9780857095602.1.48.

[83] S. Vats, M. Anyfantakis, L. W. Honaker, F. Basoli, and J. P. F. Lagerwall, "Stable Electrospinning of Core-Functionalized Coaxial Fibers Enabled by the Minimum-Energy Interface Given by Partial Core–Sheath Miscibility," *Langmuir*, vol. 37, no. 45, pp. 13265–13277, Nov. 2021, doi: 10.1021/acs.langmuir.1c01824.

[84] H. Sun, W. Mu, X. Cui, Z. Xu, T. Zhang, and Y. Zhao, "Polymer-Encapsulated Aerogel Fibers Prepared via Coaxial Wet Spinning with Stepwise Coagulation for Thermal Insulation," *ACS Appl Polym Mater*, vol. 5, no. 1, pp. 552–559, Jan. 2023, doi: 10.1021/acsapm.2c01648.

[85] M. He, H. Jiang, R. Wang, Y. Xie, and C. Zhao, "Fabrication of metronidazole loaded poly (ε-caprolactone)/zein core/shell nanofiber membranes via coaxial electrospinning for guided tissue regeneration," *J Colloid Interface Sci*, vol. 490, pp. 270–278, Mar. 2017, doi: 10.1016/j.jcis.2016.11.062.

[86] A. ur R. Khan *et al.*, "Multifunctional bioactive core-shell electrospun membrane capable to terminate inflammatory cycle and promote angiogenesis in diabetic wound," *Bioact Mater*, vol. 6, no. 9, pp. 2783–2800, Sep. 2021, doi: 10.1016/j.bioactmat.2021.01.040.

[87] H. Zhao and H. Chi, “Electrospun Bead-on-String Fibers: Useless or Something of Value?,” in *Novel Aspects of Nanofibers*, InTech, 2018. doi: 10.5772/intechopen.74661.

[88] J. Anu Bhushani and C. Anandharamakrishnan, “Electrospinning and electrospraying techniques: Potential food based applications,” *Trends Food Sci Technol*, vol. 38, no. 1, pp. 21–33, Jul. 2014, doi: 10.1016/j.tifs.2014.03.004.

[89] R. M. Nezarati, M. B. Eifert, and E. Cosgriff-Hernandez, “Effects of Humidity and Solution Viscosity on Electrospun Fiber Morphology,” *Tissue Eng Part C Methods*, vol. 19, no. 10, pp. 810–819, Oct. 2013, doi: 10.1089/ten.tec.2012.0671.

[90] P. K. Szewczyk and U. Stachewicz, “The impact of relative humidity on electrospun polymer fibers: From structural changes to fiber morphology,” *Adv Colloid Interface Sci*, vol. 286, p. 102315, Dec. 2020, doi: 10.1016/j.cis.2020.102315.

[91] C.-L. Pai, M. C. Boyce, and G. C. Rutledge, “Morphology of Porous and Wrinkled Fibers of Polystyrene Electrospun from Dimethylformamide,” *Macromolecules*, vol. 42, no. 6, pp. 2102–2114, Mar. 2009, doi: 10.1021/ma802529h.

[92] J. Pelipenko, J. Kristl, B. Janković, S. Baumgartner, and P. Kocbek, “The impact of relative humidity during electrospinning on the morphology and mechanical properties of nanofibers,” *Int J Pharm*, vol. 456, no. 1, pp. 125–134, Nov. 2013, doi: 10.1016/j.ijpharm.2013.07.078.

[93] B. K. Park and I. C. Um, “Effect of Relative Humidity on the Electrospinning Performance of Regenerated Silk Solution,” *Polymers (Basel)*, vol. 13, no. 15, p. 2479, Jul. 2021, doi: 10.3390/polym13152479.

[94] S. Megelski, J. S. Stephens, D. B. Chase, and J. F. Rabolt, “Micro- and Nanostructured Surface Morphology on Electrospun Polymer Fibers,” *Macromolecules*, vol. 35, no. 22, pp. 8456–8466, Oct. 2002, doi: 10.1021/ma020444a.

[95] S. De Vrieze, T. Van Camp, A. Nelvig, B. Hagström, P. Westbroek, and K. De Clerck, “The effect of temperature and humidity on electrospinning,” *J Mater Sci*, vol. 44, no. 5, pp. 1357–1362, Mar. 2009, doi: 10.1007/s10853-008-3010-6.

[96] C. Wang, H.-S. Chien, C.-H. Hsu, Y.-C. Wang, C.-T. Wang, and H.-A. Lu, “Electrospinning of Polyacrylonitrile Solutions at Elevated Temperatures,” *Macromolecules*, vol. 40, no. 22, pp. 7973–7983, Oct. 2007, doi: 10.1021/ma070508n.

[97] N. M. Jalal, A. R. Jabur, and S. Allami, “Effect of Electro-spinning applied Voltage on Electro-spun EPS Membranes Thickness and Fibers Diameters,” *J Phys Conf Ser*, vol. 1879, no. 3, p. 032085, May 2021, doi: 10.1088/1742-6596/1879/3/032085.

[98] L. A. Can-Herrera, A. I. Oliva, M. A. A. Dzul-Cervantes, O. F. Pacheco-Salazar, and J. M. Cervantes-Uc, "Morphological and Mechanical Properties of Electrospun Polycaprolactone Scaffolds: Effect of Applied Voltage," *Polymers (Basel)*, vol. 13, no. 4, p. 662, Feb. 2021, doi: 10.3390/polym13040662.

[99] D. Rodoplu and M. Mutlu, "Effects of Electrospinning Setup and Process Parameters on Nanofiber Morphology Intended for the Modification of Quartz Crystal Microbalance Surfaces," *J Eng Fiber Fabr*, vol. 7, no. 2, p. 155892501200700, Jun. 2012, doi: 10.1177/155892501200700217.

[100] Y. Duan, L. Kalluri, M. Satpathy, and Y. Duan, "Effect of Electrospinning Parameters on the Fiber Diameter and Morphology of PLGA Nanofibers," *Dental Oral Biology and Craniofacial Research*, pp. 1–7, May 2021, doi: 10.31487/j.DOBCR.2021.02.04.

[101] N. Joy, R. Anuraj, A. Viravalli, H. N. Dixit, and S. Samavedi, "Coupling between voltage and tip-to-collector distance in polymer electrospinning: Insights from analysis of regimes, transitions and cone/jet features," *Chem Eng Sci*, vol. 230, p. 116200, Feb. 2021, doi: 10.1016/j.ces.2020.116200.

[102] A. H. Hekmati, A. Rashidi, R. Ghazisaeidi, and J.-Y. Drean, "Effect of needle length, electrospinning distance, and solution concentration on morphological properties of polyamide-6 electrospun nanowebs," *Textile Research Journal*, vol. 83, no. 14, pp. 1452–1466, Sep. 2013, doi: 10.1177/0040517512471746.

[103] S. Suresh, A. Becker, and B. Glasmacher, "Impact of Apparatus Orientation and Gravity in Electrospinning—A Review of Empirical Evidence," *Polymers (Basel)*, vol. 12, no. 11, p. 2448, Oct. 2020, doi: 10.3390/polym12112448.

[104] H. Yuan, Q. Zhou, and Y. Zhang, "Improving fiber alignment during electrospinning," in *Electrospun Nanofibers*, Elsevier, 2017, pp. 125–147. doi: 10.1016/B978-0-08-100907-9.00006-4.

[105] S. Zargham, S. Bazgir, A. Tavakoli, A. S. Rashidi, and R. Damerchely, "The Effect of Flow Rate on Morphology and Deposition Area of Electrospun Nylon 6 Nanofiber," *J Eng Fiber Fabr*, vol. 7, no. 4, p. 155892501200700, Dec. 2012, doi: 10.1177/155892501200700414.

[106] Q. Wei, D. Tao, and Y. Xu, "Nanofibers: principles and manufacture," in *Functional Nanofibers and their Applications*, Elsevier, 2012, pp. 3–21. doi: 10.1533/9780857095640.1.1.

[107] M. S. Mu'min *et al.*, "Electrospun phosphonated poly(pentafluorostyrene) nanofibers as a reinforcement of Nafion membranes for fuel cell application," *J Memb Sci*, vol. 685, p. 121915, Nov. 2023, doi: 10.1016/j.memsci.2023.121915.

[108] C. J. Angammana and S. H. Jayaram, “Analysis of the Effects of Solution Conductivity on Electrospinning Process and Fiber Morphology,” *IEEE Trans Ind Appl*, vol. 47, no. 3, pp. 1109–1117, May 2011, doi: 10.1109/TIA.2011.2127431.

[109] Z. Sun, J. M. Deitzel, J. Knopf, X. Chen, and J. W. Gillespie, “The effect of solvent dielectric properties on the collection of oriented electrospun fibers,” *J Appl Polym Sci*, vol. 125, no. 4, pp. 2585–2594, Aug. 2012, doi: 10.1002/app.35454.

[110] Y.-K. Wu, L. Wang, J. Fan, W. Shou, B.-M. Zhou, and Y. Liu, “Multi-Jet Electrospinning with Auxiliary Electrode: The Influence of Solution Properties,” *Polymers (Basel)*, vol. 10, no. 6, p. 572, May 2018, doi: 10.3390/polym10060572.

[111] K. Yan, Y. Le, H. Mengen, L. Zhongbo, and H. Zhulin, “Effect of Solution Miscibility on the Morphology of Coaxial Electrospun Cellulose Acetate Nanofibers,” *Polymers (Basel)*, vol. 13, no. 24, p. 4419, Dec. 2021, doi: 10.3390/polym13244419.

[112] J. H. Yu, S. V. Fridrikh, and G. C. Rutledge, “Production of Submicrometer Diameter Fibers by Two-Fluid Electrospinning,” *Advanced Materials*, vol. 16, no. 17, pp. 1562–1566, Sep. 2004, doi: 10.1002/adma.200306644.

[113] Z. Sun, E. Zussman, A. L. Yarin, J. H. Wendorff, and A. Greiner, “Compound Core–Shell Polymer Nanofibers by Co-Electrospinning,” *Advanced Materials*, vol. 15, no. 22, pp. 1929–1932, Nov. 2003, doi: 10.1002/adma.200305136.

[114] D.-G. Yu, J.-H. Yu, L. Chen, G. R. Williams, and X. Wang, “Modified coaxial electrospinning for the preparation of high-quality ketoprofen-loaded cellulose acetate nanofibers,” *Carbohydr Polym*, vol. 90, no. 2, pp. 1016–1023, Oct. 2012, doi: 10.1016/j.carbpol.2012.06.036.

[115] G. Larsen, R. Spretz, and R. Velarde-Ortiz, “Use of Coaxial Gas Jackets to Stabilize Taylor Cones of Volatile Solutions and to Induce Particle-to-Fiber Transitions,” *Advanced Materials*, vol. 16, no. 2, pp. 166–169, Jan. 2004, doi: 10.1002/adma.200306021.

[116] D. Han and A. J. Steckl, “Superhydrophobic and Oleophobic Fibers by Coaxial Electrospinning,” *Langmuir*, vol. 25, no. 16, pp. 9454–9462, Aug. 2009, doi: 10.1021/la900660v.

[117] J. E. Díaz, A. Barrero, M. Márquez, and I. G. Loscertales, “Controlled Encapsulation of Hydrophobic Liquids in Hydrophilic Polymer Nanofibers by Co-electrospinning,” *Adv Funct Mater*, vol. 16, no. 16, pp. 2110–2116, Oct. 2006, doi: 10.1002/adfm.200600204.

[118] A. K. Moghe and B. S. Gupta, “Co-axial Electrospinning for Nanofiber Structures: Preparation and Applications,” *Polymer Reviews*, vol. 48, no. 2, pp. 353–377, May 2008, doi: 10.1080/15583720802022257.

[119] M. Li, Y. Zheng, B. Xin, and Y. Xu, “Coaxial Electrospinning: Jet Motion, Core–Shell Fiber Morphology, and Structure as a Function of Material Parameters,” *Ind Eng Chem Res*, vol. 59, no. 13, pp. 6301–6308, Apr. 2020, doi: 10.1021/acs.iecr.9b05866.

[120] R. P. Gonçalves, F. F. F. da Silva, P. H. S. Picciani, and M. L. Dias, “Morphology and Thermal Properties of Core-Shell PVA/PLA Ultrafine Fibers Produced by Coaxial Electrospinning,” *Materials Sciences and Applications*, vol. 06, no. 02, pp. 189–199, 2015, doi: 10.4236/msa.2015.62022.

[121] Y. Liu *et al.*, “Phase separation of a PVDF–HFP film on an ice substrate to achieve self-polarisation alignment,” *Nano Energy*, vol. 106, p. 108082, Feb. 2023, doi: 10.1016/j.nanoen.2022.108082.

[122] P. Filip, J. Zelenkova, and P. Peer, “Electrospinning of a Copolymer PVDF-co-HFP Solved in DMF/Acetone: Explicit Relations among Viscosity, Polymer Concentration, DMF/Acetone Ratio and Mean Nanofiber Diameter,” *Polymers (Basel)*, vol. 13, no. 19, p. 3418, Oct. 2021, doi: 10.3390/polym13193418.

[123] W. W.-F. Leung and Q. Sun, “Charged PVDF multilayer nanofiber filter in filtering simulated airborne novel coronavirus (COVID-19) using ambient nano-aerosols,” *Sep Purif Technol*, vol. 245, p. 116887, Aug. 2020, doi: 10.1016/j.seppur.2020.116887.

[124] W. W.-F. Leung, C.-H. Hung, and P.-T. Yuen, “Effect of face velocity, nanofiber packing density and thickness on filtration performance of filters with nanofibers coated on a substrate,” *Sep Purif Technol*, vol. 71, no. 1, pp. 30–37, Jan. 2010, doi: 10.1016/j.seppur.2009.10.017.

[125] Z. Wang, C. Zhao, and Z. Pan, “Porous bead-on-string poly(lactic acid) fibrous membranes for air filtration,” *J Colloid Interface Sci*, vol. 441, pp. 121–129, Mar. 2015, doi: 10.1016/j.jcis.2014.11.041.

[126] N. Mao, “Nonwoven fabric filters,” in *Fibrous Filter Media*, Elsevier, 2017, pp. 133–171. doi: 10.1016/B978-0-08-100573-6.00005-8.

[127] Geng, X., Kwon, O. H., & Jang, J. (2005). Electrospinning of chitosan dissolved in concentrated acetic acid solution. Biomaterials, 26(27), 5427–5432.

[128] Sencadas, V., Correia, D. M., Areias, A., Botelho, G., Fonseca, A. M., Neves, I. C., Gomez Ribelles, J. L., & Lanceros Mendez, S. (2012). Determination of the parameters affecting electrospun chitosan fiber size distribution and morphology. Carbohydrate Polymers, 87(2), 1295–1301.

[129] Zargham, S., Bazgir, S., Tavakoli, A., Rashidi, A. S., & Damerchely, R. (2012). The effect of flow rate on morphology and deposition area of electrospun nylon 6 nanofiber. Journal of Engineered Fibers and Fabrics, 7(4), 42–49.

[130] Le, N. T., Myrick, J. M., Seigle, T., Huynh, P. T., & Krishnan, S. (2018). Mapping electrospray modes and droplet size distributions for chitosan solutions in unentangled and entangled concentration regimes. Advanced Powder Technology, 29(12), 3007–3021. https://doi.org/10.1016/j.apt.2018.10.006 [5]Pakravan, M., Heuzey, M. C., & Ajji, A. (2011). A fundamental study of chitosan/PEO electrospinning. Polymer, 52(21), 4813–4824.

[131] Sener, A. G., Altay, A. S., & Altay, F. (2011). Effect of voltage on morphology of electrospun nanofibers. ELECO 2011 - 7th International Conference on Electrical and Electronics Engineering, January 2011.

[132] V. Paolucci *et al.*, "Sustainable Liquid-Phase Exfoliation of Layered Materials with Nontoxic Polarclean Solvent," *ACS Sustain Chem Eng*, vol. 8, no. 51, pp. 18830–18840, Dec. 2020, doi: 10.1021/acssuschemeng.0c04191.

[133] N. M. Salih, U. Hashim, N. Nafarizal, C. F. Soon, and M. Z. Sahdan, "Surface Tension Analysis of Cost-Effective Paraffin Wax and Water Flow Simulation for Microfluidic Device," *Adv Mat Res*, vol. 832, pp. 773–777, Nov. 2013, doi: 10.4028/www.scientific.net/AMR.832.773.

[134] J. Movaffagh, T. Nourollahian, S. Khalatbari, N. Amiri, B. S. F. Bazzaz, and F. Kalalinia, "Fabrication of Zein-Chitosan-Zein Sandwich-Like Nanofibers Containing Teicoplanin as a Local Antibacterial Drug Delivery System," *J Pharm Innov*, vol. 18, no. 3, pp. 911–922, Sep. 2023, doi: 10.1007/s12247-022-09686-2.

[135] A. Haider, S. Haider, and I.-K. Kang, "A comprehensive review summarizing the effect of electrospinning parameters and potential applications of nanofibers in biomedical and biotechnology," *Arabian Journal of Chemistry*, vol. 11, no. 8, pp. 1165–1188, Dec. 2018, doi: 10.1016/j.arabjc.2015.11.015.

[136] V. Agrahari, V. Agrahari, J. Meng, and A. K. Mitra, "Electrospun Nanofibers in Drug Delivery," in *Emerging Nanotechnologies for Diagnostics, Drug Delivery and Medical Devices*, Elsevier, 2017, pp. 189–215. doi: 10.1016/B978-0-323-42978-8.00009-7.

# VITA AUCTORIS

| | |
|---|---|
| NAME: | Grzegorz Gajewski |
| PLACE OF BIRTH: | Warsaw, PL |
| YEAR OF BIRTH: | 1991 |
| EDUCATION: | Catholic Central High School, Windsor, ON, 2009 |
| | University of Windsor, B.Sc., Windsor, ON, 2020 |
| | University of Windsor, M.Sc., Windsor, ON, 2024 |